Title
The Role of Cation/Proton Exchanger NHE9 in Synaptic Transmission & Autism

Author
Ullman, Julia Collier

Publication Date
2015

Peer reviewed|Thesis/dissertation

The Role of Cation/Proton Exchanger NHE9 in Synaptic Transmission & Autism

By

Julia Collier Ullman

A dissertation submitted in partial satisfaction of the

requirements for the degree of

Doctor in Philosophy

in

Molecular and Cell Biology

in the

Graduate Division

of the

University of California, Berkeley

Committee in charge:

Professor Robert H. Edwards, Co-Chair
Professor Ehud Isacoff, Co-Chair
Professor Richard Kramer
Professor Daniela Kaufer

Spring 2015

The Role of Cation/Proton Exchanger NHE9 in Synaptic Transmission & Autism

Julia Collier Ullman

Abstract

The Role of Cation/Proton Exchanger NHE9 in Synaptic Transmission & Autism

By

Julia Collier Ullman

Doctor of Philosophy in Molecular and Cell Biology

University of California, Berkley

Professor Robert H. Edwards Co-Chair

Professor Ehud Y. Isacoff, Co-Chair

Autism spectrum disorders (ASD) are neurodevelopmental syndromes that affect an estimated 1.5 million people in the United States alone. While ASDs arising from single gene mutations are rare, the study of these conditions provides a powerful and effective approach toward understanding the molecular basis for ASD as well as normal social behaviors. Recently, the cation/hydrogen exchanger Nhe9 has surfaced as a locus for inherited autism, with mutations confirmed to abolish expression. In addition, gene expression analysis from thousands of idiopathic ASD patients has shown altered Nhe9 gene expression as a more general feature of ASD. Interestingly, Nhe9 has also been identified as the single most significant locus for attention deficit hyperactivity disorder. Multiple lines of evidence thus implicate Nhe9 in the development of normal social behavior. In non-neural cells, NHE9 localizes to late endosomes where it mediates a H+ leak from these organelles, thus increasing their pH, and loss of NHE9 from these cells has been shown to hyper-acidify the vesicles. However, to date nothing is known about the function of NHE9 in neurons. This work seeks to understand the neurobiology of ASDs by investigating NHE9 knockout mice at behavioral, synaptic and cellular levels.

To understand the role of NHE9 in autism, we created a conditional KO mouse lacking Nhe9 only in the central nervous system. The first goal of the study was to determine whether these animals exhibit behaviors analogous to human autism. Using a wide range of behavioral assays we determined that NHE9 cKO mice have altered sociability, repetitive behaviors, and impaired olfactory communication making them a suitable model for autism in mice. Immunostaining of cultured neurons localized NHE9 to both dendritic and axonal endosomes. As a protein of known biochemical function, we hypothesized that loss of NHE9 from these endosomal vesicles would result in over-acidification of those compartments, and indeed NHE9 KO neuron endosomes are more acidic than their WT counterparts. The physiological consequence of this hyper-acidification was investigated through electrophysiological recordings in acute hippocampal slices. These measurements revealed that loss of NHE9 impairs transmitter release by a reduction in release probability and decreased quantal size. Further investigation into the nature of this impairment, using VGLUT1-pHluorin imaging, discovered that hyper-acidic synaptic vesicles have a reduced rate of exocytosis and that acute neutralization of the pH gradient rescues this impairment. While it has yet to be determined how vesicular pH directly influences vesicle exocytosis, these findings reveal a new role for ΔpH in synaptic vesicle

biology. Vesicles that are too acidic result in reduced excitatory transmission and yet dissipation of the proton gradient will collapse the driving forces required for retention of glutamate in the vesicles and abolish synaptic transmission. Thus, this study highlights the importance of the finely tuned balance in the proton-electrochemical gradient inside synaptic vesicle and the potential challenge of targeting this system to treat ASDs.

Table of Contents

Abstract 1

Chapter 1: Introduction to Cation/Hydrogen Exchange in Cell Physiology and Autism

1.1 Overview of the NHE protein family 1
1.2 Plasma Membrane NHEs 3
1.3 Organellar NHEs 3
1.4 Autism Spectrum Disorders: Man to Model Mice 5
1.5 NHE6 & NHE9 in Autism Spectrum Disorders 7
1.6 Chapter 1 References 9

Chapter 2: Dysregulation of the Synaptic Vesicle pH Gradient Impairs Neurotransmitter Release in a Mouse Model of Autism

2.1 Abstract 15
2.2 Introduction 15
2.3 Experimental Procedures 17
2.4 Results 26
2.5 Discussion 46
2.6 Acknowledgments 50
2.7 Chapter 2 References 51

Chapter 3: Physiological Role of NHE6 in Neurons

3.1 Introduction 57
3.2 Experimental Procedures 57
3.3 Results & Discussion 59
3.4 Chapter 3 References 63

Chapter 4: Future Directions & Closing Remarks

4.1 Future Directions 64
4.2 Closing Remarks 66

List of Figures

Chapter 2:

2.1 Conditional Knockout and Developmental Time Course of NHE9 26
2.S1 Conditional Inactivation of NHE9 27
2.2 The NHE9 cKO Exhibits Behavioral Features Characteristic of ASD 29
2.S2 NHE9 cKO Mice Exhibit Normal Locomotor Activity, Anxiety and Olfaction 30
2.3 NHE9 Localizes to Dendritic Endosomes and Synaptic Vesicles 33
2.S3 Subcellular localization of NHE9. 34
2.4 Loss of NHE9 Dysregulates the pH of Dendritic Endosomes and Synaptic Vesicles 36
2.S4 Surface Expression of the pHluorin Reporters and Endolysosomal Degradation 37
2.5 Loss of NHE9 Impairs Neurotransmitter Release 38
2.S5 Loss of NHE9 Does Not Affect Spine Number, Morphology or Vesicular Glutamate Transport Activity 40
2.6 Loss of NHE9 Impairs Synaptic Vesicle Exocytosis 41
2.S6 Loss of NHE9 Does Not Affect Readily Releasable Pool Size or the Level of Synaptic Proteins 43
2.7 Inhibition of the H+ Pump Rescues Synaptic Vesicle Exocytosis 44
2.S7 Bafilomycin Dissipates Synaptic Vesicle ΔpH 45

Chapter 3:

3.1 NHE6 protein levels over development 59
3.2 NHE6 sediments with synaptic vesicle proteins in equilibrium gradient fractionation 60
3.3 Co-Immunoisolation of NHE6 with neurotransmitter transporters 61
3.4 K+ stimulation of glutamate uptake is normal in NHE6 KO vesicles 61
3.5 Loss of NHE6 KO does not alter synaptic vesicle cycling 62

Chapter 1: Introduction to Cation/Hydrogen Exchange in Cell Physiology and Autism

1.1: Overview of the NHE Protein Family

The concentration gradient of monovalent cations across cell membranes is a powerful biophysical driving force in cellular physiology. These gradients set the excitability of cells, drive the active transport of solutes across membranes, and influence pH, amongst other important roles. The cation/proton antiporter (CPA) superfamily is a large group of integral membrane proteins that utilize these gradients to perform the electroneutral exchange of one cation for one proton. This superfamily is highly conserved from prokaryotes to eukaryotes thus highlighting their biological significance. Multiple isoforms of CPA family proteins are found in all cells from single celled organisms to humans where they collectively function to regulate the pH and cation composition of various membrane bound compartments.

CPA family members are commonly known as Na^+/H^+ antiporters or exchangers (NHA/NHE/NHX). The mammalian NHE protein family includes 13 distinct isoforms subdivided by their evolutionary relationships. In humans and mice, the NHE gene families are known as Solute Carrier SLC9 and further subdivided into three subfamilies. The first cluster includes SLC9A1-9, the NHE subfamily. The second group is the NHA subfamily and is made up of SLC9B1-2. Finally, the most functionally and evolutionarily distinct subfamily are the mammalian sperm-NHE like genes in the SLC9C1-2 cluster.

There are nine NHE proteins in the NHE subfamily, and all of those studied catalyze the electroneutral exchange of one cation (Na+ or K+) for one H+. While no structure has been solved for a mammalian NHE protein, a lot of structural information is known about these isoforms. Ranging in size from 645-896 amino acids (aa), they all have an amino (N)-terminus of ~450 aa with 12 membrane spanning domains and a carboxy (C)-terminus of varying length (~125-440 aa). Cation/proton exchange activity occurs within the transmembrane domains. The c-terminus is known to be a target for post-translational modification and these modifications influence both the exchange activity as well as the localization of the protein (Kondapalli et al., 2013). While transport function requires only monomeric protein, the mammalian NHEs nonetheless exist as homodimers; with some speculating that this feature enhances protein stability (Donowitz et al., 2013).

The nine NHE proteins in the mammalian NHE subfamily are further subdivided into two groups. The plasma membrane isoforms (NHE1-5) utilize the extracellular Na^+ gradient, generated by the Na^+/K^+-ATPase, to exchange protons across the plasma membrane thus regulating cytoplasmic pH and cell osmolarity (Orlowski et al., 2004). However, we know much less about the four intracellular isoforms (NHE6-9) that exchange either Na^+ or K^+ for H^+ and have been hypothesized to regulate organellar pH (Nakamura et al., 2005, Orlowski et al., 2007). These isoforms presumably drive cations into vesicles using the high proton gradient inside the vesicles generated by the vacuolar-type H+ ATPase (V-ATPase) in exchange for the high cytosolic K^+ levels.

While known cytosolic and organellar ion concentrations allow predictions to be made about the directionality of NHE transport these hypotheses must be tested. Cytosolic ion concentrations have been assayed directly however accurate measurements of vesicular ion concentrations are still lacking. Furthermore, ion flux in cells changes dynamically and the flux

of one cation can influence another rapidly altering gradients. Thus, when considering the function of NHE activity in a living cell it must be clear that the forces governing active transport for either plasma membrane or organellar isofoms is strictly dependent on the combined chemical gradients of the ions. This driving force can therefore be defined as:

$$\Delta\mu(Na^+/H^+\,exchange) = \Delta\mu\,(Na^+) - \Delta\mu\,(H^+)$$
$$= RT \cdot \ln\left([Na^+]_i/[Na^+]_o\right) - RT \cdot \ln\left([H^+]_i/[H^+]_o\right)$$

where Na^+ represents either Na^+ or K^+, R is the gas constant, T is the temperature in degrees Kelvin, and subscripts $_i$ and $_o$ refer respectively to the intracellular (cytosolic) and extracellular (or lumen) concentration of ions (Orlowski et al., 2011, Pederson et al., 2006). These calculations are based on the assumption that the exchange stoichiometry is one for one. While some have suggested that it is possible that specific isoforms may exchange two for two, there is no empirical evidence yet to support this conclusion (Orlowski et al., 2011). Using the above equation, the driving force for exchange in different cell compartments can thus be determined. For the plasma membrane isoforms the driving forces are quite clear. The Na^+ gradient is very high, (extracellular [~145 mM] to cytosolic [~10 mM]), and the pH gradient is substantial as well, with the cytosol set at ~0.3 pH units lower than the extracellular space. However, the potential driving forces are less clear for the organellar compartments where quantitative measurements of ions have been difficult to determine. Additionally, for vesicles along the endosomal pathway it is likely that the concentration of ions changes from compartment to compartment. Immediately following endocytosis, endosomal vesicles are filled with contents representative of the extracellular space, thus containing high Na^+ and slightly more alkaline pH. The prediction would be that NHEs present on these vesicles might initially be activated upon endocytosis to transport Na^+ out of the vesicle and contribute to filling the vesicle with protons. However, this scenario is presumably short lived as the V-ATPase works very quickly (~15 sec) to acidify vesicles down to pH set points of 6.8-4.5 depending on the vesicle sub-type (Egashira et al., 2015). Once this equilibrium is reached, the driving force for exchange no longer favors Na^+ but reverses direction coupling the high cytosolic K^+ concentration to the high lumen proton concentration. The exchange activity is also sensitive to the apparent affinity for cations and various isoforms range in Na^+ K_m from 5-50 mM (Orlowski et al., 2011). Furthermore, this affinity is sensitive to pH, presumably by proton competition at the cation-binding site (Orlowski et al., 2011). There is also evidence from the plasma membrane isoforms of a cytosolic proton modifier site that limits NHE activity above a certain pH (Hayashi et al., 2002, Levine et al., 1993, Kapus et al., 1994). This pH set point varies by isoform but ultimately accomplishes the same thing- it prevents over-alkalization of the cytosol. If plasma membrane NHE exchange activity were to persist until Na^+ equilibrium was reached the cytosolic pH would exceed 8.0, which would likely be fatal for the cell. While this allosteric modulation has been clearly demonstrated for the plasma membrane isoforms, there is no direct evidence for this property amongst the organellar isoforms. However, testing this possibility is extremely difficult in live cells within endogenous compartments. Nonetheless, given the high evolutionary and functional conservation within the family it is quite possible that with more precise experiments this will be demonstrated and a better understanding of the stoichiometry, allosteric modulation and cation affinity will be known for the organellar NHE isoforms.

1.2: Plasma Membrane NHEs

The plasma membrane NHE isoforms (NHE1-5) differ from the organellar isoforms (NHE6-9) by substrate recognition as well as cellular localization. The plasma membrane isoforms utilize the high extracellular Na+ gradient to catalyze the electroneutral exchange of one Na^+ (or in some instances Li^+ or NH_4^+) for one cytosolic proton. In so doing they contribute to cytosolic cell volume control, fluid secretion, renal Na^+ reabsorption, and homeostatic regulation of cytosolic pH. While NHE1 and 2 are ubiquitously expressed, NHE3 expression is highest in kidney and intestines, NHE4 is enriched in stomach cells and NHE5, while expressed in most tissues, is expressed at very high levels in neurons (Donowitz et al., 2013).

Human studies and knock-out (KO) mice (for NHE1-4) have yielded important insights into the physiological roles of the plasma membrane isoforms. Highlighting the essential role of the ubiquitous isoform, NHE1 knock-out mice die prematurely and are severely impaired while they are alive. They exhibit seizures as a result of excessive neuronal excitability, slow wave epilepsy, extreme ataxia and overall growth retardation (Bell et al., 1999, Cox et al., 1997). In humans, increased activity of NHE1 is correlated with cardiac hypertrophy and heart failure. Transgenic mice over-expressing NHE1 also develop cardiac hypertrophy and die from heart failure, further supporting a role for NHE1 in these disorders (Nakamura et al., 2008). While there is no evidence for NHE2 dysfunction in human disease, NHE2 KO mice exhibit hypochlorhydria, impaired gastric parietal cell viability, intestinal barrier dysfunction and elevated renal renin content (Shultheis et al., 1998a). Variations in NHE3 expression have been implicated in human disease with decreased expression correlating with irritable bowel disorder and increased brain stem expression with sudden infant death syndrome (SID) (Sullivan et al., 2009, Poetsch et al., 2010). While the SID studies remain somewhat controversial, there is additional evidence supporting the correlation between decreased NHE3 expression and features of IBD. Indeed, NHE3 KO mice display altered kidney/intestine Na^+ homeostasis and mild diarrhea (Shultheis et al., 1998b). Consistent with its enrichment in the stomach, NHE4 KO mice exhibit stomach inflammation, gastric necrosis and hypochlorhydria (Gawenis et al., 2005). NHE5 is the least well-understood of the plasma membrane isoforms. Studies in neurons have revealed that NHE5 constitutively recycles through the endocytic pathway to the plasma membrane, where it is dynamically retained in response to AMP-activated protein kinase phosphorylation (Diering et al., 2009, Jinadasa et al., 2014). Recent work has demonstrated a neuronal role for NHE5 in dendrite morphology with overexpression blocking activity dependent spine growth and knockdown resulting in spontaneous spine outgrowth, however the physiological consequence of this regulation has yet to be defined (Diering et al., 2011, Diering et al., 2014).

1.3: Organellar NHEs

In comparison to the plasma membrane isoforms, very little is known about the organellar NHE proteins (NHE6-9). While they are generally regarded as ubiquitously expressed throughout the body, in recent years quantitative comparisons of transcript levels in specific cell types has revealed striking expression level differences (Orlowski et al., 2011, Donowitz et al., 2013). For example NHE6 is abundant across all regions of the brain whereas NHE9 expression is highly restricted to specific cortical areas (Kandapalli et al., 2013, Kandapalli et al., 2014). Much of what is hypothesized about the possible function of these isoforms derives from studies of Nhx1, the sole intracellular NHE isoform present in *Saccharomyces cerevisiae*. NHE6, NHE7 and NHE9 all evolved from Nhx1, the K^+ and Na^+/H^+

antiporter found on yeast prevacuolar and vacuolar membranes (Brett et al., 2005a). Nhx1 functions to exchange lumenal H^+ for cytosolic K^+, and in so doing influences both the cytosolic and vacuolar pH (Kondapalli et al., 2014). Nhx1 exchange activity affects both vesicular trafficking from the late endosome to the vacuole as well as fusion of these vesicles with the vacuolar membrane (Brett et al., 2005b). However, extrapolation of Nhx1 findings to form hypotheses about the role of mammalian isoforms has proven challenging.

This is no small part due to the complexity of the endo-lysosomal pathway in mammalian cells. The electrochemical gradient of mammalian endosomes and lysosomes, just like the yeast vacuole, is driven primarily by the V-ATPase. The V-ATPase pumps protons into the lumen and this activity provides the driving force for intracellular chloride channels (CLC) proteins to electrogenically load Cl^- into the vesicles (Scott et al., 2010). Without anion accumulation to counter-balance the charge of the protons, the high membrane potential would eventually inhibit the V-ATPase activity and prevent a substantial pH gradient from forming. It was long thought that these two proteins were the main drivers controlling the various pH set-points along the endo-lysosomal pathway. In recent years various CLC KO mice were created and all of the animals exhibited functional disturbances in the endo-lysosomal pathway. The prediction for these mice was that loss of the CLCs from endosomal vesicles would result in neutral vesicular pH values. However, only the CLC5 KO mice have neutral vesicle pH and surprisingly the CLC3 & 4 knockout mice retain acidic vesicular pH (Wellhauser et al., 2010). These findings highlight redundancies in the family that ensure proper vesicular pH by chloride. Yet, given the other functional disturbances observed, these studies also reveal an intriguing role of Cl^- independent of pH, which suggests that the absolute Cl^- concentration may have a broader regulatory role (Scott et al., 2010). In parallel to the CLC work, Orlowski and Rao's groups were independently formulating what is now called the NHE pump-leak hypothesis for endosomal pH regulation (Orlwoski et al., 2007, Kondapalli et al., 2014). This hypothesis suggests that NHE proteins, present in various parts of the endo-lysosomal compartment, exchange alkali cations for lumenal protons providing a regulated proton leak that achieves the various pH set points observed along the endosomal pathway. NHE6 and NHE9 have clearly been implicated in endosomal pH regulation and the evidence supporting this hypothesis will be presented in greater detail in the following sections. Nonetheless, it suffices to say that there are multiple forces influencing pH regulation of vesicles along the endo-lysosomal pathway and disturbances in this balance result in a multitude of cellular abnormalities. Precise lumenal pH (and likely ion concentrations) are required for proper endocytosis, processing of receptor ligand complexes, cargo sorting, lipid sorting, protease activity, receptor recycling and neurotransmitter filling. It is for these reasons that understanding the unique contribution of each organellar NHE isoform is so important.

While yeast functions with a single organellar isoform, Nhx1, mammalian cells require four isoforms all of which share similar alkali cation affinity properties (K+>>Na+ but not Li+ or Rb+) but are localized to separate intracellular compartments. NHE6 and NHE9 are the two isoforms most closely related to Nhx1 and both have been localized to compartments within the endosomal pathway. In a variety of mammalian cells, NHE6 localizes to early and recycling endosomes, where it recycles through the plasma membrane (Brett et al., 2002, Nakamura et al., 2005, Hill et al., 2006, Gillfillan et al., 2008, Gabern et al., 2010, Deane et al., 2013, Ouyang et al., 2013). Originally, NHE9 was shown to be restricted to vesicles of the late endosome and lysosome. However, more recent studies show no overlap with lysosomal markers and instead localization to early, late and recycling endosomes (Nakamura et al., 2005, Hill et al., 2006,

Kondapalli et al., 2013, Kondapalli et al., 2015). While NHE6 and NHE9 reside primarily on endosomal vesicles in the majority of cell types, this is not true for the highly polarized hair cells of the inner ear. In these specialized cells, both NHE6 and NHE9 are enriched at the cell membrane where they facilitate the removal of cytosolic protons by using the high external K+ endolymph (Hill et al., 2006). Furthermore, NHE6 association with RACK1 leads to enrichment of this isoform at the plasma membrane, demonstrating that NHE6 localization can be dynamically regulated in non-neural cells as well (Ohgaki et al., 2008). Further discussion of the functional roles subserved by NHE6 and NHE9 are presented in the following sections.

NHE7 and NHE8 function within the broader golgi network. Specifically, NHE7 localizes to the trans-golgi network (TGN) (Numata et al., 2001, Nakamura et al., 2005, Lin et al., 2005, Fukura et al., 2010). Interestingly, while overexpression of NHE7 alkalized TGN compartments, a recent study has challenged the role of NHE7 as proton leak pathway for the TGN (Nakamura et al., 2005, Milosavljevic et al., 2014). Milosavljevic et al., expressed NHE7 at the plasma membrane and found that it did not transport K^+ only Na^+, and that it is constitutively active at cytosolic pH. From this work, the prediction would be that NHE7 at the TGN would serve to acidify this compartment; however this conflicts with the earlier overexpression experiments that demonstrated clear alkalization (Nakamura et al., 2005, Milosavljevic et al., 2014). Further experiments are thus needed to reconcile these apparently disparate findings. NHE8 is the most evolutionarily distinct isoform within the organellar NHE clade (Brett et al., 2005a). It localizes primarily to the mid to trans-golgi network and over-expression of this isoform alkalizes these compartments (Nakamura et al., 2005, Lawrence et al., 2010, Xia et al., 2015). However, a very small percentage of NHE8 has been observed on small vesicles within multivesicular bodies (MVB) and NHE8 knockdown alters the morphology and function of MVBs arguing for its additional importance at this site (Lawrence et al., 2010).

1.4: Autism Spectrum Disorders: man to model mice

Autism spectrum disorders (ASD) are neurodevelopmental syndromes that affect an estimated 1.5 million people in the United States alone. They present a tremendous financial burden to individual families as well as to society given that the overwhelming majority of autistic adults cannot live independently. The most recent CDC statistics describe a striking prevalence of ASD at 1 in 68 children, with boys being predominantly affected at a ratio of 4:1 over girls (Baio 2014). While it has been argued that a large proportion of the prevalence increase is due to increased diagnosis, this does not take away from the fact that ASDs are largely intractable conditions that have become a worldwide public health concern.

In humans, ASDs arise from heterogeneous constellations of neurodevelopmental deficits with behavioral outcomes negatively impacting the quality of life for the patient. The most recent diagnostic manual for mental disorders (DSM version 5) has both broadened and reprioritized the scope of behaviors required for a diagnosis of autism. The core ASD diagnostic features now include: 1) deficits in social interaction and communication (independent of gross developmental delay, eg. intellectual disability), 2) restricted or repetitive behaviors or interests, 3) onset of behaviors during early childhood and 4) collectively, the atypical behaviors negatively impact quality of life (American Psychiatric Association 2013). Deficits in social interaction and communication often manifest as a lack of social-emotional reciprocity, inability to interpret or engage in nonverbal communication, and failure to develop and maintain age appropriate relationships. The second feature for diagnosis, restricted or repetitive behaviors or interests, requires presentation in at least two out of four behavioral areas. These four areas include: 1)

stereotyped speech, movements or use objects, 2) excessive adherence to routines and resistance to change, 3) highly restricted, intense and abnormal preoccupation with either objects or interests, and 4) hyper or hypo-reactivity to sensory input. In addition to these primary diagnostic features, individuals with ASD have high comorbidity rates with intellectual disability, seizures, and attention deficit hyperactivity disorders (ADHD) (Canitano 2007, Amr et al., 2012, Anthshel et al., 2013). Monozygotic twin studies have revealed a very strong genetic underpinning for ASD, however ASDs arising from single gene mutations are rare accounting for less than one percent of all diagnosed cases (Folstein et al., 2001, Delvin et al., 2012). Over the past several years, genetic screens of autistic patients have revealed that de novo mutations, copy number variations and rare variants account for the vast majority of ASD (Pinto et al., 2014, Chen et al. 2015).

While hundreds of genes have thus far been implicated in autism very few have been studied in great detail at the molecular level. However, from these a picture has emerged of autism resulting from cellular dysfunction at the synapse. These genes cluster broadly into groups important for neuronal cell adhesion, post-synaptic translation, activity dependent regulation, synaptic plasticity and an imbalance in excitation and inhibition (Berg et al., 2012, Ebrahimi-Fakhari et al., 2015). Thus, while ASDs arising from single gene mutations are rare, the study of these conditions has to date provided a powerful and effective approach toward understanding the molecular basis for ASD as well as normal social behaviors. The development of targeted and effective therapies for ASD relies on understanding the molecular basis of these behavioral deficits. Future progress in ASD research requires not only greater understanding of the genes already implicated but also validation of new candidate autism genes.

To date, cellular research into ASD genes has relied prominently on mouse models. In order for a mouse model to be an effective tool for ASD research the animal should exhibit three primary features: 1) construct validity, 2) face validity and 3) predictive validity (Silverman et al., 2010, Ey et al., 2011, Roullet et al., 2011). Construct validity refers to the specific genetic mutation identified in humans; eg. loss of function versus duplication. The face validity of the mouse model speaks to whether the mutation results in behavioral features mice analogous to human autism. Finally, the predictive validity of the animal highlights the importance of the goal that these models ultimately be useful for testing drugs or therapies to ameliorate specific ASD behavioral deficits. The first validity feature is typically straightforward to interpret; however the other two can be quite challenging. Mice are innately very social creatures, however they express their sociability very differently than humans (Crawley 2004, Nadler et al., 2004). Furthermore, the laboratory environments used to house mice are quite unnatural and can mask or exacerbate certain behaviors. Despite these limitations, many ASD behavioral assays have been developed and validated for specific aspects of mouse sociability, communication, and repetitive/restricted behaviors (Silverman et al., 2010, Ey et al., 2011, Roullet et al., 2011). Analysis of ASD model mice has demonstrated that the pathogenic mutations in mice result in behavioral phenotypes as heterogeneous as their human counterparts. For example, null mutations in the serotonin transporter (SlC6A4) result in overall low sociability and lack of preference for social novelty (Moy et al., 2009), but mice that are haploinsufficient for SLC6A4 have normal social interest but impaired social recognition (Page et al., 2009). A mouse model with chromosomal duplication of the analogous region to human 15q11-13 displays low sociability, altered ultrasonic vocalizations and impaired reversal learning (Nakatani et al., 2009). Neuroligin (NLGN1) null mice have no defects in sociability, normal preference for social novelty, unchanged reciprocal social interactions but altered nest building (Blundell et al., 2010). As a

final example, Shank3 null mice have altered social interactions and self-injurious repetitive grooming (Peca et al., 2011). One of the best-studied autism models is the FMR1 null mouse, a model for Fragile X syndrome, which was first created more than two decades ago (Bakker et al., 1994). Hundreds of research articles have been published on these animals and it has taken two decades of research to fully understand the molecular dysfunction such that promising clinical trials are only now underway (Erickson et al., 2014). Continued research into the molecular basis of autism-like behaviors, using these model mice, will undoubtedly yield new insights and pathways targetable for therapeutic interventions.

1.5: NHE6 & NHE9 in Autism Spectrum Disorders

Recent human genetic studies have implicated the two intracellular cation/proton exchangers NHE6 and NHE9 in autism and other neuropsychiatric disorders. X-linked developmental brain disorders are the most prevalent form of intellectual disability and mutations in NHE6 rank amongst the top leading causes (Tarpey 2009). ASD causing mutations in NHE6 were first identified in a group of patients diagnosed with Angelman-like Syndrome (AS) (Gillfillan et al, 2008). However, as more patients with NHE6 mutations were identified it became clear that they presented a unique syndrome. Numerous mutations in NHE6 have now been identified and today all of those patients are diagnosed with Christianson Syndrome (CS) named for the person who first described the unique set of phenotypes caused by NHE6 mutations (Christianson et al., 1999, Pescosolido et al., 2014). CS is a syndromic autism spectrum disorder, with features of classic autism and physiological traits unique to CS including microcephaly, non-verbal status, epilepsy, intellectual disability, and ataxia (Pelc et al., 2008, Ouyang et al., 2013). Interestingly, mutations in NHE6 have also been identified in patients with features of autism combined with tau-positive neurodegeneration, and in patients with schizophrenia (Gabern et al., 2010, Piton et al., 2011).

NHE9 has similarly been implicated in autism, as well as ADHD. Mutations in the promoter region of NHE9 were originally identified from homozygosity mapping of autism patients with shared ancestries (Morrow et al., 2008). This study also investigated non-consanguineous patients with autism and epilepsy, and discovered non-sense mutations in NHE9 predicted to truncate the protein between the 11^{th} and 12^{th} transmembrane domains (Morrow et al., 2008). Additional studies have now also identified loss of function mutations in the NHE9 gene in formerly idiopathic ASD patients (Ben-David et al., 2011, Wagle et al., 2014). Several of these mutations were recently investigated in cell culture assays and they were all determined to result in loss of the catalytic activity of the protein (Kondapalli et al., 2013). This same study investigated the physiological consequence of NHE9 loss of function by knocking down the gene in cultured fibroblasts and astrocytes, and found that this resulted in endosomes that were hyper-acidifed (Kondapalli et al., 2013). In contrast to the loss of function mutations, differential gene expression analysis of post-mortem brain tissue comparing autistic to non-autistic controls identified strong up-regulation of NHE9 as well as down-regulation of NHE6 in ASD brains (Schwede et al., 2014). This suggests that the correct dosage of NHE9 is important for normal behavior and brain function. This observation is further supported by the strong correlation of NHE9 with ADHD. Quantitative trait locus (QTL) mapping of ADHD patients genomes identified the NHE9 locus, and in a separate study a pericentric inversion of chromosome 3 disrupting NHE9 was found in ADHD patients with intellectual disability (Fischer et al., 2002, de Silva et al., 2003). Since its identification in these early screens, spontaneous disruption of NHE9 has also been discovered to be the genetic dysfunction in the WKY/NCrl rat model of

ADHD, which exhibits behavioral phenotypes analogous to human ADHD (Zhang-James et al., 2011, Zhang-James et al., 2012). However, the functional consequences of these ADHD mutations have yet to be characterized. Most recently, in a sample set comparing over 900 children with ADHD to their parents, NHE9 was identified as the single most significant locus for attention deficit hyperactivity disorder (Lasky-Su et al., 2008). These findings highlight the importance of NHE6 and NHE9 in normal cognition and behavior, yet we know little about their function in neurons or how their loss can produce such profound behavioral disorders.

1.6: Chapter 1 References

American Psychiatric Association. (2013). Diagnostic and statistical manual of mental disorders: DSM-5. Washington, D.C: American Psychiatric Association.

Amr M, Raddad D, El-Mehesh F, bakr A, Sllam K, Amin T. (2012) Comorbid psychiatric disorders in Arab children with autism spectrum disorders. Res. Autism Sectr. Disord., 6: 240-248.

Antshel KM, Zhang-James Y, Farone SV. (2013) The comorbidity of ADHD and autism spectrum disorder. Expert Rev. Neurother., 13: 1117-1128.

Baio J. (2014) Prevalence of autism spectrum disorders among children aged 8 years autism and neurodevelopmental disabilities monitoring network, 11 sites, United States, 2010.] MMWR. Surveill. Summ. 63(Suppl.2), 1-21.

Bakker CE, Verheij C, Willemsen R, van der Helm R, Oerlemans F, Vermey M, Bygrave A, Hoogeveen AT, Oostracorrespondence BA, Reyniers E, De Boule K, D'Hooge R, Cras, van Velzen PD, Nagels G, Martin JJ, De Deyn PP, Darby JK, Willems PJ. (1994) Fmr1 knockout mice: A model to study fragile X mental retardation. Cell, 78: 23-33.

Bell SM, Schreiner CM, Schultheis PJ, Miller ML, Evans RL, Vorhees CV, Shull GE, Scott WJ (1999) Targeted disruption of of the murine NHE1 locus induces ataxia, growth retardation and seizures. Am. J. Physiol. 276: C788-C795.

Ben-David E, Granot-Hershkovitz E, Monderer-Rothkoff G, Lerer E, Levi S, Yaari M, Ebstein RP, Yirmiya N, Shifman S. (2011) Identification of a functional rare variant in autism using genome-wide screen for monoallelic expression. Hum Mol. Genet.,20:363-3641.

Berg JM, Geschwind DH. (2012) Autism genetics: searching for specificity and convergence. Genome Biology, 13: 247.

Blundell J, Blaiss CA, Etherton MR, Espinosa F, Tabuchi K, Walz C, Bolliger MF, Südhof TC, Powell CM. (2010) Neuroligin-1 deletion results in impaired spatial memory and increased repetitive behavior. J Neuroscience, 30: 2115-2129.

Brett CL, Wei Y, Donowitz M, Rao R. (2002) Human Na+/H+ exchanger isoform 6 is found in recycling endosomes of cells, not mitochondria. Am. J. Physiol. 282, C1031-1041.

Brett CL, Donowitz M, Rao R. (2005a) Evolutionary origins of eukaryotic sodium/proton exchangers. Am. J. Physiol. 288, C223-239.

Brett CL, Tukaye DN, Mukherjee S, Rao R. (2005b) The yeast endosomal Na+(K+)/H+ exchanger Nhx1 regulates cellular pH to control vesicle trafficking. Molecular Biology of the Cell, 16: 1396–1405.

Canitano R. (2007) Epilepsy in autism spectrum disorders. European Child Adolescence Psychiatry, 16: 61-66.

Chen JA, Penagarikano O, Belgard TG, Swarup V, Geschwind DH. (2015) The emerging picture of autism spectrum disorder: genetics and pathology. Ann. Rev. Pathology, 10: 111-144.

Christianson AL1, Stevenson RE, van der Meyden CH, Pelser J, Theron FW, van Rensburg PL, Chandler M, Schwartz CE. (1999) X linked severe mental retardation, craniofacial dysmorphology, epilepsy, ophthalmoplegia, and cerebellar atrophy in a large South African kindred is localised to Xq24-q27. J Med Genet, 36:759-766.

Cox GA, Lutz CM, Yang CL, Biemesderfer D, Bronson RT, Fu A, Aronson PS, Noebels JL, Frankel WN (1997) Sodium/hydrogen exchanger gene defect in slow wave epilepsy mutant mice. Cell 91: 139-148.

Crawley JN. (2004) Designing mouse behavioral tasks relevant to autistic-like behaviors. Mental

Retardation and Developmental Disabilities Research Reviews, 10: 248-258.
de Silva MG, Elliott K, Dahl HH, Fitzpatrick E, Wilcox S, Delatycki M, Williamson R, Efron D, Lynch M, Forrest S. (2003) Disruption of a novel member of a sodium/hydrogen exchanger family and DOCK3 is associated with an attention deficit hyperactivity disorder-like phenotype. J Med Genet., 40: 733-740.
Deane, E.C., Ilie, A.E., Sizdahkhani, S., Das Gupta, M., Orlowski, J., and McKinney, R.A. (2013). Enhanced recruitment of endosomal na+/h+ exchanger nhe6 into dendritic spines of hippocampal pyramidal neurons during nmda receptor-dependent long-term potentiation. J. Neurosci. *33*, 595-610.
Delvin B, Scherer SW. (2012) Genetic architecture in autism spectrum disorders. Current Opinions Genetics and Development, 22: 229-237.
Diering GH, Chruch J, Numata M. (2009) Secretory carrier membrane protein 2 regulates cell surface targeting of brain enriched Na+/H+ exchanger NHE5. J. Biol. Chem., 284: 13892-13903.
Diering GH, Mills F, Bamji SX, Numata M. (2011) Regualtion of dendritic spine growth through activity dependent recruitment of the brain enriched Na+/H+ exchanger NHE5. Mol. Biol. Cell, 22: 2246-2257.
Diering GH, Numata M. (2014) Endosomal pH in neuronal signaling and synaptic transmission: role of Na(+)/H(+) exchanger NHE5. Front Physiol, 13: 400-412.
Donowitz M, Mohan S, Zhu CX, Chen TE, Lin R, Cha B, Zachos NC, Murtazina R, Sarker R, Li X (2009) NHE3 regulatory complexes. J. Exp. Biol. 212: 1638-1646.
Donowitz M, Ming Tse C, Fuster D. (2013) SLC9/NHE gene family, a plasma membrane and organellar family of Na+/H+ exchangers. Molecualr Aspects of Medicine 34: 236-251.
Ebrahimi-Fakhari D, Sahin M. (2015) Autism and the synapse: emerging mechanisms and mechanism-based therapies. Current Opinions Neurology, 28: 91-102.
Edwards RH. (2007) The neurotransmitter cycle and quantal size. Neuron, 55: 835-858.
Egashira Y, Takase M, Takamori S. (2015) Monitoring of vacuolar-type H+ ATPase mediated proton influx into synaptic vesicles. Journal of Neuroscience, 35:3701-3710.
Erickson CA, Veenstra-Vanderweele JM, Melmed RD, McCracken JT, Ginsberg LD, Sikich L, Scahill L, Cherubini M, Zarevics P, Walton-Bowen K, Carpenter RL, Bear MF, Wang PP, King BH. (2014) STX209 (arbaclofen) for autism spectrum disorders: an 8-week open-label study. J Autism Dev Disord., 44: 958-64.
Ey E, Leblond CS, Bourgeron T. (2011) Behavioral profiles of mouse models for autism spectrum disorders. Autism Research, 4: 1-12.
Fisher SE, Francks C, McCracken JT, McGough JJ, Marlow AJ, MacPhie IL, Newbury DF, Crawford LR, Palmer CG, Woodward JA, Del'Homme M, Cantwell DP, Nelson SF, Monaco AP, Smalley SL. (2002) A genomewide scan for loci involved in attention deficit/hyperactivity disorder. Am J Hum Genet., 70: 1183 1196.
Folstein SE, Rosen-Shiedley B. (2001) Genetics of autism: complex aeitology for a heterologous disorder. Nature Review Genetics, 2: 943-955.
Fukura N, Ohgaki R, Matsushita M, Nakamura N, Mitsui K, Kanazawa H. (2010) A membrane-proximal region in the C-terminal tail of NHE7 is required for its distribution in the trans-Golgi network, distinct from NHE6 localization at endosomes. J Membr Biol., 234:149-58.

Gabern JY, Neumann M, Trojanowski JQ, Lee VM, Feldman G, Norris JW, Friez MJ, Schwartz CE, Stevenson R, Sima AA. (2010) A mutation affecting the sodium/proton exchanger, Slc9a6, causes mental retardation with tau deposition. Brain,133:1391-1402.

Gawenis LR, Greeb JM, Prasad V, Grisham C, Sanford LP, Doetschman T, Andringa A, Miller ML, Shull GE (2005) Impaired gastric acid secretion in mice with a targeted disruption of the NHE4 Na+/H+ exchanger. J. Biolo. Chem. 280: 12781 12789.

Gillfillan GD, Selmer KK, Roxrud I, Smith R, Kyllerman M, Eiklid K, Kroken M,Mattingsdal M, Egeland T, Stenmark H, Sjoholm H, Server A, Samuelsson L, Christianson A, Tarpey P, Whibley A, Stratton MR, Futreal PA, Teague J, Edkins S, Gecz J, Turner G, Raymond FL, Schwarz C, Stevenson RE, Undlien DE, Stromme P. (2008) SLC9A6 mutations cause X-linked mental retardation, microcephaly, epilepsy, and ataxia, a phenotype mimicking Angelman syndrome. American Journal of Human Genetics, 82: 1003-10.

Goh GY, Huang H, Ullman J, Borre L, Hnasko TS, Trussell LO, Edwards RH. (2011) Presynaptic regulation of quantal size: K+/H+ exchange stimulates vesicular glutamate transport. Nature Neuroscience, 14: 1285-1292.

Greer PL, Hanayama R, Bloodgood BL, Mardinly AS, Lipton DM, Flavell SW, Kim TK, Griffith EC, Waidon Z, Maehr R, Ploegh HL, Chowdhury S, Worley PF, Steen J, Greenberg M. (2010) The Angelman sydrome protein Ube3a regulates synapse development by ubiquitinating Arc. Cell, 140: 704-716.

Gronborg M, Pavlos NJ, Brunk I, Chua JJ, Munster-Wandowskit A, Reidel D, Ahnert HIlger G, Urlaub H, Jahn R. (2010) Quantitative comparison of glutamatergic and GABAergic synaptic vesicles unveils selectivity for few proteins including MAL2, a novel synaptic vesicle protein. Journal of Neuroscience, 30: 2-12.

Hayashi H, Szaszi K, Grinstein S. (2002) Multiple modes of regulation of Na+/H+ exchangers. Ann. N.Y. Acad. Sci. 976: 248-258.

Hartinger J, Jahn R. (1993) An anion binding site that regulates transporter of synaptic vesicles. Journal of Biological Chemistry, 268: 23122-7.

Hill JK, Brett CL, Chyou A, Kallay LM, Sakaguchi M, Rao R, Gillespie PG. (2006) Vestibular hair bundles control pH with (Na+, K+)/H+ exchangers NHE6 and NHE9. Journal of Neuroscience, 26: 9944-9955.

Jinadasa T, Szabó EZ, Numat M, Orlowski J. (2014) Activation of AMP-activated protein kinase regulates hippocampal neuronal pH by recruiting Na(+)/H(+) exchanger NHE5 to the cell surface. J Biol Chem. 289(30): 20879-97.

Juge N, Yoshida Y, Yatsushiro S, Omote H, Moriyama Y. (2006) Vesicular glutamate transporter contains two independent transport machineries. Journal of Biological Chemistry, 281: 39499-506.

Kapus A, Grisntein S, Wasan S, Kandasamy R, Orlowski J. (1994) Functional characterization of the Na+/H+ exchanger stably expressed in chinese hamster ovary cells, ATP dependence, osmotic sensitivity and role in cell proliferation. J. Biol Chem, 269: 23544-23552.

Kondapalli KC, Hack A, Schushan M, Landau M, Ben-Tal N, Rao R. (2013) Functional evaluation of autism-associated mutations in NHE9. Nature Communications, 4:2510.

Kondapalli KC, Prasad H, Rao R. (2014) An inside job: how endosomal Na+/H+ exchangers link to autism and neurological disease. Frontiers in Cellular Neuroscience, 8: 1-21.

Kondapalli KC, Llongueras JP, Capilla-González V, Prasad H, Hack A, Smith C, Guerrero

Cázares H, Quiñones-Hinojosa A, Rao R. (2015) A leak pathway for luminal protons in endosomes drives oncogenic signaling in glioblastoma. Nature Communications, 6:6289.

Lasky-Su J, Neale BM, Franke B, Anney RJ, Zhou K, Maller JB, Vasquez AA, Chen W, Asherson P, Buitelaar J, Banaschewski T, et al. (2008) Genome-wide association scan of quantitative traits for attention deficity hyperactivity disorder identifies novel associations and confirms candidate gene associations. American Journal of Medicinal Genetics B Neuropyschiatric Genetics, 147B: 1345-54.

Lawrence SP, Bright NA, Luzio JP, Bowers K. (2010) The sodium/proton exchanger NHE8 regulates late endosomal morphology and function. Molecular Biology of the Cell, 21: 3540-3551.

Levine SA, Montrose MH, Tse CM, Donowitz M. (1993) Kinetics and regulation of three cloned mammalian Na+/H+ exchangers stably expressed in a fibroblast cell line. J. Biol. Chem. 268: 25527-25535.

Lin PJ, Williams WP, Luu Y, Molday RS, Orlowski J, Numata M. (2005) Secretory carrier membrane proteins interact and regulate trafficking of the organellar (Na+,K+)/H+ exchanger NHE7. J Cell Science, 118: 1885-1897.

Lukashova V, Jinadasa T, Ilie A, Verbich D, Cooper E, Orlowski J. (2013) The Na(+)/H (+) exchanger NHE5 is sorted to discrete intracellular vesicles in the central and peripheral nervous systems. Adv Exp Med Biol. 961: 397-410.

Maycox PR, Deckerwerth T, Hell JW, Jahn R. (1988) Glutamate uptake by brain synaptic vesicles. Energy dependence of transport and functional reconstitution in proteoliposomes. Journal of Biological Chemistry, 263: 15423-28.

Milosavljevic N, Monet M, Léna I, Brau F, Lacas-Gervais S, Feliciangeli S, Counillon L, Poët M. (2014) The intracellular Na(+)/H(+) exchanger NHE7 effects a Na(+) coupled, but not K(+)-coupled proton-loading mechanism in endocytosis. Cell Rep., 7:689-96.

Morrow EM, Yoo SY, Flavell SW, Kim TK, Lin Y, Hill RS, Mukaddes NM, Balkhy S, Gascon G, Hashmi A, Al-Saad S, et al. (2008) Identifying autism loci and genes by tracing recent shared ancestry. Science, 321: 218-23.

Moy SS, Nadler JJ, Young NB, Nonneman RJ, Grossman AW, Murphy DL, D'Ercole AJ Crawley JN, Magnuson TR, Lauder JM. (2009) Social approach in genetically engineered mouse lines relevant to autism. Genes Brain Behav. 8, 129–142

Nadler JJ, Moy SS, Dolf G, Trang D, Simmons N, Perez A, Young NB, Barbaro RP, Piven J, Magnuson TR, Crawley JN, (2004) Automated apparatus for quantitation of social approach in mice. Genes, Brain and Behavior, 3: 303-314.

Nakamura N, Tanaka S, Teko Y, Mitsui K, Kanazawa H. (2005) Four Na+/H+ exchanger isoforms are distributed to Golgi and post-golgi compartments and are involved in organelle pH regulation. J Biol Chem, 280: 1561-72.

Nakamura TY, Iwata Y, Arai Y, Komamura K, Wakabayashi S. (2008) Activation of Na+/H+ exchanger 1 is sufficient to generate Ca2+ signals that induce cardiac hypertrophy and heart failure. Circ Res. 103: 891-899.

Nakatani J1, Tamada K, Hatanaka F, Ise S, Ohta H, Inoue K, Tomonaga S, Watanabe Y, Chung YJ, Banerjee R, Iwamoto K, Kato T, Okazawa M, Yamauchi K, Tanda K, Takao K, Miyakawa T, Bradley A, Takumi T. (2009) Abnormal behavior in a chromosome engineered mouse model for human 15q11-13 duplication seen in autism. Cell, 137: 1235-124.

Numata M, Orlowski J. (2001) Molecular cloning and characterization of a novel (Na+,

K+)/H+ exchanger localized to the trans-golgi network. J Biol Chem, 276: 17387 17394.
Ohgaki R, Fukura N, Matsushita M, Mitsui K, Kanazawa H. (2008) Cell surface levels of organellar Na+/H+ exchanger isoform 6 are regulated by interaction with RACK1. J. Biol Chem, 283: 4417-4429.
Orlowski J, Grinstein S. (2004) Diversity of the mammalian sodium/proton exchanger SLC9 gene family. Pflugers Archive European Journal of Physiology, 447: 549 565.
Orlowski J, Grinstein S. (2007) Emerging roles of alkali cation/proton exchangers in organellar homeostasis. Current Opinions in Cell Biology, 19: 483-92.
Orlowski J, Grinstein S. (2011) Na+/H+ exchangers. Comprehensive Physiology, 1: 2083-2100.
Ouyang, Q., Lizarraga, S.B., Schmidt, M., Yang, U., Gong, J., Ellisor, D., Kauer, J.A., and Morrow, E.M. (2013). Christianson syndrome protein nhe6 modulates trkb endosomal signaling required for neuronal circuit development. Neuron *80*, 97-112.
Page DT, Kuti OJ, Prestia C, Sur M. (2009) Haploinsuffiency for Pten and Serotonin transporter cooperatively influences brain size and social behavior. PNAS, 106: 1989 1994.
Peça J, Feliciano C, Ting JT, Wang W, Wells MF, Venkatraman TN, Lascola CD, Fu Z, Feng G. (2011) Shank3 mutant mice display autistic-like behaviours and striatal dysfunction. Nature, 472: 437-442.
Pedersen SF, O'Donnell ME, Anderson SE, Cala PM. (2006) Physiology and pathophysiology of Na+/H+ exchange and Na+ - K+ - 2Cl- cotransport in the heart, brain and blood. Am. J. Phys. Regul. Integr. Comp. Physiol, 291:R1-R25.
Pelc K, Cheron G, Dan B. (2008) Behavior and neuropyschiatric manifestations inAngelman syndrome. Neuropyschiatric Disease Treatment, 4: 577-84.
Pescosolido MF, Stein DM, Schmidt M, El Achkar CM, Sabbagh M, Rogg JM, Tantravahi U, McLean RL, Liu JS, Poduri A, Morrow EM. (2014) Genetic and phenotypic diversity of NHE6 mutations in Christianson syndrome. Ann Neurol., 76: 581-593.
Pinto D, Delaby E, Merico D, Barbosa M, Merikangas A, Klei L, Thiruvahindrapuram B, Xu X, Ziman R, et al. (2014) Convergence of genes and cellular pathways dysregulated in autism spectrum disorders. Am J Hum Genet., 94: 677-694
Piton A, Gauthier J, Hamdan FF, Lafrenière RG, Yang Y, Henrion E, Laurent S, Noreau A, Thibodeau P, Karemera L, et al. (2011) Systematic resequencing of X chromosome synaptic genes in autism spectrum disorder and schizophrenia. Molecular Psychiatry, 16: 867-880.
Poetsch M, Nottebaum BJ, Wingenfeld L, Frede S, Vennemann M, Bajanowski T.(2010) Impact of sodium/proton exchanger 3 gene variants on sudden infant deathsyndrome. Journal of Pediatrics, 156: 44-48.
Rotin D, Kumar S. (2009) Physiological functions of the HECT family of ubiquitin ligases. Nature Review Molecular Cell Biology, 10: 398-409.
Roullet FI, Crawley JN. (2011) Mouse models of autism: testing hypotheses about molecular mechanisms. Current Topics in Behavioral Neuroscience.
Roxrud I, Raiborg C, Gilfillan GD, Stromme P, Stenmark H. (2009) Dual degradation mechanisms ensure disposal of NHE6 mutant protein associated with neurologicaldisease. Experimental Cell Research, 315: 3014-27.
Scott C, Greunberg J. (2010) Ion flux and the function of endosomes and lysosomes: pH is the just the start. Bioessays Journal, 33: 103-110.
Schenck S, Wojcik SM, Brose N, Takamori S. (2009) A chloride conductance in VGlut1

underlies maximal glutamate loading into synaptic vesicles. Nature Neuroscience, 12: 156-62.

Schultheis PJ, Clarke LL, Meneton P, Harline M, Boivin GP, Stemmermann G, Duffy JJ, Doetschman T, Miller ML, Shull GE. (1998a) Targeted disruption of the murine Na+/H+ exchanger isoform 2 gene causes reduced viability of gastric parietal cells and loss of net acid secretion. J Clin Invest, 101: 1243-1253.

Schultheis PJ, Clarke LL, Meneton P, Miller ML, Soleimani M, Gawenis LR, Riddle TM,Duffy JJ, Doetschman T, Wang T, Giebisch G, Aronson PS, Lorenz JN, Shull GE. (1998b) Renal and intestinal absorptive defects in mice lacking NHE3 Na+/H+ exchanger. Nature Genetics, 19: 282-285.

Schwede M, Garbett K, Mirnics K, Geschwind DH, Morrow EM. (2014) Genes for endosomal NHE6 and NHE9 are misregulated in autism brains. Mol Psychiatry, 19: 277-279.

Shroer RJ, Holden KR, Tarpey PS, Matheus MG, Griesemer DA, Friez MJ, Fan JZ, Simensen RJ, Stromme P, Stevenson RE, Stratton MR, Schwartz CE. (2010) Natural history of Christianson syndrome. American Journal of Medicinal Genetics A, 152: 2775-83.

Silverman JL, Yang M, Lord C, Crawley JN. (2010) Behavioural phenotyping assays for mouse models of autism. Nature Reviews Neuroscience, 11: 490–502.

Strømme P, Dobrenis K, Sillitoe RV, Gulinello M, Ali NF, Davidson C, Micsenyi MC, Stephney G, Ellevog L, Klungland A, Walkley SU. (2011) X-linked Angelman like syndrome caused by Slc9a6 knockout in mice exhibits evidence of endosomal-lysosomal dysfunction. Brain, 134: 3369-3383.

Sullivan S, Alex P, Dassopoulos T, Zachos NC, Iacobuzio-Donahue C, Donowitz M, Brant SR, Cuffari C, Harris ML, Datta LW, Conklin L, Chen Y, Li X. (2009) Downregulation of sodium transporters and NHERF proteins in IBD patients and mouse colitis models: potential contributors to IBD-associated diarrhea. Inflamm Bowel Dis. 15: 261-274.

Tabb JS, Kish PE, Van Dyke R, Ueda T. (1992) Glutamate transport into synaptic vesicles. Roles of membrane potential, pH gradient, and intravesicular pH. Journalof Biological Chemistry, 267: 15412-18.

Tarpey PS, Smith R, Pleasance E, Whibley A, Edkins S, Hardy C, O'Meara S, Latimer C, Dicks E, et al. (2009) A systematic, large-scale resequencing screen of X chromosome coding exons in mental retardation. Nature Genetics, 41: 535-543.

Wagle M, Holder J. (2014) Exonic deletion of Slc9a9 in autism with epilepsy. Neurology, 82: P4.338.

Wellhauser L, D'Antonio C, Bear CE. (2010) CLC transporters: discoveries and challenges in defining the mechanisms underlying functional and regulation of CLC5. Pflugers Arch, 460: 543-557.

Xia CH, Liu H, Cheung D, Tang F, Chang B, Li M, Gong X. (2015) NHE8 is essential for RPE cell polarity and photoreceptor survival. Science Reports, 5:9358.

Zhang-James Y, Middleton FA, Sagvolden T, Faraone SV. (2012) Differential expressionof SLC9A9 and interacting molecules in the hippocampus of rat models for attention deficit/hyperactivity disorder. Dev Neurosci., 34: 218-227.

Zhang-James Y, DasBanerjee T, Sagvolden T, Middleton FA, Faraone SV. (2011)SLC9A9 mutations, gene expression, and protein-protein interactions in rat models of attention deficit/hyperactivity disorder. Am J Med Genet B Neuropsychiatr Genet., 156B: 835-843.

Chapter 2: Dysregulation of the Synaptic Vesicle pH Gradient Impairs Neurotransmitter Release in a Mouse Model of Autism

2.1 Abstract

The weak base character of multiple psychoactive compounds such as chloroquine and amphetamine has suggested that they act at least in part by accumulating inside acidic intracellular compartments where they dissipate the pH gradient. However, the physiological mechanisms that normally regulate vesicular pH remain poorly understood. Interestingly, recent human genetic studies have implicated the intracellular Na^+/H^+ exchanger NHE9 in both autism spectrum disorders (ASD) and ADHD. Plasma membrane NHEs control cytosolic pH but the role of intracellular isoforms has remained unclear. We now find that the inactivation of NHE9 in mice reproduces behavioral features of ASD including impaired social interaction, repetitive behaviors and altered olfactory communication. The mechanism involves defects in synaptic transmission due to impaired synaptic vesicle filling and exocytosis. Indeed, acute dissipation of the H^+ electrochemical gradient rescues the defect in exocytosis. The physiological regulation of vesicular pH thus has an important role in synaptic transmission and behavior.

2.2 Introduction

Flux across intracellular membranes generally relies on a H^+ electrochemical gradient. Mitochondria use this force to produce ATP, and lysosomes require a low pH to activate degradative enzymes. Neurotransmitters also depend on a H^+ electrochemical gradient for transport into synaptic vesicles (Edwards, 2007). The psychoactive properties of many drugs that act as a weak base to dissipate the chemical component of this gradient (ΔpH) attests to its importance for physiology and behavior. Amphetamines promote flux reversal by plasma membrane monoamine transporters, but this effect relies on their ability to dissipate ΔpH, release vesicular stores and increase cytosolic monoamine levels (Sulzer and Rayport, 1990; Sulzer et al., 1995). Their efficacy in the treatment of attention deficit hyperactivity disorder (ADHD) presumably reflects this activity (Del Campo et al., 2011). The antimalarial compound chloroquine also dissipates ΔpH and has a variety of psychoactive effects, from vivid dreams to psychosis (Rab, 1963). In addition, a number of antipsychotic compounds accumulate in synaptic vesicles due to their behavior as weak bases, and release from this source may contribute to their therapeutic efficacy (Tischbirek et al., 2012). A disturbance in the vesicular H^+ electrochemical gradient may therefore contribute to neuropsychiatric disease, but the mechanisms that normally regulate this gradient remain poorly understood.

A vacuolar-type H^+-ATPase creates the H^+ electrochemical gradient across membranes of the secretory pathway (Stevens and Forgac, 1997). However, the expression of this gradient as either ΔpH or membrane potential ($\Delta\psi$) depends on other factors. The formation of ΔpH generally requires anion entry to relieve inhibition of the H^+-ATPase by the accumulating positive $\Delta\psi$, and Cl^- is considered the main anion responsible. Intracellular members of the ClC chloride carrier family control acidification in the endolysosomal pathway (Stauber and Jentsch, 2013), but other anions such as the excitatory transmitter glutamate have a similar role in synaptic vesicles (Gras et al., 2008; Hnasko et al., 2010). In contrast to the vesicular transport of other classical transmitters, which generally relies on ΔpH, vesicular glutamate transport depends on and hence consumes $\Delta\psi$, thereby creating ΔpH. Multiple anions thus contribute to the

formation of ΔpH. It has nonetheless been difficult to understand how differences in anion flux alone could account for progressive acidification in the endolysosomal pathway.

The family of Na^+/H^+ exchangers includes plasma membrane isoforms that regulate cytosolic pH, but recent work has uncovered a series of isoforms that localize to membranes of the secretory pathway (Orlowski and Grinstein, 2004; Ohgaki et al., 2011). The organellar isoforms exchange cytosolic Na^+ or K^+ for lumenal H^+ and can thus function with anion carriers to determine organelle pH. In addition to effects on ΔpH, the single common yeast ancestor *Nhx1* influences membrane trafficking (Brett et al., 2005; Kojima et al., 2012), and a mammalian homologue has been reported to affect endocytosis (Xinhan et al., 2011).

Since many psychoactive drugs also dissipate ΔpH across internal cell membranes, the organellar NHE isoforms might be expected to influence synaptic transmission. Indeed, we identified an NHE activity on synaptic vesicles that dissipates ΔpH to promote the Δψ driving glutamate transport into synaptic vesicles (Goh et al., 2011). Studies in culture implicate organellar isoform NHE6 in dendrite morphology and NHE9 in glutamate uptake by glia (Kondapalli et al., 2013). However, the actual role of organellar NHEs in synaptic transmission and behavior has remained unclear.

Interestingly, human genetic studies have recently implicated the organellar NHEs in a range of neuropsychiatric conditions, from intellectual disability and autism spectrum disorders (ASD) to attention deficit hyperactivity disorder (ADHD). Recessive mutations in the X-linked endosomal isoform NHE6 produce Christianson syndrome, a developmental disorder with severe intellectual disability and seizures (Gilfillan et al., 2008). The condition apparently reflects both endolysosomal dysfunction and a profound defect in neuronal morphology due to reduced expression of the brain-derived neurotrophic factor (BDNF) receptor TrkB (Stromme et al., 2011; Ouyang et al., 2013).

More recently, mutations in the organellar isoform NHE9 have been identified in ASD (Morrow et al., 2008). ASD form a group of related neurodevelopmental conditions defined by defects in social interaction (including abnormal communication) and often accompanied by restricted interests, repetitive, stereotyped behavior and impaired sensory reactivity (Lord and Bishop, 2015). Mutations in NHE9 produce seizures as well as ASD but the disability is considerably milder than that produced by loss of NHE6. Originally identified in consanguineous families, NHE9 mutations were subsequently found in non-consanguineous families as well, suggesting that heterozygotes can also express the phenotype (Morrow et al., 2008). Complementation in yeast and astrocytes indicates that the mutations produce a loss of function (Kondapalli et al., 2013). In addition, changes in the regulation of NHE6 and 9 have been observed more generally in patients with ASD (Schwede et al., 2013). NHE9 has also been implicated in ADHD. Among the candidate genes identified in a genome-wide association study, NHE9 had the highest overall association (Fisher et al., 2002; de Silva et al., 2003; Lasky-Su et al., 2008). A condition treated by an agent that dissipates vesicular ΔpH (amphetamine) may thus involve a specific disturbance in the endogenous mechanisms that regulate this gradient.

To understand how the loss of NHE9 contributes to organelle pH homeostasis, synaptic transmission and ultimately behavior, we inactivated the gene in mice.

2.3 Experimental Procedures

Mouse breeding and genotyping

To produce a conditional knockout (cKO) of NHE9, JM8A3.N1 embryonic stem (ES) cells (derived from C57Bl/6) were transfected with the targeting vector described in Figure S1A, selected in G418 and screened by long-range PCR for homologous recombination at a single NHE9 allele (Knockout Mouse Project). To generate chimeras, the appropriately targeted ES cells were then injected into C57Bl/6 recipient blastocysts (University of California at Davis Mouse Biology Program). The resulting chimeras were bred to C57BL/6 mice to produce heterozygotes, and the heterozygotes bred to mice expressing FLPe under the control of the beta-actin promoter (Tg(ACTFLPe)9205Dym) to remove the lacZ reporter and selectable marker (Rodriguez et al., 2000). To inactivate NHE9 in the nervous system, inbred mice homozygous for loxP sites flanking exon 5 (fl/fl) were crossed with heterozygous (fl/+) mice expressing cre under the control of the nestin promoter (Tg(Nes-cre)1Kln) (Tronche et al., 1999). Since nestin-cre inactivates NHE9 at low frequency in gametes, we also used these animals to produce unconditional heterozygotes (fl/- without cre) as well as cKO animals (fl/-; cre/+). We also used mice fully recombined at the NHE9 locus (-/-) for hippocampal primary culture as well as acute hippocampal slice recording. It is important to note that the ES cells and all subsequent mice used to mate with the NHE9 KO animals were on a C57Bl/6 background, eliminating the requirement for back-crossing.

Genotyping was performed by PCR using the primers indicated (all from 5' to 3'). For wild type NHE9, we used the 5' homology arm primer Slc9a9-F: GGCCAGACTTTGGTTGGTCATTCC, and a primer from the sequences deleted by homologous recombination (WT-R only): GGCTATGTACCATGCATATCCTTTTGG. To detect the original insertion event, we used a primer through the most 3' loxP site (CSD-loxP-F): GAGATGGCGCAACGCAATTAATG and the 3' homology arm primer Slc9a9-R: ACCCCGATTCTGATTAAGCCTCTAGC. To detect the presence of the lacZ reporter, we used the primer pair LacZ-F: GTGCGGATTGAAAATGGTCT and LacZ-R: TATTGGCTTCATCCACCACA. To detect the neomycin-resistance marker, we used the primer pair NEO-F: GCCATCACGAGATTTCGATT and Slc9a9 Exon 5-R: GCACCATGGCTTTCACAAA. To detect the nestin-cre transgene, we used the primer pair Nestin CRE-F: AATGCTTCTGTCCGTTTGC and Nestin CRE-R: TAGCGCCGTAAATCAATCG. To detect deletion of exon 5, we used a combination of Slc9a9-F with either Slc9a9-R or Slc9a9 Exon 5-R

To confirm targeting of the conditional allele, mouse tail DNA was subjected to Southern analysis. Briefly, genomic DNA was digested with restriction enzymes Spe I and/or Sbf I, which cut the Slc9a9 locus upstream of the 5' homology arm and downstream of the 3' homology arms respectively. The DNA was blotted onto Zeta-probe GT (Bio-rad) cationized mylon membranese and hybridized with sequences outside the homology arms that were amplified by PCR and labelled using Rediprime (Amersham).

NHE9 mRNA expression

At each time point, the brains of 3 C57Bl/6 mice were rapidly frozen in liquid nitrogen and total RNA extracted using Trizol reagent. Purified RNA (1 μg) was converted into cDNA with oligodT primers, and the primers used were tested for efficiency using a ten-fold dilution of cDNA. To amplify Slc9a9 sequences by PCR, we used the following primers: exon 5-6 forward primer (TTGTGAAAGCCATGGTGCAT) and reverse primer

(GACTATGGCCACCGCATCAT); ACT forward (CGTCGACAACGGCTCCGGCA) and reverse primers (CCCATTCCCACCATCACACCCTGGT). qRT-PCR was performed in triplicate using SYBRgreen and the mean fluorescence used to calculate the delta-delta cycle threshold (CT) fold change for each transcript (Schmittgen and Livak, 2008).

Behavioral assays

Mice. The subject mice used for all of the behavioral tests on adults were 3-12 month old male cKO (fl/-;cre/+) and HET (fl/-) mice with WT (fl/fl) littermates as controls. Mice were housed with enrichment, in the same cohort of 4-5 animals/cage for the entire testing period. C57Bl/6 males 4-8 weeks old were used as control novel mice. Before and after each test, all equipment was cleaned thoroughly with soap and water, and then with ethanol. Unless otherwise stated, all experiments were performed during the light cycle from 9 am-6 pm, and at the same time frame for each experiment. Only one test/animal was performed each day. All behavioral studies were performed and analyzed blind to genotype. All experiments with animals were performed according to the National Institutes of Health Guide for Care and Use of Laboratory Animals and were approved by the University of California San Francisco Institutional Animal Care and Use Committee.

Open field. Open field activity was assessed as previously described (McFarlane et al., 2008; Martin et al., 2010; Spencer et al., 2011; Sadakata et al., 2012). Mice were habituated to the testing room for 30 minutes, then habituated to the chamber for 30 minutes before testing. The chamber was a clean plexiglass rat cage (44 x 20 x 30 cm) with opaque sides. Video was recorded for 30 min of open field exploration. At the end of the trial, a wire cup was placed in the center of the cage for the novel object exploration, and video was recorded for an additional 30 minutes. Automated video analysis was performed with Ethiovision XT tracking software (Noldus Technology) by setting the arena space (44 x 20 x 30 cm), the center space (14 x 12 cm centered), tracking the mouse, and recording the total distance moved and total time spent in each arena. All data are presented as mean ± s.e.m. and analyzed by one-way ANOVA with Bonferroni post-hoc comparison.

Elevated plus maze. Mice were habituated to the test room for 60 minutes and the test performed essentially as described (Han et al., 2012). The maze platform was elevated 50 cm off the ground. Comprised of two closed arms (10 x 50 cm), it was surrounded by 40 cm high non-transparent walls and two open arms (10 x 50 cm). During the 5 minute trial, times spent in closed, center, and open arms, and as well as total number of entries/quadrant were tallied in real time by investigator blind to genotype. All data are presented as mean ± s.e.m. and analyzed by 2-way ANOVA.

Rotarod. Mice were habituated to the test room for 30 minutes and placed walking forward in their respective lane on the rotarod with the machine rotating at 4 rpm. With all animals on the rotarod, acceleration increased at a steady rate from 4 to 40 rpm over 300 seconds. The latency to fall off was recorded for each animal. The trial was repeated three times, with 15 minute ITIs. All data are presented as mean ± s.e.m. and analyzed by 2-way ANOVA.

Juvenile play. Juvenile play was assessed as previously described (McFarlane et al., 2008). Briefly, three week old mice were habituated to the testing environment one day before the test for one hour in standard individual mouse cages with food and water. Every animal was weighed so that play pairs could be weight matched, and half the animals received a mark on their tails with a silver sharpie so that the individuals in a pair could be distinguished more easily during analysis. On the day of testing, mice were habituated to the room for one hour and then to

the test cage (standard clean mouse cage) for 10 minutes. Paired mice not housed together (novel mice) were allowed to interact for 30 minutes while videotaped. The behaviors scored included investigative (sniffing or following the other mouse), affiliative (allogrooming, close physical contact), play soliciting (crawling over/under, touching while pushing past, lodging under) (McFarlane et al., 2008). For each animal, the time spent engaged in specific activities was scored by experimenter blind to genotype for the entire 30 minute recording. Data are presented as mean ± s.e.m. and analyzed using one-way ANOVA with Bonferroni post-hoc comparison.

Three chamber test for sociability. The three chamber test was performed as previously described (Silverman et al., 2010; Yang et al., 2011). Male C57Bl/6 mice housed separately from the subject animals were habituated to the testing room for one hour, then placed under a wire cup for 30 minutes before use as novel test animals. The chamber used for testing was constructed of clear plexiglass with overall dimensions and left/center/right chamber dimensions as previously described, but with no automated doors or infrared beams to detect movement. This chamber was encased in a larger opaque plastic box with a hole at the top for a video camera. Subject mice were habituated to the testing room for one hour, then placed into the center chamber with both doors closed for 5 minutes. The doors were then opened, and the mice were allowed to explore all three chambers for ten minutes. Analysis of the time spent in each chamber during this phase enabled us to conclude that there was no chamber bias (data not shown). Next, an upside-down novel wire cup was placed in one chamber, a wire cup enclosing a novel mouse in the other chamber, and the subject mouse was allowed to explore all three chambers for ten minutes while recorded. For the final ten minutes of recording, the empty wire cup was replaced with a different wire cup enclosing a new novel test mouse and this phase recorded for an additional ten minutes. Movement, time spent per chamber and time spent investigating the wire cups was automatically measured using Ethiovision XT tracking software (Noldus Technology). All data are presented as mean ± s.e.m. and analyzed by two-way ANOVA with Bonferroni post-hoc comparison.

Social recognition. The social recognition test was performed as previously described (Hitti and Siegelbaum, 2014). Briefly, subject and novel test C57Bl/6 mice were habituated to the testing room for 60 minutes. The subject mouse was then habituated to the test chamber (a clean standard mouse cage) for 5 minutes before adding the novel test mouse (M1) for 5 minutes. After an additional 60 minutes, M1 was reintroduced for five minutes, and at 120 minutes, a new novel mouse (M2) was added for five minutes. Total time spent by the subject mouse investigating (sniffing, allogrooming, following within 2 cm) the novel mice was determined in real time blind to genotype. Results are expressed as mean ± s.e.m. and analyzed by one-way ANOVA with Bonferroni post-hoc comparison.

Tube test. Mice were habituated to the testing room for one hour before the trial and the tube test performed as previously described (Moretti et al., 2005; Spencer et al., 2011). A clear acrylic tube 30 cm in length with an inner diameter of 3.5 cm and glued to 0.5" square plastic feet was placed in the center of the testing space. Clean standard mouse cages housing each animal were positioned 5" away from each end of the tube. The two mice were picked up simultaneously and inserted into the ends of the tube. Matches were allowed to continue for five minutes or until one animal backed out of the tube with all four feet out. A loser was defined as the animal who backed out. A tie was recorded if no mouse backed out within five minutes. Scoring for analysis was 1.0 Win, 0.0 Lose, 0.5 Tie. The average score per genotype was determined to be statistically significant in a one sample t-test with theoretical mean of 0.5, indicating 50% wins/50% losses.

Marble burying. Mice were habituated to the testing room for 60 minutes before the actual test, which was performed as previously described (Thomas et al., 2009; Silverman et al., 2010). The test cage was a standard mouse cage containing 4.5 cm sani-chip bedding with 20 marbles (blue, glass, 1.5 cm diameter) placed in a regular array (4x5) across the top of the bedding. Subject mice were placed in the test cage and left for 30 minutes. The animals were removed at the end of this time and the total number of marbles buried at least 2/3 in the bedding recorded for each cage. Average marbles buried per genotype were statistically compared by one-way ANOVA.

Olfactory response, habituation and dishabituation. Mice were habituated to the testing room for 30 minutes before testing and the test performed as previously described (Silverman et al., 2010). The test cage was a standard mouse cage with a small hole in the lid for a scent applicator. Cotton tip applicators were soaked in odorants in this order: water, almond extract (frontier 1:100), banana extract (frontier 1:100), or swiped across the bottom of a dirty cage (unchanged for a week) from novel males or novel females (both C57Bl/6). The test mouse was habituated to the test cage for 2 minutes with an untreated cotton swab suspended from the lid. Odorant swabs were then individually presented through the lid for 2 minutes each, then removed for an inter-trial interval (ITI) of one minute and returned for 2 additional exposures. The cumulative time spent sniffing the cotton swab was recorded per exposure. Data are presented as mean ± s.e.m. and analyzed by two-way ANOVA with Bonferroni post-hoc comparison.

Buried cookie. As previously described (Yang and Crawley, 2009), mice were habituated to novel food (one ~1.5 g teddy graham cookie per mouse per day) for three days before testing. The evening before the test, all food was removed from the home cage. The next morning, mice were habituated to the test room for 60 minutes. A single cookie was hidden in a cage buried under 3 cm sani-chip bedding. Mice were habituated to sani-chip bedding in a separate cage for 5 minutes before entering the test cage. Once in the test cage with the hidden cookie, the time required to find the buried cookie was recorded. The average delay was calculated per genotype and the results analyzed by one-way ANOVA.

Adult stereotypies. Stereotypies were assessed as previously described (Kelley, 2001; Silverman et al., 2010). Briefly, mice were habituated to the testing room 60 minutes before the test and to the test cage (standard clean mouse cage) for ten minutes before video recording. Behavior was taped for 30 minutes, then scored offline for total time spent engaged in sniffing, self-grooming, biting/gnawing at the cage, handling/gnawing pellet bedding, circling, roof climbing, rearing and sleeping. For each animal, the time spent engaged in specific activities were scored by experimenter blind to genotype for the entire 30 minute recording. Data are presented as mean ± s.e.m. and analyzed by one-way ANOVA with Bonferroni post-hoc comparison.

Neuronal culture

Hippocampal neurons were isolated from newborn mouse pups following guidelines approved by the UCSF IACUC. Hippocampi were digested for 20 minutes in Hanks buffered saline + 0.36% glucose (HBS+) containing 0.00025% trypsin, washed three times with HBS+ and triturated thirty times in 2.25 ml MEM containing 21 mM glucose, 5% FBS, 2% B27 and 1x Glutamax (Serum Neuronal Media, SNM). Coverslips pretreated with L-polylysine (PLL) were rinsed in water and dried before plating neurons. For live cell imaging experiments, neurons in SNM were plated into 10 mm cloning rings secured onto 25 mm coverslips at a density of 30-

35,000/79mm^2. For immunofluorescence, neurons were plated onto 12 mm coverslips at a density of 45,000/113 mm^2. For biochemical experiments, neurons were plated directly onto PLL-coated wells of a 12-well plate at a density of 150,000/380mm^2. The next day, 50% of the SNM media was removed and 3 volumes Neurobasal Media (NBM) DIV1 (NBM with 2% B27, 1.3X Glutamax) was added. At 7 days *in vitro* (DIV7), 50% of the media was removed and one volume NBM DIV7 (1 part SNM: 3 part NBM DIV1, 4 μM AraC) added. Neurons were transfected using calcium phosphate at DIV6, resulting in transfection efficiencies ~15%. For biochemical experiments, neurons were infected with lentiviral supernatant at DIV7 resulting in 100% transduction efficiency. For the ss-flag-DOR lysosomal degradation assay, DOR agonist DADLE was applied at a final concentration of 10 μM directly into culture media for the times indicated.

Immunofluorescence

Cultured neurons were fixed at DIV14 in phosphate-buffered saline (PBS) containing 2% paraformaldehyde for 30 minutes at 27° C. The cells were then washed three times for 5 minutes each in PBS, and permeabilized/blocked for 60 minutes at 27° C in PBS, 0.01% Saponin, 2%NGS. Primary antibody incubation was performed in the same buffer for 60 minutes, followed by washing, then secondary incubation for 60 minutes in the same buffer. Coverslips were mounted with fluoromount. Images were acquired using a Zeiss LSM 510 confocal scanning microscope. Antibody source and titer used for immunostaining: TfR (Invitrogen, 1:500), VAMP2 (Synaptic Systems, 1:2000), VGLUT1 (Chemicon, 1:5000), VGAT (Synaptic Systems, 1:1000), GluR2 (Millipore, 1:1000), LAMP1 (Developmental Studies Hybridoma Bank, 1:400), NHE6 (gift of J. Orlowski, adsorbed), GFAP (Zymed, 1:1000). Cy3, Cy5- conjugated secondary antibodies (Jackson Immuno Research) and Alexa 488, 555 or 649-conjugated secondary antibodies (Invitrogen) were used at a dilution of 1:1000.

Live Neuron Imaging

pH. Cultured neurons were imaged at DIV 12–14 to measure both vesicular and cytosolic pH. For vesicular measurements, pHluorin fusions to transferrin receptor (TfR) and vesicle-associated membrane protein 2 (VAMP2) were respectively used as post- and presynaptic vesicle reporters because both have high plasma membrane as well as total expression, enabling calibration to the surface protein. pHluorin was imaged using 470/40 nm excitation and 525/50 nm emission filters. Glutamate receptor antagonists 6-cyano-7 nitroquinoxaline-2,3-dione (CNQX, 10 μM) and D,L-2-amino- 5-phosphonovaleric acid (APV, 50 μM) were included in the external solution for all imaging experiments. Lumenal pH (pHi) was measured as previously described (Mitchell and Ryan, 2004) assuming a pKa for pHluorin ~7.1. Total pHluorin emission is a combination of surface and intravesicular fluorescence. Baseline fluorescence was obtained as an average of 5 frames collected at 0.2 Hz in Tyrode's solution (mM: 100 NaCl, 2.5 KCl, 2 $CaCl_2$, 2 $MgCl_2$, 10 glucose and 25 HEPES, pH 7.4). To determine the fraction quenched at low pH, we imaged the neurons during fast perfusion with Tyrode's solution, pH 5.5 [mM: 100 NaCl, 2.5 KCl, 2 $MgCl_2$, 2 $CaCl_2$, 10 glucose, 25 MES, pH 5.5], cellecting 5 frames at 0.2 Hz and using the lowest fluorescence values for the pH 5.5 calculuations. During the same image acquisition period, intracellular compartments were alkalinized by fast perfusion with Tyrode's solution, pH 7.4 with 50 mM NH_4Cl [mM: 50 NaCl, 2.5 KCl, 2 $MgCl_2$, 2 $CaCl_2$, 50 NH_4Cl, 10 glucose, 25 HEPES, pH 7.4], thus revealing the lumenal pHluorin quenched by low pH. In principle, pHi was calculated as f(pHi) = (average

baseline fluorescence – average pH 5.5 fluorescence)/peak fluorescence NH_4Cl, and more precisely according to:

$$f(pHi) = \frac{\epsilon}{(1 - \phi(pHi) + \propto (pHi)(1 - \epsilon)}$$

where

$$\epsilon = (F_0 - F_{pH5.5})/F_0$$
$$\phi(pHi) = \frac{1/(1 + 10^{pK-5.5})}{1/(1 + 10^{pK-5.5})}$$
$$\alpha(pHi) = \frac{\Delta[X]}{[X]_0} = \frac{(1/(1 + 10^{pK-7.4}) - 1/(1 + 10^{pK-pHi})}{1/(1 + 10^{pK-pHi})}$$

Regions of interest (ROIs) of 10 x 10 pixels were selected for the TfR and 5 x 5 pixels for VAMP2. Background was determined by averaging 10 representative background regions of interest (ROIs) of similar size without cells and the subtracted from each experimental ROI of similar size imaged. A minimum of 25 puncta per neuron from 3-5 neurons per coverslip were analyzed.

To measure cytosolic pH, cultured neurons were incubated with 1 μM BCECF-AM for 15 minutes in Tyrode's solution, pH 7.4. Images of the soma and processes were acquired with 436/10 and 495/10 nm excitation and 530/35 nm emission filters. After imaging steady-state cytosolic pH, neurons were perfused with calibration solution (containing in mM: 100 KCl, 20 NaCl, 2.5 MgCl2, 25 HEPES (pH 8, 7.5, 7) or MES (pH 6.5, 6, 5.5) and 50 μM nigericin. The ratio of fluorescence produced at the two excitation wavelengths for each pH was then used to produce a calibration curve. This curve was then used to calculate the pH for each ROI imaged, and the difference between averages for each genotype assessed for significance using the Student's t-test.

VGLUT1-pHluorin. To image the cycling of synaptic vesicles, cultured neurons were imaged at DIV14–17 as previously described (Voglmaier et al., 2006; Nemani et al., 2010; Hua et al., 2011). VGLUT1-pHluorin with a C-terminal cytosolic mCherry tag was imaged with 470/40 nm excitation and 525/50 nm emission filters for the pHluorin, and with 572/30 nm excitation and 632/60 nm emission filters for mCherry. mCherry images were collected once each at the start and end of acquisition, and used to identify transfected boutons in DIV14 neurons. pHluorin images were acquired at 0.5 Hz, and the fluorescence normalized to total intracellular fluorescence (in NH_4Cl) after subtracting the initial fluorescence, or $F_{NH4Cl} - F_{initial.}$. Background fluorescence was determined by translating 5 x 5 pixel ROIs 10 pixels over into an area of representative adjacent background, and subtracted from the fluorescence of each puncta in each frame. Endocytosis kinetics at the end of 10 Hz stimulation were determined by fitting the data to single-exponential decay using PRISM (Graphpad). To calculate exocytosis rate and total recycling pool size, DIV14 neurons were stimulated at 10 Hz for 150 s in 600 nM Bafilomycin. The average initial rate of exocytosis was determined for each neuron, and the average for each genotype compared using the Student's t-test. Recycling pool size was determined as the plateau reached during stimulation as a fraction of F_{NH4Cl}, averaged for each genotype and the effect of genotype compared using the Student's t-test. Imaging DIV17 neurons at 1 Hz, the readily releasable pool size was measured as the peak response to 40 action

potentials delivered at 20 Hz for 2 s, and the mean for each genotype compared by Student's t-test. Calcium sensitivity was similarly determined using DIV17 neurons imaged at 1 Hz, and the VGLUT1-pHluorin peak response to stimulation normalized as described above. The experimental protocol involved stimulating the same coverslip 3 times each at 10 Hz for 30 seconds with 10 minute interval between stimuli, first with 2 mM, then 1 mM and finally 4 mM Ca^{++}, followed by NH_4Cl.

FM dye. FM2-10 (50 μM) was loaded into synaptic vesicles of DIV 14 hippocampal neurons by stimulating at 10 Hz for 120 s in culture media since it contains physiological bicarbonate buffer and only 10 mM HEPES. Bafilomycin (600 nM) was loaded simultaneously with FM2-10, followed by a rapid rinse with Tyrode's solution, then Advasep (1 mM) in culture media for 2 minutes and finally constant perfusion in Tyrode's solution for 10 minutes before unloading FM2-10 by stimulating at 10Hz for 150s. Images were acquired at 1 Hz using 470/40 nm excitation and 525/50 nm emission filters. The time constant (tau) for destaining was calculated by nonlinear curve fitting of a plateau with one-phase decay using PRISM. The mean taus per genotype per experimental condition were compared by 2-way ANOVA and Bonferroni post-hoc.

Biochemistry

Hippocampus. After euthanasia, the hippocampi were dissected rapidly in cold Hepes-buffered saline (HBS), flash frozen in liquid nitrogen and stored on dry ice until homogenization. The hippocampi were disrupted in 300 μl buffer containing 150 mM NaCl, 50 mM Tris, pH 7.5, 1 mM EGTA, 1% Triton-X 100, 0.5 % Na-deoxycholate and 1x Roche protease inhibitor cocktail using a Dounce homogenizer by hand for 60 seconds and by rotation at 4° C for 30 minutes. The homogenate was then sedimented at 1000 *g* for 10 minutes at 4° C to sediment large debris. The supernatant was then transferred to a new tube, total protein concentration determined by BCA, equal amounts of protein added to SDS loading buffer with 100mM DTT and 5% BME. The samples were incubated at 27° C for 30 minutes before separation by electrophoresis through SDS-polyacrylamide (10-15%) and immunoblotting.

Culture. Lysates were prepared from primary dissociated culture using lysis buffer (150 mM NaCl, 50 mM Tris, pH 7.5, 1% Triton-X 100, 0.1% SDS and 1x Roche protease inhibitor cocktail) at 100 μl/well. The plates were rocked at 27° C for 5 minutes, then transferred to eppendorf tubes and solubilized by rocking at 4° C for 60 minutes. Insoluble material was sedimented at 16000 G for 10 minutes at 4°C, protein concentration determined by BCA to equalize loading and aliquots stored at -80°C until western blotting as described above.

Antibodies. We used the following antibodies at the titer indicated: VGLUT1 (Bellocchio et al., 1998) at 1:2000, VGLUT2 (Fremeau et al., 2004) at 1:1000, VGAT (Chaudhry et al., 1998) at 1:2000, SV2 (Developmental Studies Hybridoma Bank at 1:1000, P38 (Sigma) at 1:2000, SYT1 (Synaptic Systems) at 1:1000, VAMP2 (Synaptic Systems at 1:1000, Syntaxin 1 (Sigma) at 1:1000, SNAP25 (Synaptic Systems) at 1:1000, Munc18 (BD Biosciences) at 1:500, GluR2 (Millipore) at 1:1000, NR1 (BD Biosciences) at 1:1000, PSD95 (Neuromab) at 1:1000, TfR (Invitrogen) at 1:500, RAB3 (Synaptic Systems) at 1:500, RAB5 (Synaptic Systems) at 1:500, RAB7 (Sigma) at 1:500, LAMP1 (Developmental Studies Hybridoma Bank) at 1:500, VATPase H subunit (Santa Cruz) at 1:100, Na^+/K^+ pump (Abcam) at 1:1000, α -ATP synthase (Abcam) at 1:1000, GFAP (Zymed) at 1:250, CPE-c term (P. Loh) at 1:500, Actin (Millipore) at 1:1000, FLAG (Sigma) at 1:2000. IR dye-conjugated secondary antibodies (LI-COR) were used for western blotting at 1:50,000.

Quantification. Western blots were quantified using the Odyssey system (LI-COR). Briefly, tiff files of imaged gels including the proteins of interest and actin (loading control) were analyzed in ImageJ by subtracting the background for each channel, measuring average pixel intensity for each band (in a fixed area), and normalizing each sample to actin. Results are presented as mean ± s.e.m. for 4 animals/genotype. The significance of the difference was assessed by Student's t-test.

Synaptic vesicle isolation. Synaptic vesicles were purified as described before (Clift-O'Grady et al., 1990; Goh et al., 2011). Briefly, the standard buffer for glutamate uptake contained 148 mM choline or potassium gluconate, 2 or 20 mM choline or KCl, 4 mM MgATP, 10 mM HEPES-Tris, pH 7.4, 1 mM choline glutamate, and 40 μCi ml^{-1} [^{3}H]L-glutamate (Perkin Elmer). Transport was initiated by adding 100 μg LP2 protein to 200 μl reaction buffer (pre-warmed to 30° C). The reaction was incubated at 30° C for 10 min and stopped by rapid filtration and washing four times with 2 ml cold reaction buffer with no glutamate. Bound radioactivity was detected by liquid scintillation, and background transport measured in the presence of 100 μM Evans Blue subtracted. In every experiment, each condition was assayed in triplicate and at least three independent experiments were performed using at least three different synaptic vesicle preparations. Results are presented as mean ± s.e.m and the statistics analyzed by two-way ANOVA test with Bonferroni post-hoc comparison.

Electrophysiology

Acute hippocampal slices. Acute hippocampal slices (350 μm thickness) were prepared from 3-4 week KO and WT mice. Animals were deeply anesthetized by exposure to isoflurane and decapitated immediately. The brain was rapidly removed and immersed in ice-cold, aerated (95% O_2–5% CO_2) slicing solution (containing, in mM 228 sucrose, 2.5 KCl, 1 NaH_2PO_4, 7 $MgSO_4$, 0.5 $CaCl_2$, 26 $NaHCO_3$, and 11 dextrose). Vibratome (Leica VT1000S)-cut slices were transferred to artificial cerebrospinal fluid (ACSF) (containing, in mM 119 NaCl, 2.5 KCl, 1.3 $MgSO_4$, 2.5 $CaCl_2$, 26 $NaHCO_3$, 1 NaH_2PO_4, and 11 dextrose; 315 Osm; pH 7.4) at 35° C and allowed to recover for a minimum of 1 hr before recording. Hippocampal slices were visualized using an upright infrared differential interference contrast (IR-DIC) microscope (Olympus BX50WI) and perfused with standard ACSF at room temperature while recording. Electrical stimulation (100 μs) pulses were generated by Master-8 and isolator (W.P.I.), and were delivered through a bipolar metal electrode (FHC MX21AEW). For field potentials, synaptic strength was quantified as the initial slope of the evoked response using ACSF-filled microelectrodes (1 to 2 MΩ). For whole cell recording of evoked EPSCs and miniature EPSPs, the pipette solution contained (in mM) 136 $CsMeSO_4$, 7 CsCl, 0.25 EGTA, 10 HEPES, 2 MgATP, 0.3 Na_2GTP, 8 NaCl, 0.1 Spermine and 7 Phosphocreatine. QX-314 (5 mM) was added to the internal solution to block sodium channels. For miniature IPSC recording, CsCl in the pipette solution was increased to 75 mM to magnify the GABA response at -70 mV. Tetrodotoxin (TTX), picrotoxin (PTX), or CNQX and APV were added to the standard external solution to distinguish miniature EPSCs and IPSCs, respectively. Results are presented as mean ± s.e.m. The results were analyzed by either Student's *t*-test or two-way ANOVA.

Golgi stain

P21 mice were euthanized by CO_2, their brains dissected and immediately immersed in rapid golgi stain reagents (FD Neurotech), following the manufacturer's instructions. Briefly, the brains were incubated in solution A/B for 3 weeks, cryoprotected in solution C 48 hours, flash

frozen in isopentane and stored at -80° C. Sections (100 μm) were cut with a cryostat (Leica CM3050S), mounted onto slides coated with 3% gelatin, air dried for 24 hours, stained, dehydrated following the manufacturer's instructions, and mounted using Permount. Single plane images of spine segments in CA1 were collected 60-100 μm from the soma using a Leica DMRB microscope with Leica PL FLUOTAR 100X/1.30 DIL oil objective. The images were used only if >25 spines remained in focus per segment. Image acquisition and analysis were performed by different experimenters, with analysis blind to genotype. The results are presented as mean ± s.e.m. The data were analyzed by two-way ANOVA with Bonferroni post-hoc comparison.

2.4 Results

To produce a conditional knockout (cKO) of NHE9, we used homologous recombination in embryonic stem cells to introduce loxP sites surrounding exon 5 of the gene. Exon 5 encodes sections of transmembrane domains (TMD) 4 and 5, and the frameshift that results from its deletion places a stop codon in-frame immediately downstream (Figures 2.1A, 2.S1A). We inactivated NHE9 specifically in the nervous system using the nestin-cre transgene that expresses cre recombinase in all neurons and glia (Knoepfler et al., 2002).

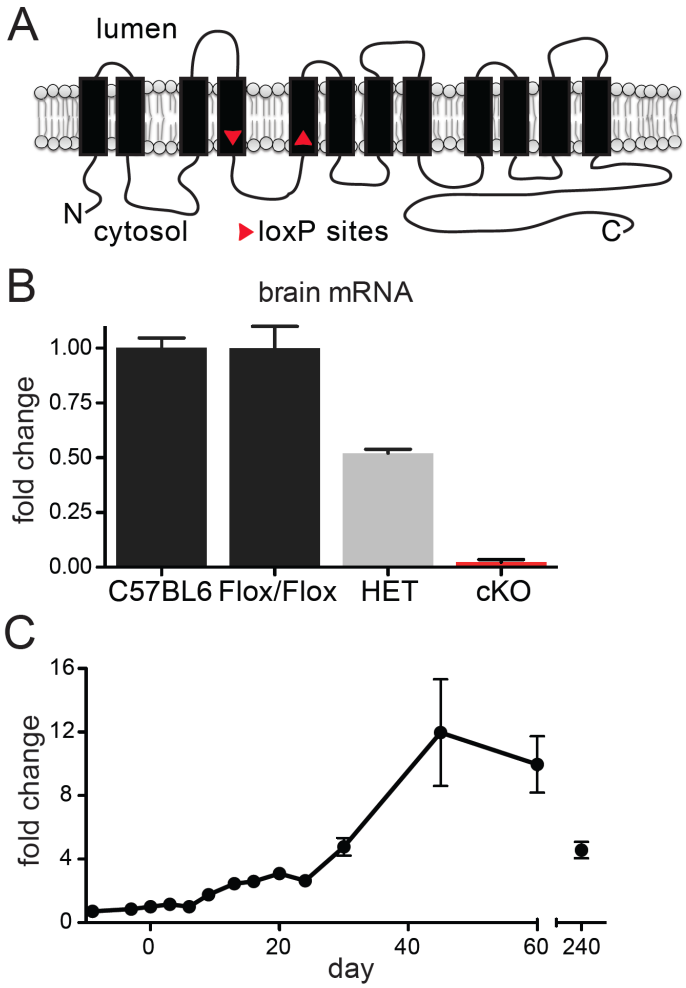

Figure 2.1. Conditional Knockout and Developmental Time Course of NHE9
(A) NHE9 contains 12 predicted transmembrane domains (TMDs) and two loxP sites (red arrowheads) were inserted into TMD4 and 5.
(B) Quantitative RT-PCR demonstrates the reduction and loss of NHE9 mRNA in brain mRNA from, respectively, heterozygous and conditional knock-out (cKO) animals relative to WT animals and those with unrecombined alleles (Flox/Flox). Bars indicate the mean and error bars s.e.m. n=2-4 animals/genotype
(C) Quantitative RT-PCR indicates the time course of NHE9 expression in the brain from the embryo to adulthood in wild type C57Bl/6 mice. The graph shows mean ± s.e.m. n=3 mice/day

To determine whether the cKO eliminates expression of NHE9, we first attempted to use several available antibodies. Although these antibodies recognize the mouse protein expressed in

heterologous cells, they fail to detect a signal in brain extracts from wild type (WT) mice that is not also present in the NHE9 cKO (Figure 2.S1C). The levels of endogenous NHE9 thus appear too low to be detected using these antibodies. For this reason, we used PCR to quantify the mRNA transcripts encoding NHE9. Figure 1B shows that in the brain, NHE9 mRNA is reduced ~50% in the heterozygote and eliminated in the cKO.

NHE9 cKO animals are born in expected mendelian ratios and show normal survival, with several living up to 3 years (data not shown). They do show a small but significant reduction in body weight as early as 30 days after birth that persists to at least 4 months (Figure 2.S2A). However, the brain shows no reduction in weight. The phenotype thus appears considerably milder than that observed for loss of NHE6 (Stromme et al., 2011; Ouyang et al., 2013).

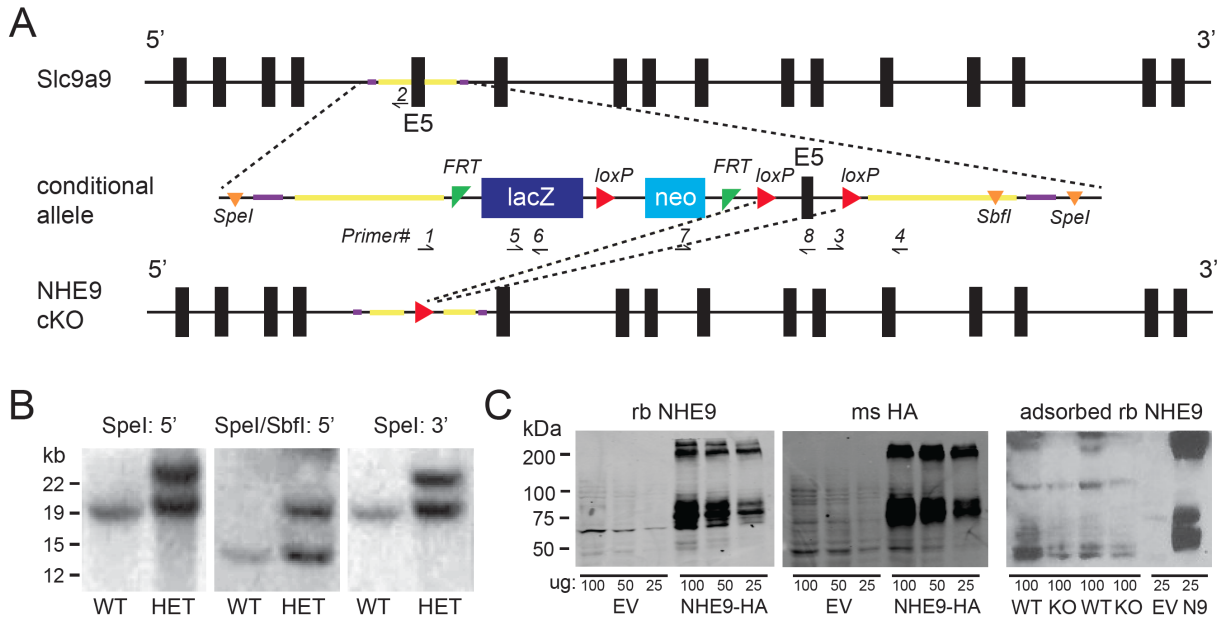

Figure 2.S1. Conditional Inactivation of NHE9

(A) Organization of the Slc9a9 gene locus in *Mus musculus*, with exon 5 (E5) indicated and the homology arms used for recombination shown in yellow (top). The middle panel shows the predicted conditional allele after homologous recombination, with SpeI and SbfI restriction sites (orange arrowheads), lacZ and neomycin-resistance genes indicated. The probes used for Southern analysis are indicated in purple, the FRT sites in green and the loxP sites in red. The numbers indicate the position of 8 primers used for genotyping. The bottom panel shows the final recombined state of the allele after recombination by both FlpE and cre recombinase.

(B) Southern blot of DNA from WT and heterozygous mice using probes outside the 5' and 3' homology arms confirms homologous recombination of one allele.

(C) Affinity purified antibodies specific to mouse NHE9 do not detect endogenous NHE9 protein. Left, rabbit anti-NHE9 antibody (a generous gift from J. Orlowski, McGill) specifically detects mouse NHE9-HA overexpressed in HEK cells with cell extract loaded at 25-100 μg protein per lane. Middle panel shows an immunoblot of the same samples probes with HA antibody, confirming the identity of the protein identified as NHE9. Since western blotting revealed no specific bands in WT relative to KO brains (data not shown), we adsorbed the NHE9 antibody with an acetone extract made from the brains of NHE9 KO mice. Right panel, adsorption

improved the signal in cells transfected with NHE9-HA relative to empty vector, but still do not identify any proteins specific to the WT. We similarly adsorbed several commercial antibodies as well as those generated in other labs, all of which could detect NHE9-HA over-expressed in HEK cells, but did not find any capable of detecting a protein in the WT that was not also present in the KO (data not shown). We also tried to enrich for NHE9 by separating brain membranes by differential centrifugation and density gradient fractionation, but again observed no specific bands. Immunofluorescence similarly failed to identify a signal in the WT that was not also present in the KO (data not shown).

NHE9 cKO Mice Display Behavioral Features of ASD

NHE9 cKO mice show no gross defects in motor behavior as assessed by performance on the accelerating rotarod (Figure 2.S2C) or by distance travelled and time spent exploring in the open field and novel object tests (Figure 2.S2D). In addition, they do not differ from heterozygous or WT littermates in the elevated plus maze, a measure of anxiety (Figure 2.S2E). Although a subset of patients with ASD due to mutations in NHE9 have seizures (Morrow et al., 2008), we observed only a single generalized tonic-clonic seizure in one animal out of hundreds studied.

In contrast to the normal behavior displayed by the NHE9 cKO mice in these assays, they exhibit several core features characteristic of ASD. First, NHE9 cKO mice exhibit deficits in social interaction. As juveniles, they show considerably reduced play soliciting, such as crawling under and over other mice (Figure 2.2A). They also spend less time engaged in affiliative behavior (e.g., allogrooming, huddling) and investigative behavior (e.g., sniffing, following)(Figure 2.2A). Consistent with the ASD phenotype observed in non-consanguineous families with rare, presumably heterozygous, mutations in NHE9, heterozygous mice also show a defect in play soliciting and investigative behavior. However, the defect in affiliative behavior requires loss of both alleles.

Adult NHE9 cKO mice also show defects in specific social interactions. In the three chamber test, very similar to WT animals, they spend more time in the chamber with a novel mouse than in one with a novel object, and more time with a novel than with a familiar mouse (Figure 2.2B). NHE9 cKO mice thus exhibit normal interest in social interactions. In a test for social recognition, WT mice spend less time investigating a subject mouse upon repeat exposure, but cKO and heterozygous animals fail to habituate, suggesting that they do not recognize the subject (Figures 2.2B) (Hitti and Siegelbaum, 2014). Importantly, WT mice show no reduction in time spent investigating a novel test animal on second exposure (Figure 2.S2G), indicating that the test specifically assesses social recognition. The tube test for social dominance also shows that cKO mice consistently lose in confrontation with a WT (or HET) animal (Figure 2.2B). In addition to the defect in social recognition, NHE9 cKO mice thus exhibit a highly penetrant submissive phenotype.

Second, we investigated NHE9 cKO mice for repetitive and stereotyped behavior characteristic of ASD. cKO animals bury more marbles than WT or heterozygous mice (Figure 2.2C), indicating an increase in repetitive digging behavior (Thomas et al., 2009). They also spend more time than WT climbing, but less time manipulating pellets, rearing and grooming (Figure 2.S2H). Similar to the selective defects in social interaction, the impairment thus affects some repetitive behaviors but not others.

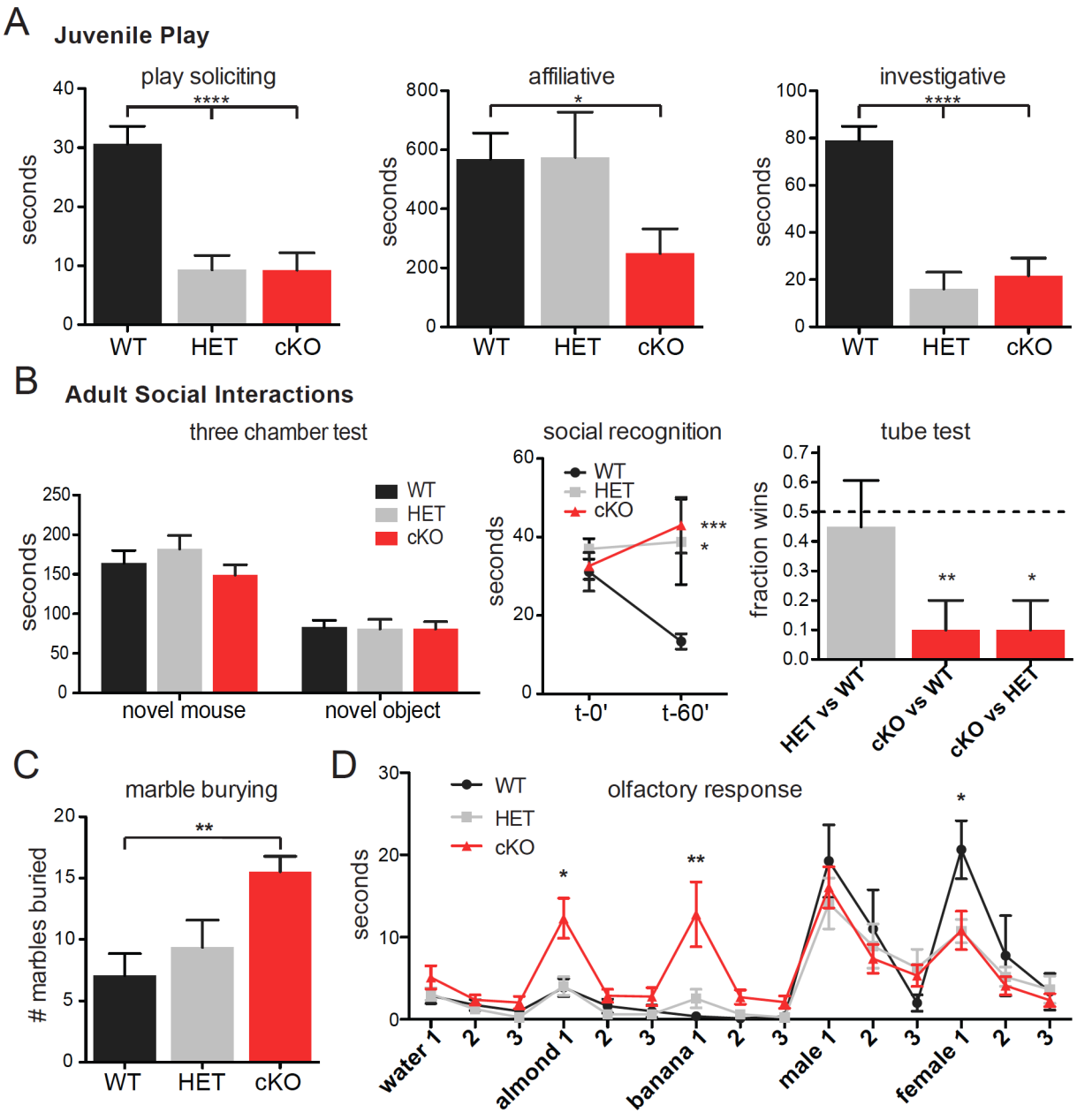

Figure 2.2. The NHE9 cKO Exhibits Behavioral Features Characteristic of ASD

(A) Postnatal day 21 (P21) mice were videotaped for 30 minutes and the amount of time soliciting play, in affiliative and investigative behavior was scored. ****, $p<0.0001$ by one-way ANOVA with Bonferroni multiple comparison. *, $p=0.016$ by two-tailed Student's t-test comparing WT and cKO animals. WT, n=12; HET, n=10; cKO, n=11

(B) Adult NHE9 cKO mice show selective defects in social interaction. Left panel, the three chamber test shows no difference between cKO and WT mice in the intrinsic interest of a novel mouse or novel object although all genotypes spend more time investigating a novel mouse. WT, n=10; HET, n=10; cKO n=12 Middle panel, NHE9 HET and cKO mice display deficits in social recognition. Total time spent investigating (sniffing, close following) a novel mouse (at t-0') was compared with the time spent investigating the same mouse one hour later (t-60'). *, $p<0.05$; ***,

p<0.001. WT, n=8; HET, n=5; cKO, n=8. Right panel, tube test for social dominance shows that NHE9 cKO mice are submissive. Pairs matched by weight were placed at opposite ends of a tube and the first animal to back out designated a loser, with a score of 0 for a loss, 0.5 for a tie and 1.0 for a win. Mean performance per genotype was compared by one sample t-test with a theoretical mean of 0.5. cKO v WT (n=10), p=0.003; cKO v HET (n=5), p=0.016; WT v HET, n=10

(C) cKO mice exhibit repetitive digging behavior in the marble burying test. The number of marbles buried by each genotype was counted at the end of thirty minutes. **, p<0.01 by one-way ANOVA with Bonferroni comparison. WT, n=14; HET, n=14; cKO, n=21

(D) NHE9 cKO mice do not distinguish between social and non-social odorant cues. The olfactory habituation and dishabituation test shows that all three genotypes habituate normally to an odorant presented multiple times and dishabituate on exposure to a new odor. However, cKO mice show heightened interest in non-social cues and both cKO and HET mice show decreased interest in female scent. *, p<0.05, **, p<0.01 by one-way ANOVA with Bonferroni comparison. WT, n=8; HET, n=11; cKO n=18

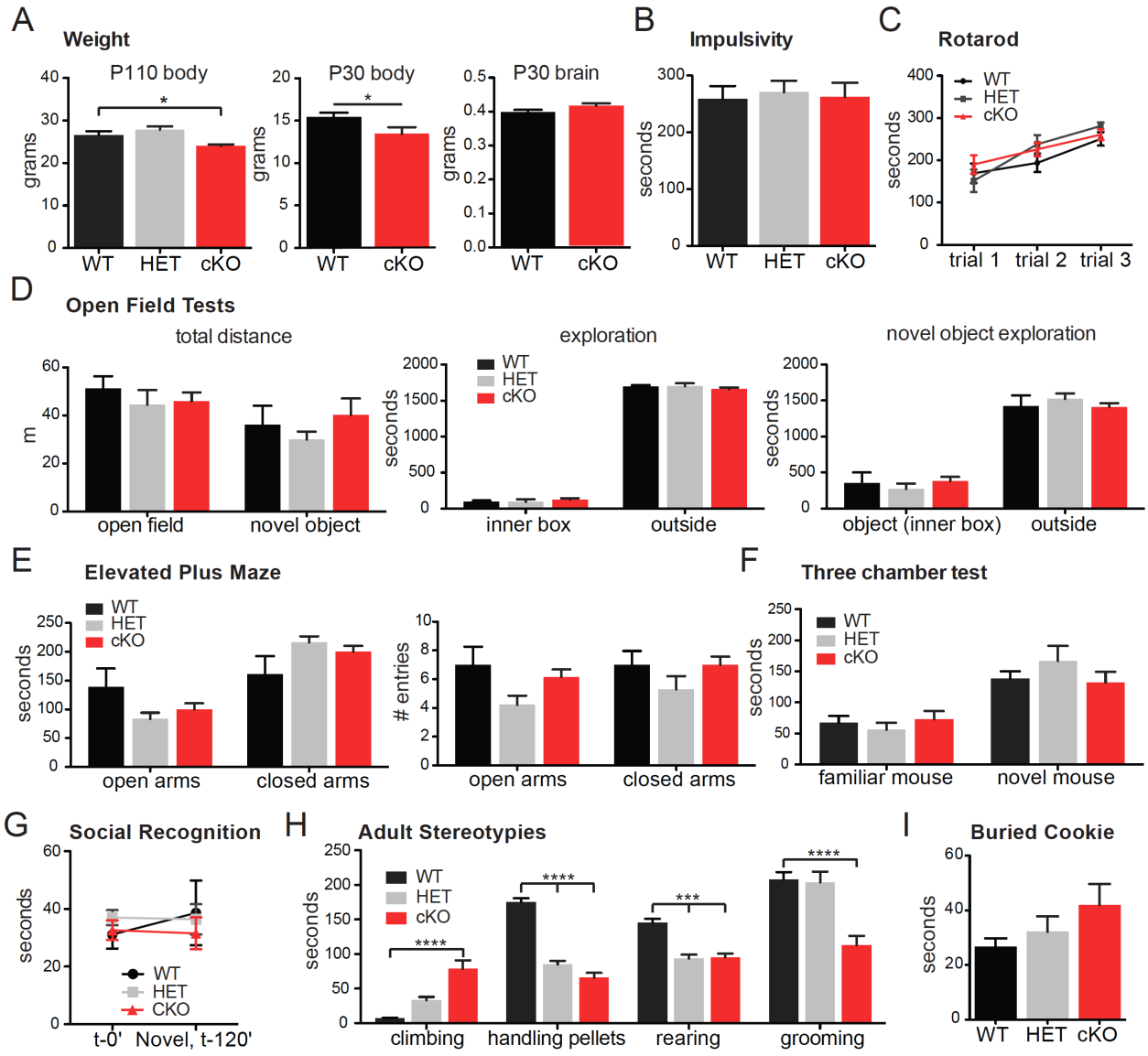

Figure 2.S2, NHE9 cKO Mice Exhibit Normal Locomotor Activity, Anxiety and Olfaction.
(A) The adult (P110) body weight of NHE9 cKO mice (n=21) is significantly less than WT (n=7) or HET animals (n=12). *, $p<0.05$ by one-way ANOVA with Bonferroni. Juvenile cKO (n=16) body weight is also less than WT (n=19) but cKO brain weight (n=16) is the same as WT (n=22). *, $p<0.05$ by Student's t-test.
(B) All genotypes showed similar, low impulsivity in the cliff test. WT, n=17; HET, n=18; cKO, n=15
(C) Performance on the rotarod over multiple trials showed no difference in baseline coordination or motor learning between the genotypes. WT, n=14; HET, n=12; cKO, n=20
(D) Open field activity levels and area exploration do not differ from WT in the HET and cKO mice. Left, the total distance explored in both the open field and open field with a novel object was determined using Ethiovision tracking software. For the same two experiments (middle and right panels), the time spent in the inner box versus outer perimeter of the arena was also determined and also found not to differ from WT. WT, n=6; HET, n=13; cKO, n=21
(E) Behavior in the elevated plus maze shows normal anxiety in the NHE9 cKO. All genotypes explored the open and closed arms for similar amounts of time (left) with similar entry numbers (right). WT, n=6; HET, n=13; cKO, n=21
(F) The three chamber test shows cKO mice show the same preference for a novel over a familiar mouse. WT, n=10; HET, n=10; cKO, n=12
(G) In the social recognition assay, all genotypes investigate a novel mouse to the same extent two hours (t-120') after exposure to another. WT, n=8; HET, n=5; cKO, n=8
(H) NHE9 cKO mice differ from WT in multiple aspects of stereotyped behavior. Mice were individually housed in a clean empty cage and recorded for thirty minutes. Over 30 minutes, activity was scored for the stereotypic behaviors indicated and the average time spent in each compared by two-way ANOVA with Bonferroni post hoc comparison. ***, $p<0.001$, ****, $p<0.0001$ WT, n=10; HET, n=11; cKO, n=10
(I) The buried cookie test shows that basic olfaction remains intact in NHE9 HET and cKO mice. WT, n=14; HET, n=16; cKO n=21 Bars indicate mean ± s.e.m.

Finally, we examined NHE9 cKO animals for defects in communication. Since rodents rely on olfactory cues to communicate, w e tested their ability to distinguish social from non-social olfactory cues. In WT mice, sequential exposure to male and female mouse odor elicits a substantially larger response than almond or banana odor (Figure 2.2D). In contrast, cKO mice respond almost equally to non-social (almond and banana) as to social (male and female) scents, although they habituate normally to each of these odors on repeat exposure. Thus, they appear to have a specific defect in olfactory discrimination. Since this might simply reflect impaired olfaction, we also tested this sensory modality by determining how long it takes the mice to find a buried cookie after fasting for 16 hours. The cKO animals do not differ significantly from WT in this test (Figure 2.S2I), suggesting that the defect in olfactory discrimination reflects a specific problem in sensory integration likely to affect communication. In summary, NHE9 cKO mice reproduce several defining behavioral features of ASD, including deficits in social interaction, repetitive behavior and impaired communication.

Although the NHE9 cKO did not show differences from WT in open field activity (Figure 2.S2D), the association of NHE9 with ADHD (Fisher et al., 2002; de Silva et al., 2003; Lasky-Su et al., 2008) led us to investigate impulsiveness. However, NHE9 cKO do not differ from WT in the time waited before jumping off a high platform (Figure 2.S2B), suggesting normal impulse control as well as locomotor activity.

The Localization of NHE9 in Neurons and Its Role in the Regulation of ΔpH

The biochemical function of NHEs in cation/H^+ exchange suggests that loss of NHE9 disturbs organellar ΔpH. To determine when and where this might occur, we characterized the pattern of NHE9 expression. Since ASD begin early in childhood, we first determined the time course of NHE9 expression, relying on quantitative PCR to detect mRNA transcripts due to the low level of endogenous protein. Figure 1C indeed shows very low levels of brain NHE9 mRNA that increase slowly for 3 weeks after birth, then rise dramatically (a total of ~12-fold) 3-6 weeks after birth. The highest levels of NHE9 thus occur after synaptogenesis, suggesting a role for the protein in function of the mature brain rather than specifically in development. The Allen Brain Atlas further shows that in the adult, expression of NHE9 appears restricted to the olfactory bulb, superficial cortex and hippocampus (Lein et al., 2007). Since the animals exhibit a defect in social recognition, and social recognition depends on hippocampal function (Hitti and Siegelbaum, 2014), we have focused on the hippocampus.

Previous work in non-neuronal cells has suggested localization of NHE9 as well as NHE6 to endosomes (Nakamura et al., 2005; Kondapalli et al., 2013; Kondapalli et al., 2015). Since analysis of the KO showed that none of the available antibodies recognized endogenous NHE9 in the brain (Figure 2.S1C), we transfected an epitope-tagged construct into dissociated hippocampal neurons isolated from NHE9 KO mice. Although transfection presumably results in over-expression of the transporter, the absence of endogenous NHE9 should minimize the potential for mislocalization. To distinguish presynaptic from postsynaptic processes, we also used sparse cotransfection with the green fluorescent protein (GFP). Figure 3 shows that in GFP^+ processes, the epitope-tagged protein colocalizes extensively with transferrin receptor (TfR), indicating expression in dendritic endosomes. Dendritic NHE9-HA does not colocalize with the glutamate receptor subunit GluA2, indicating exclusion of even the over-expressed NHE9 from postsynaptic sites (Figure 2.S3). The tagged NHE9 also appears in axons, where it colocalizes with the synaptic vesicle proteins vesicle-associated membrane protein 2 (VAMP2), vesicular glutamate transporter 1 (VGLUT1) and the vesicular GABA transporter (Figures 2.3 and 2.S3). However, NHE9-HA does not colocalize with all GFP^+ presynaptic boutons and occasionally labels punctae not expressing the synaptic vesicle proteins. Importantly, the introduced NHE9 shows only partial colocalization with endogenous NHE6, and less with the lysosomal protein LAMP1 (Figure 2.S3). In astrocytes, HA-NHE9 localizes more clearly to the

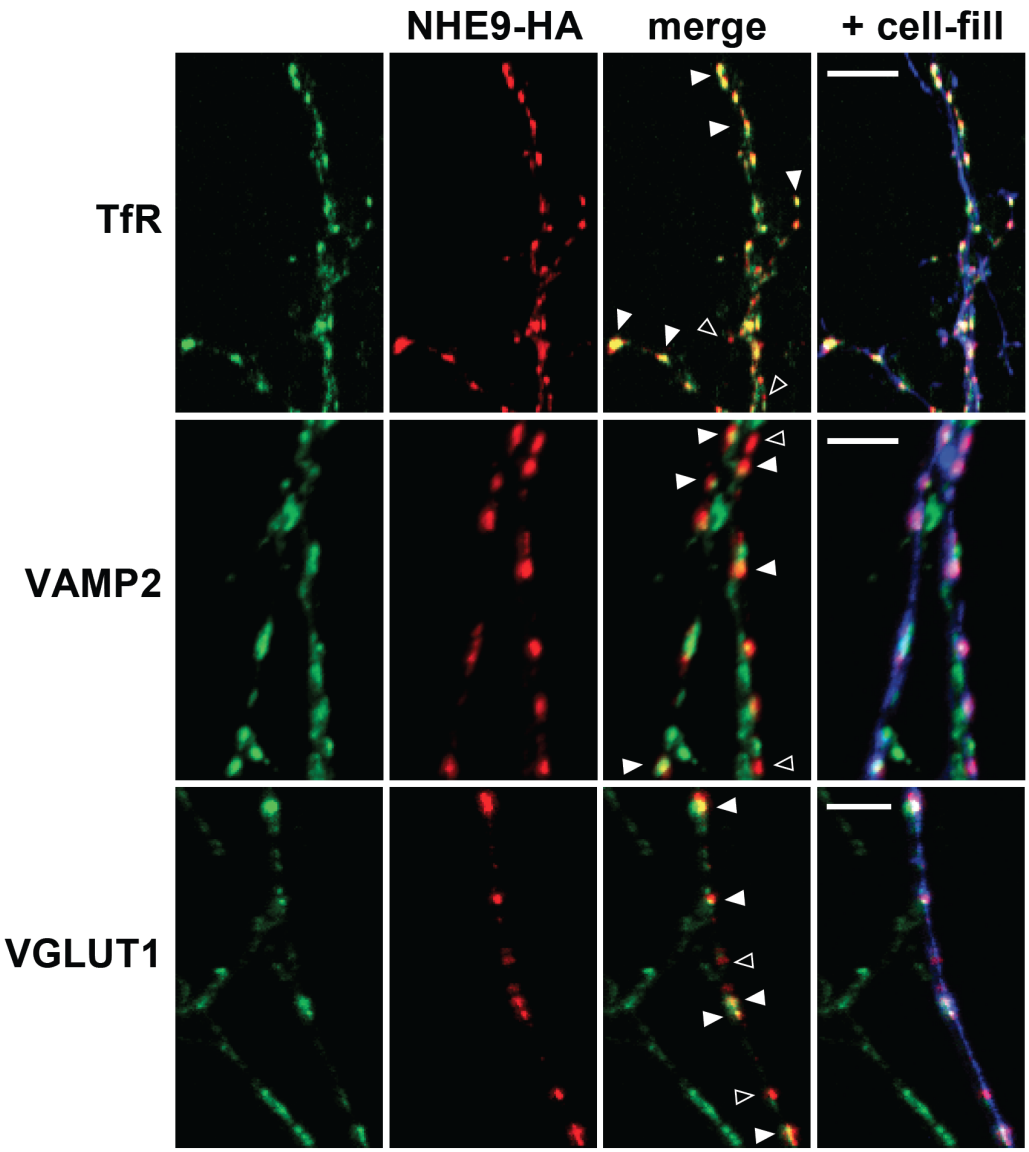

Figure 2.3. NHE9 Localizes to Dendritic Endosomes and Synaptic Vesicles
Dissociated hippocampal cultures prepared from NHE9 KO mice were co-transfected with EGFP to identify the transfected neurons and HA-tagged mouse NHE9. NHE9-HA colocalizes strongly with the transferrin receptor in dendritic endosomes. In axons, NHE9-HA colocalizes with the synaptic vesicle v-SNARE VAMP2 and VGLUT1 at some but not all boutons. White arrowheads indicate colocalization and black arrowheads HA-NHE9 alone. Scale bars all indicate 5 μm.

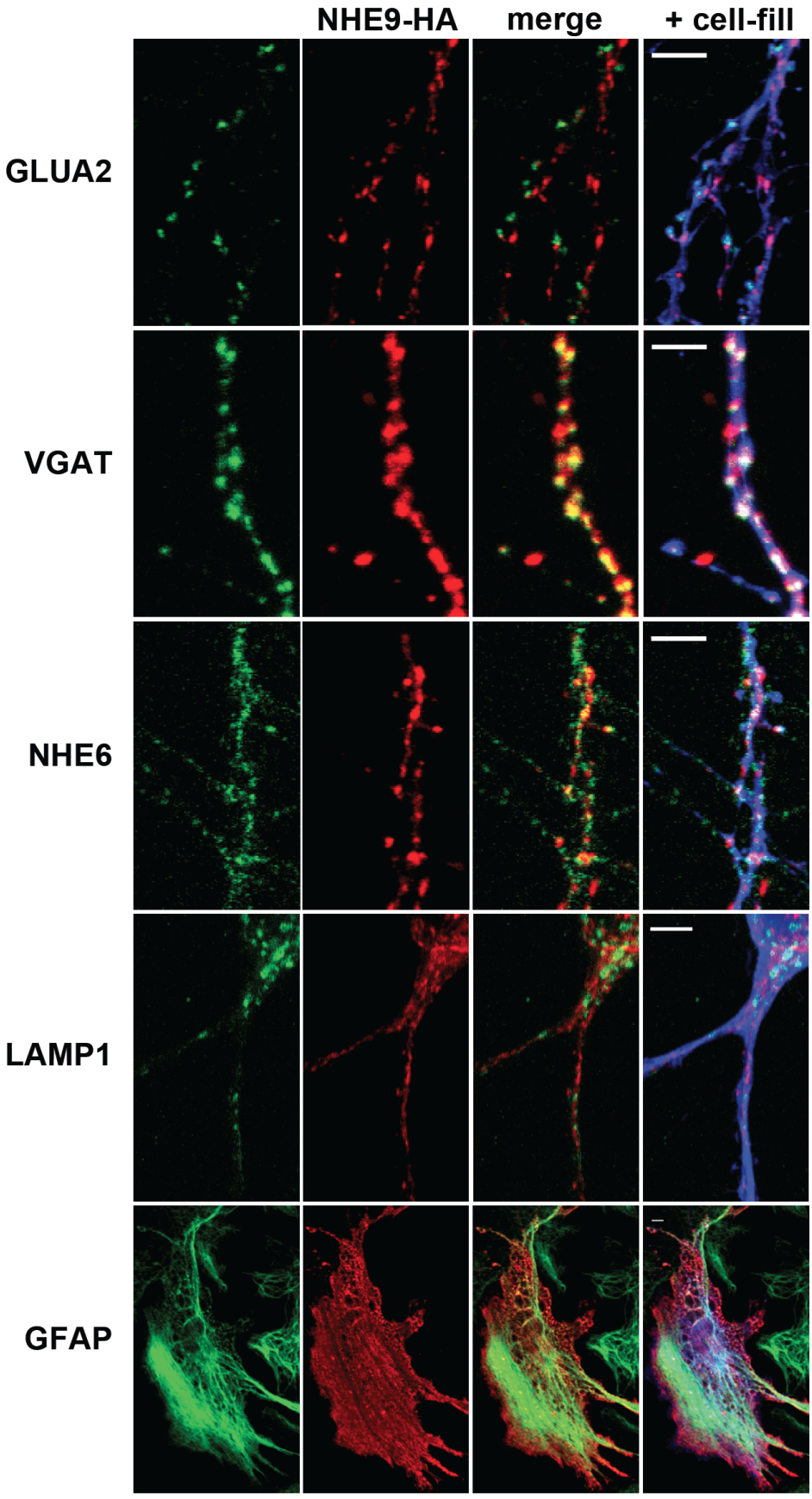
NHE9-HA
merge
+ cell-fill
GLUA2
VGAT
NHE6
LAMP1
GFAP

Figure 2.S3. Subcellular localization of NHE9.
Hippocampal neurons from NHE9 KO mice were cotransfected with EGFP and mouse NHE9 C-terminally tagged with HA (NHE9-HA). DIV14 neurons were fixed and stained for GFP, HA and the endogenous proteins indicated. NHE9 does not colocalize with the postsynaptic protein GluA2 but strongly colocalizes with the vesicular GABA transporter (VGAT). NHE9 colocalizes partially but not completely with the related isoform NHE6. NHE9-HA does not colocalize with the lysosomal protein LAMP1. In astrocytes, NHE9-HA has a diffuse distribution through the cell. Scale bars all indicate 5 μm.

plasma membrane as well as to intracellular compartments (Figure 2.S3). Nonetheless, the localization suggests that dendritic endosomes and synaptic vesicles of cKO mice may exhibit a change in lumenal pH.

Previous work has suggested a number of roles for the intracellular NHE isoforms. In yeast, *Nhx1* acts as a H^+ leak to alkalinize endosomes (Brett et al., 2005). However, mammals express multiple isoforms with diverse functions. Although heterologous expression has indicated a role for NHE6 and NHE9 in alkalinization (Hill et al., 2006; Kondapalli et al., 2015), NHE7 has recently been suggested to promote vesicle acidification, apparently because it recognizes Na^+, not K^+, and the outwardly directed endosome Na^+ gradient would promote acidification through the mechanism of H^+ exchange (Milosavljevic et al., 2014). To determine the role of endogenous NHE9 in regulation of lumenal pH, we took advantage of the ecliptic pHluorin, a form of GFP with increased pH sensitivity (Miesenböck et al., 1998; Sankaranarayanan et al., 2000). Transfecting the pHluorin-based reporters into neurons, buffer at low pH was used to quench the fluorescence of cell surface protein, leaving only the fluorescence of unquenched internal fluorophore, and ammonium chloride was used to alkalinize internal membranes, revealing the total pHluorin fusion expressed and thereby enabling calculation of the lumenal pH (Figure 2.4A) (Mitchell and Ryan, 2004). A fusion of pHluorin to the lumenal domain of TfR (TfR-pHluorin) shows that the dendritic endosomes of NHE9 cKO animals are more acidic, with a pH ~0.3 units lower than WT (Figure 2.4A). NHE9-deficient synaptic vesicles labeled with VAMP2-pHluorin show a similar reduction in pH (Figure 2.4B). NHE9 thus normally serves to dissipate the pH of dendritic endosomes and synaptic vesicles.

Yeast *Nhx1* has also been suggested to regulate cytosolic pH (Brett et al., 2005). The endosomal location might indeed serve to regulate cell surface NHE delivery and activity. We therefore also examined cytosolic pH using the ratiometric dye BCECF-AM. However, we found no difference in the pH of cell body or processes of neurons from NHE9 cKO and WT mice (Figures 2.4C, 2.S4D). NHE9 thus has a specific role in dendritic endosomes and synaptic vesicles rather than at the plasma membrane.

Previous work in yeast has further implicated *Nhx1* in membrane trafficking (Bowers et al., 2000; Brett et al., 2005; Kallay et al., 2011). In mammalian cells, over-expression of NHE9 promotes transferrin internalization (Kondapalli et al., 2013). However, we found no change in the surface fraction of TfR-pHluorin or GluA2-pHluorin in the NHE9 KO (Figure 2.S4A,C), consistent with previous work showing no effect of NHE9 RNAi on transferrin uptake (Kondapalli et al., 2013). On the other hand, we did observe a significant decrease in surface fraction of VAMP2-pHluorin, suggesting a change in trafficking of this v-SNARE (Figure 2.S4B). NHE9 over-expression has also been suggested to influence tumorigenesis through changes in the endolysosomal pathway, but we observed no effect of NHE9 inactivation on

ligand-dependent degradation of the delta opioid receptor expressed in hippocampal neurons (Figure 2.S4E).

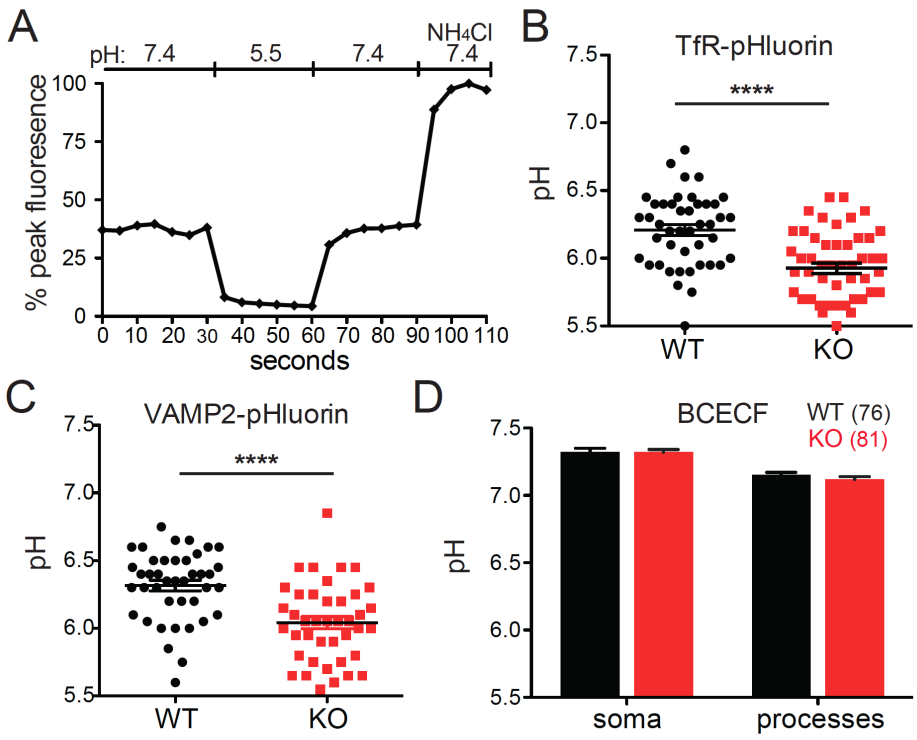

Figure 2.4. Loss of NHE9 Dysregulates the pH of Dendritic Endosomes and Synaptic Vesicles

(A) Transferrin receptor (TfR)-pHluorin was transfected into hippocampal neurons and imaged at DIV12-14. Baseline fluorescence reflects both the unquenched fluorescence of TfR-pHluorin at the plasma membrane and the residual, unquenched fluorescence of the protein in acidic membranes. Buffer at pH 5.5 quenches the surface fluorescence without affecting the intracellular pool, and ammonium chloride reveals the entire population of TfR-pHluorin. These measurements were used to calculate steady-state endosome and synaptic vesicle pH.

(B,C) Dendritic endosomes expressing TfR-pHluorin (B) and synaptic vesicles VAMP2-pHluorin (C) exhibit a lower pH in NHE9 KO neurons than WT. ****, $p<0.0001$ by unpaired two-tailed Student's t-test. WT, n=41-46 neurons/3cultures; KO, n= 41-52 neurons/3 cultures

(D) Cytosolic pH was imaged in the soma and processes using the pH-sensitive ratiometric dye BCECF. A calibration curve for the dye performed in live neurons (Figure S4) was used to calculate pH. Bars indicate mean ± s.e.m. WT, n=76 neurons/3 cultures; KO, n= 81 neurons/3 cultures

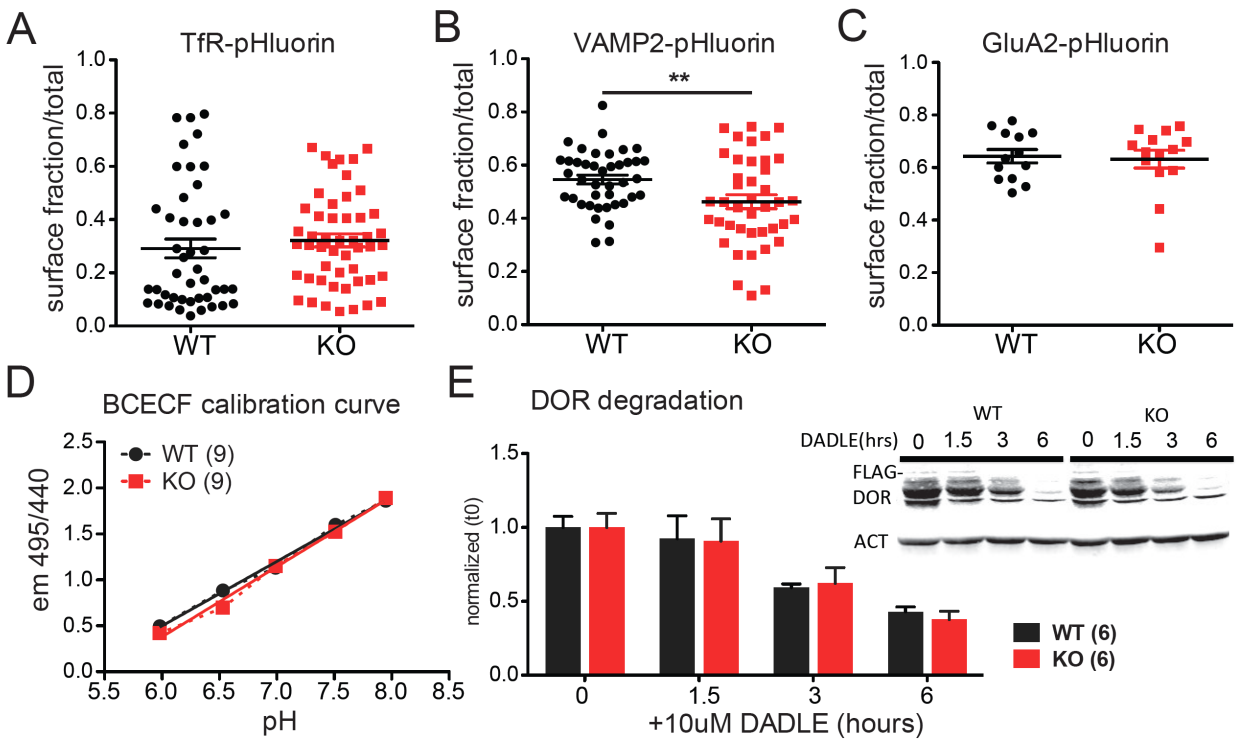

Figure 2.S4. Surface Expression of the pHluorin Reporters and Endolysosomal Degradation

(A-C) Surface expression of TfR-pHluorin (A), VAMP2-pHluorin (B) and GluA2-pHluorin (C) in transfected hippocampal neurons was determined by quenching with external acid and normalizing to total, unquenched fluorescence in NH_4Cl. NHE9 KO neurons show no difference from WT for TfR-pHluorin or GluA2-pHluorin. WT, n=46 neurons/3cultures for TfR-pHluorin and 13 neurons/1 culture for GluA2-pHluorin; KO, n=52 neurons/3 cultures, for TfR-pHLuorin and 14 neurons/1 culture for GluA2-pHluorin. However, VAMP2-pHluorin shows reduced cell surface expression in the NHE9 KO, p=0.009, F-test to compare variance p=0.006. WT and KO, n=41 neurons/3 cultures

(D) BCECF was calibrated using live neurons loaded with BCECF and external solutions at the pH indicated in the presence of ionophores nigericin and valinomycin to equilibrate vesicular with buffer pH. The lines were fit by linear regression, and WT R^2=0.995, KO R^2=0.992. WT, n=9 neurons/3cultures; KO, n=9 neurons/3 cultures

(E) A cDNA encoding the epitope-tagged, G protein-coupled delta-opioid receptor (DOR) was transfected into hippocampal neurons and the cells at DIV14 stimulated with the agonist DADLE (10 μM) to monitor degradation in the endolysosomal pathway. Western blotting for the FLAG epitope shows that DOR rapidly internalizes in response to DADLE and then undergoes degradation. WT and KO, n=6 wells/3 cultures. Bars indicate mean ± s.e.m.

The Role of NHE9 in Synaptic Transmission

The relatively subtle behavioral phenotype of NHE9 cKO mice suggested that it might be difficult to identify the physiological changes responsible. On the other hand, the dysregulation of synaptic vesicle and dendritic endosome pH raised the possibility of direct effects on pre- and postsynaptic machinery. We therefore examined the synapses formed by Schaffer collaterals in

stratum radiatum of hippocampal region CA1, where both presynaptic CA3 and postsynaptic CA1 pyramidal cells express NHE9 (Lein et al., 2007). In acute hippocampal slices, the NHE9 KO shows a small but significant reduction relative to WT in field excitatory postsynaptic potentials (fEPSPs) normalized to the axonal fiber volley (Figure 2.5A). The paired-pulse ratio also increases, suggesting a reduced probability of vesicle release (Figure 2.5B). Whole cell recording of evoked excitatory postsynaptic currents (EPSCs) confirms the increased paired-pulse ratio (Figure 2.5C). The defect in excitatory transmission thus appears to reflect at least in part impaired synaptic vesicle fusion.

We also examined the properties of spontaneous transmitter release by NHE9 KO mice. Miniature inhibitory postsynaptic currents (mIPSCs) recorded in TTX to block action potential generation show a reduction in amplitude without a change in frequency (Figure 2.5D), suggesting a change in either GABA receptor expression or vesicular GABA transport although we did not observe a difference in GABA uptake by synaptic vesicles from the NHE9 KO (data not shown). In contrast, miniature EPSCs (mEPSCs) show increased frequency in the absence of NHE9 (Figure 2.5E). Since the response to paired-pulse stimulation indicates reduced release probability, the increase in mEPSC frequency might reflect an increase in synapse number. However, the architecture of the hippocampus appears normal in NHE9 KO animals by Nissl stain (Figure 2.S5A), and the Golgi stain shows normal spine density in CA1 stratum radiatum (Figure 2.S5B,C). The increase in mEPSC frequency thus does not appear to reflect an anatomic increase in synapse number.

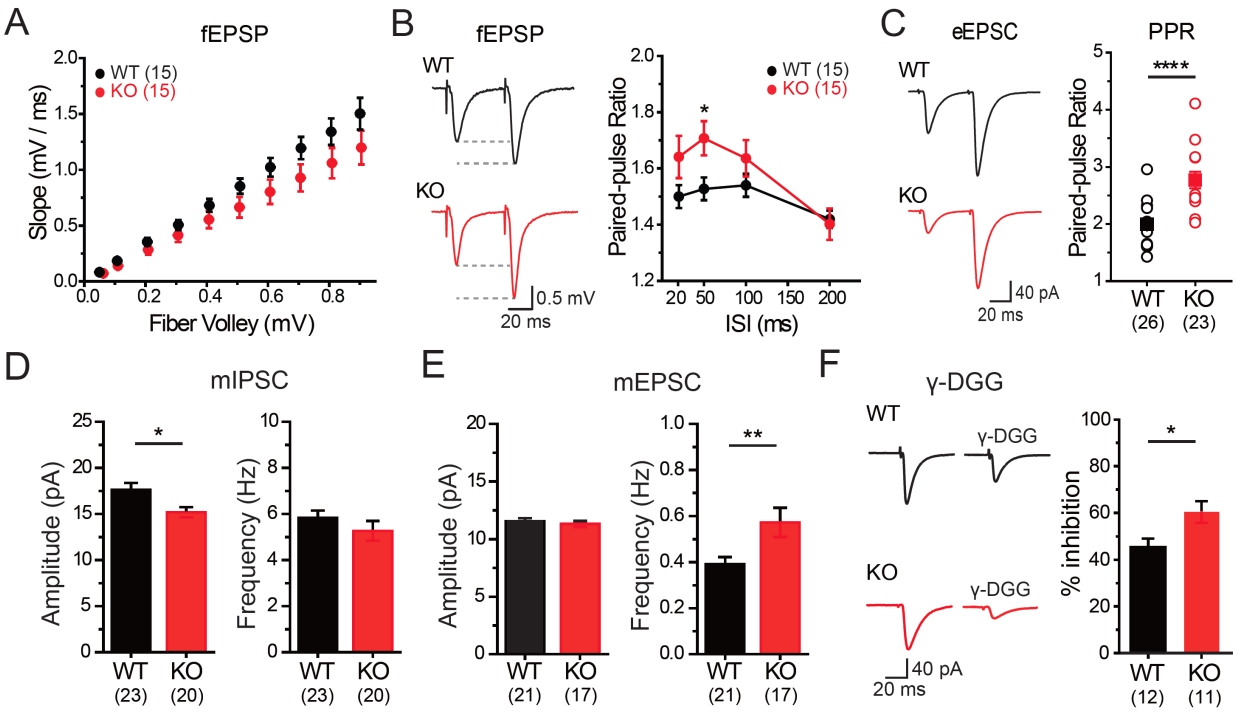

Figure 2.5. Loss of NHE9 Impairs Neurotransmitter Release

(A) fEPSPs recorded in CA1 stratum radiatum are reduced in acute hippocampal slices from NHE9 KO mice. Symbols indicate mean ± s.e.m. p=0.0002 for the difference between genotypes by two-way ANOVA. WT, n=15 neurons/3 mice; KO, n=15 neurons/3 mice

(B) The paired-pulse ratio of fEPSP response at multiple interstimulus intervals (ISIs) shows a significant increase in NHE9 KO slices. Representative traces are shown on the left and mean mean ± s.e.m. are plotted in the graph at the right. *, $p<0.05$ by unpaired two-tailed Student's t-test. WT, n=15 neurons/3 mice; KO, n= 15 neurons/3 mice
(C) Whole cell recordings of evoked EPSC from pyramidal neurons in CA1 also show increased PPR at 50 ms ISI in NHE9 KO slices. ****, $p<0.0001$ by unpaired two-tailed Student's t-test. WT, n=26 neurons/4 mice; KO n= 23neurons/4 mice
(D) mIPSC amplitude is reduced and the frequency unchanged in NHE9 KO neurons. $p=0.011$ by unpaired two-tailed Student's t-test. WT, n=23 neurons/4 mice; KO, n=20 neurons/4 mice
(E) Whole cell recordings from CA1 neurons of NHE9 KO mice show normal mEPSC amplitude but increased frequency. **, $p=0.0098$, F-test $p=0.01$ by unpaired two-tailed Student's t-test. WT, n=21 neurons/4 mice; KO, n=17 neurons/4 mice
(F) The competitive, low affinity AMPA receptor antagonist γ–DGG (500 μM) reduces evoked EPSCs to a greater extent in NHE9 KO than WT slices. Representative traces are shown on the left and averaged results on the right. *, $p<0.05$ by unpaired, two-tailed Student's t-test. WT, n=12 neurons/3 mice; KO, n=11 neurons/3 mice. Bar graphs in D-F indicate mean ± s.e.m.

Since synaptic vesicles express an NHE activity that influences glutamate transport (Goh et al., 2011), we also measured quantal size. Surprisingly, mEPSC amplitude shows no difference between NHE9 KO and WT (Figure 2.5E). Even though loss of NHE9 lowers synaptic vesicle pH (Figure 2.4B), which should reduce the $\Delta\psi$ driving glutamate uptake, this does not seem to affect vesicle filling. However, mEPSC amplitude reflects the postsynaptic response to neurotransmitter, and is therefore sensitive to changes in the number of glutamate receptors as well as vesicle filling. To assess specifically the amount of glutamate released, we therefore used the competitive low affinity glutamate receptor antagonist γ-DGG. Since the response in this compound is normalized to evoked release before its addition, the extent of inhibition by γ-DGG is not influenced by changes in receptor sensitivity or release probability, but rather the amount of glutamate released. Indeed, γ-DGG inhibits the evoked response in slices from the NHE9 KO to a greater extent than WT (Figure 2.5F), indicating reduced glutamate release. Since Schaffer collateral synapses release either no vesicles or a single vesicle in response to stimulation under these conditions, the increased inhibition by γ-DGG implies reduced vesicle filling. Considering the relatively small magnitude of the effect, we were not surprised to find that the biochemical measurement of glutamate uptake using synaptic vesicles from the whole brain showed no detectable difference in stimulation by K^+ between NHE9 KO and WT (Figure 2.S5D).

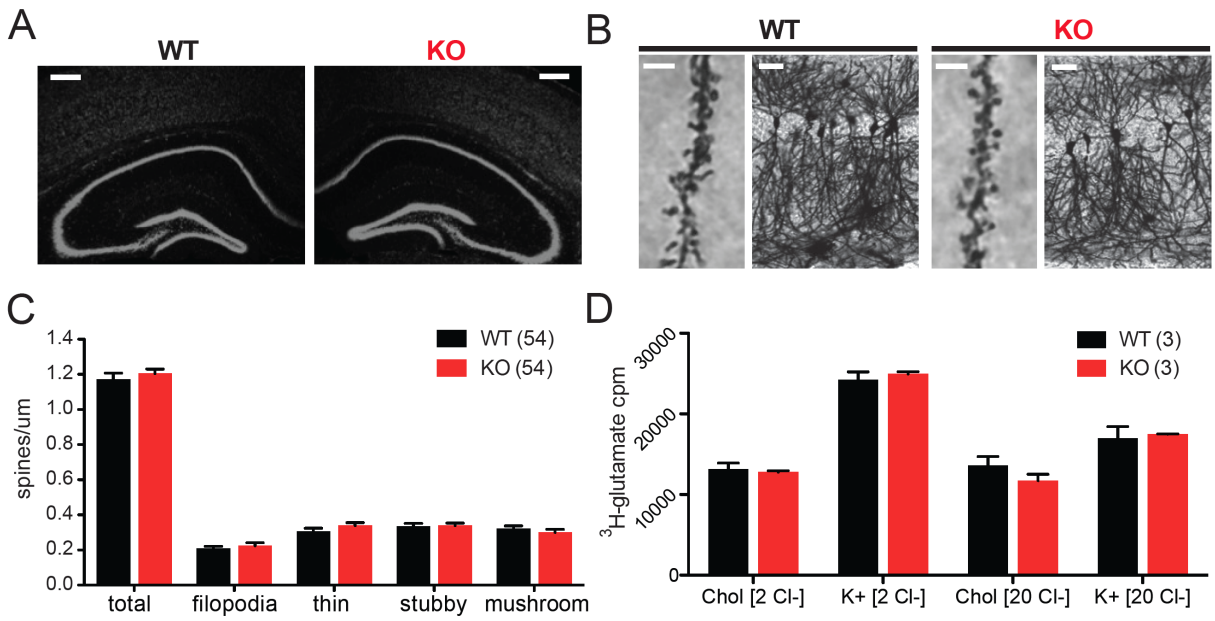

Figure 2.S5. Loss of NHE9 Does Not Affect Spine Number, Morphology or Vesicular Glutamate Transport Activity.
(A) Nissl stain of WT and NHE9 KO brain slices shows grossly normal brain architecture. Scale bar, 250 μm).
(B) Representative Golgi stain of CA1 dendritic spines and branching shows no difference between NHE9 KO and WT. Scale bars indicate 5 μm for dendritic spines (left) and 25 μm for dendritic branching (right).
(C) The analysis of spine density and shape by electron microscopy shows no difference between WT and KO hippocampal CA1 pyramidal neurons. WT, n=54 neurons/4 brains; KO, n=54 neurons/4 brains
(D) Synaptic vesicles purified from the whole brain of WT and NHE9 KO mice were incubated for 10 minutes with radiolabeled glutamate in the presence or absence of K^+ and at either physiological (20 mM) or low Cl^- (2 mM). The background in Evans Blue was subtracted. n=3 separate LP2 preparations Bars indicate mean ± s.e.m.

The Role of ΔpH in Regulation of Synaptic Vesicle Exocytosis

To characterize the defect in neurotransmitter release suggested by the increased paired-pulse ratio, we again took advantage of the ecliptic pHluorin fused to the lumenal domain of synaptic vesicle protein VGLUT1. Quenched at the low pH of synaptic vesicles, the protein increases in fluorescence when exposed to the higher external pH by exocytosis, then reacidifies rapidly after endocytosis (Voglmaier et al., 2006). Transfected into dissociated hippocampal neurons, the reporter shows substantially reduced peak fluorescence response to stimulation at 10 Hz in cells from the NHE9 KO than from WT mice (Figure 2.6A), suggesting a defect in the synaptic vesicle cycle. The impairment does not involve an identifiable subset of boutons, but rather affects the entire range including those with both large and small responses (Figure 2.6B). Although NHE activity might influence the rate of synaptic vesicle reacidification measured with

the pHluorin after stimulation, the rate of fluorescence decay appears unchanged by loss of NHE9 (Figure 2.6A), excluding effects on endocytosis as well as reacidification.

Since the fluorescence increase of VGLUT1-pHuorin during stimulation reflects a combination of both exo- and endocytosis, we also used the H^+-ATPase inhibitor bafilomycin to block the reacidification of recycling synaptic vesicles, thereby preventing the decrease in fluorescence that accompanies endocytosis, and allowing us to focus specifically on synaptic vesicle exocytosis. In the presence of bafilomycin, endocytosis is no longer detectable using the pHluorin reporter, and the fluorescence response to stimulation reflects only exocytosis. Using bafilomycin, we found that neurons from the NHE9 KO respond more slowly than WT to stimulation (Figure 2.6C). By subtracting the fluorescence response in the absence of bafilomycin from that in the presence of the drug, we also measured the endocytosis that occurs during stimulation, which can differ in mechanism from the endocytosis that follows stimulation

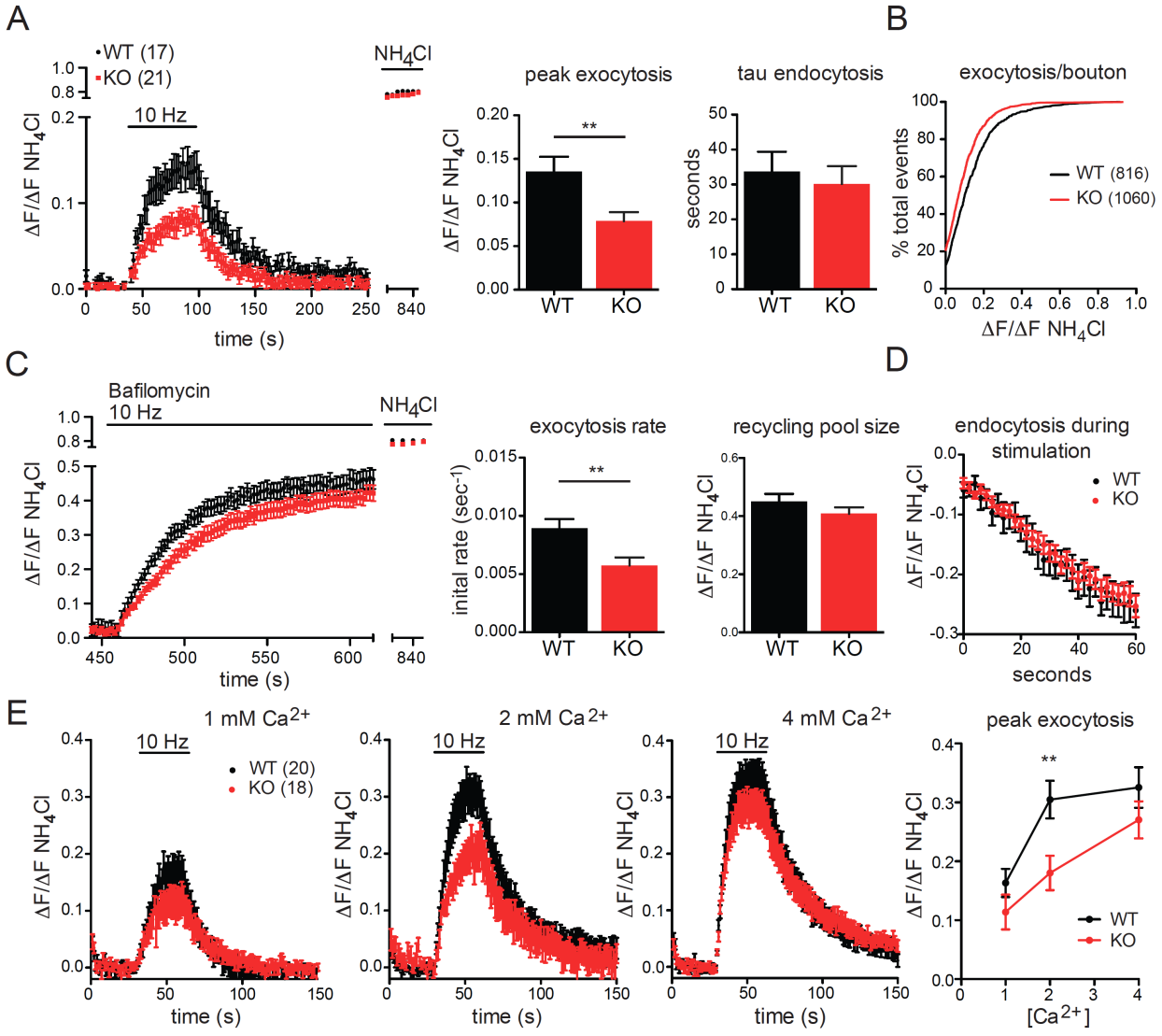

Figure 2.6. Loss of NHE9 Impairs Synaptic Vesicle Exocytosis.
(A) Cultured hippocampal neurons from NHE9 KO mice show a smaller VGLUT1-pHluorin fluorescence response to 10 Hz stimulation for 60 seconds than WT cells. The left panel plots

average fluorescence change. Middle, comparison of the peak fluorescence indicates a significant difference betweeen genotypes. **, $p<0.05$ by unpaired Student's t-test. Right panel shows there is no change in the time constant of endocytosis (tau), $p=0.65$.
(B) A cumulative frequency distribution displays the extent of exocytosis for all boutons of each genotype. $p<0.0001$ by Kolmogorov-Smirnov. WT, n=816 boutons; KO, n=1060
(C) Hippocampal neurons expressing VGLUT1-pHluorin were stimulated at 10 Hz for 60 s, then stimulated again at 10 Hz for 150 s in the presence of bafilomycin. The fluorescence change in the presence of bafilomycin (left) was used to determine the initial rate of exocytosis (middle), which is reduced for NHE9 KO neurons relative to WT, $p=0.0047$. The recycling pool size, determined by normalizing the peak fluorescence response in bafilomycin to the total fluorescence revealed in NH_4Cl (right), shows no change ($p=0.22$).
(D) The rate constant of endocytosis during stimulation was calculated by subtracting the fluorescence in the presence of bafilomycin from that in the absence. NHE9 KO neurons do not differ from WT in endocytosis during or after the stimulus. n=17 (WT) or 21 (KO) coverslips per genotype for C and D. Bar graphs indicate mean ± s.e.m.
(E) The response of VGLUT1-pHluorin to 10 Hz stimulation in 1, 2 and 4 mM Ca^{++} shows no significant difference of NHE9 KO neurons from WT at 1 and 4 mM Ca^{++} but a significant difference in 2 mM Ca^{++}. Plotting the amplitude of the peak fluorescence response against Ca^{++} concentration (right panel) shows that loss of NHE9 reduces the steepness of sensitivity to Ca^{++}. **, $p<0.01$ by two-tailed unpaired t-test. WT, n=20 coverslips; KO, n=18

(Ferguson et al., 2007). However, boutons of the NHE9 KO show no difference from WT in endocytosis during the stimulus (Figure 2.6D). NHE9 thus specifically affects synaptic vesicle exocytosis.

How does the loss of NHE9 impair synaptic vesicle exocytosis? It might affect the pool of synaptic vesicles available for release, also known as the recycling pool (Rizzoli and Betz, 2005). However, the recycling pool detected by stimulation of cells expressing VGLUT1-pHluorin in the presence of bafilomycin and normalizing to the total vesicle pool revealed in NH_4Cl shows no difference between NHE9 KO and WT (Figure 2.6C). Release also reflects the number of synaptic vesicles docked and primed for release, known as the readily releasable pool (RRP). To monitor the size of the RRP, we used stimulation at 20 Hz for 2 seconds (Rosenmund and Stevens, 1996). Figure S6A shows that NHE9 KO cells do not differ from WT in the size of the RRP, again monitored with VGLUT1-pHluorin. We also examined a wide range of pre- as well as postsynaptic proteins by quantitative western analysis of hippocampal extracts (Figure S6B). For all of these proteins, the NHE9 KO shows no difference from WT.

In the absence of a change in pool size or synaptic protein expression, we considered that a change in calcium sensitivity might be responsible for the role of NHE9 in synaptic vesicle exocytosis. We therefore tested the sensitivity of the VGLUT1-pHluorin response to stimulation in low (1 mM) and high (4 mM) Ca^{++}. Figure 6E shows that in 1 mM Ca^{++}, the amplitude of the fluorescence response by NHE9 KO neurons does not differ significantly from WT. At 4 mM Ca^{++}, the loss of NHE9 has similarly little effect on the pHluorin response. Plotting the response as a function of Ca^{++}, the loss of NHE9 thus influences the steepness of the response to Ca^{++} (Figure 2.6E).

The physiological defect in Ca^{++} sensitivity of synaptic vesicle exocytosis raises the possibility of an acute functional impairment due directly to synaptic vesicle hyperacidification.

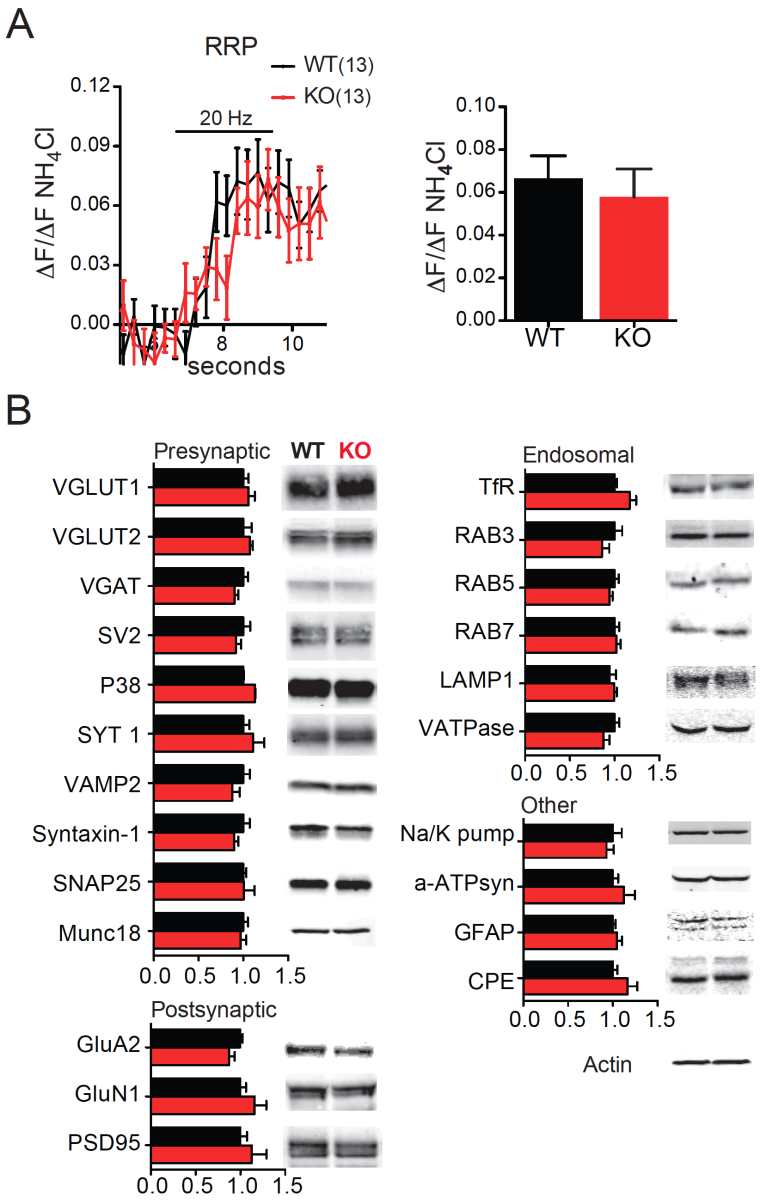

Figure 2.S6. Loss of NHE9 Does Not Affect Readily Releasable Pool Size or the Level of Synaptic Proteins.
(A) Readily releasable pool size as determined by the peak response of VGLUT1-pHluorin (expressed in hippocampal neurons) to 20 Hz stimulation for 2 seconds shows no difference between NHE9 KO and WT. WT, n=13 coverslips/3 cultures; KO, n=13 coverslips/3 cultures
(B) Extracts from P21 hippocampi were analyzed by fluorescent western blot for presynaptic, postsynaptic, endosomal and other proteins. Loss of NHE9 produced no detectable change in any of these proteins. Bars indicate mean ± s.e.m. n=4 brains/genotype

To test this possibility, we again used the H^+-ATPase inhibitor bafilomycin, in this case to dissipate the excessive pH gradient. However, H^+ pump inhibition eliminates the changes in pH required to monitor exocytosis with pHluorin-based reporters and by postsynaptic recording,

requiring an alternative, pH-independent method to assess the exocytosis of recycled vesicles. We have therefore relied on the pH-insensitive styryl dye FM2-10. Loaded into recycling synaptic vesicles during and after stimulation, the dye is destained by subsequent stimulation, providing another estimate of synaptic vesicle exocytosis. Interestingly, previous work has shown that bafilomycin does not affect subsequent FM dye destaining, suggesting that acidification has no effect on synaptic vesicle exocytosis (Zhou et al., 2000). On the other hand, a recent study has shown that vesicle filling can influence synaptic vesicle exocytosis (Herman et al., 2014), implying a clear role for the H^+ electrochemical driving force.

Using FM2-10, we found that the loss of NHE9 impairs synaptic vesicle exocytosis (Figure 2.7A,D), consistent with the postsynaptic recording and VGLUT1-pHluorin imaging. We then used bafilomycin to inactivate the H^+ pump acutely in the recycling synaptic vesicles loaded with styryl dye (Figure 7B).

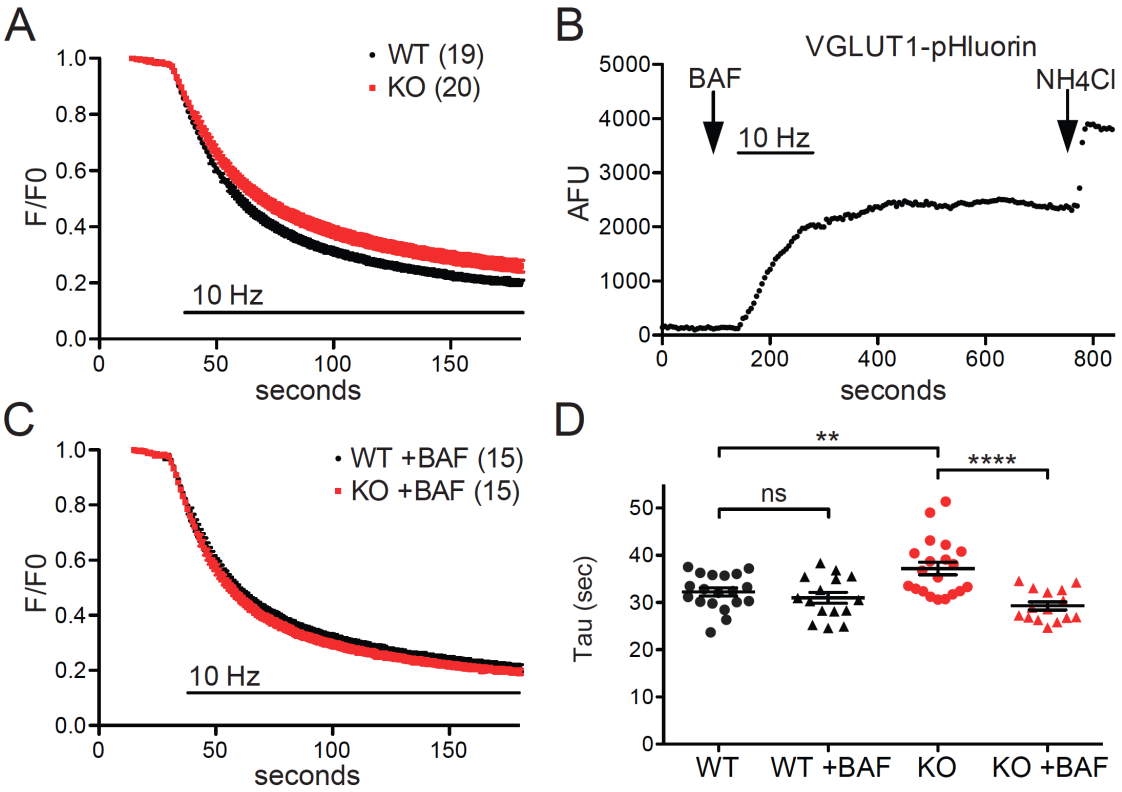

Figure 2.7. Inhibition of the H^+ Pump Rescues Synaptic Vesicle Exocytosis
(A) FM2-10 destaining confirms the defect in synaptic vesicle exocytosis. Hippocampal neurons were loaded with FM2-10 in bicarbonate-buffered media by stimulation at 10 Hz for 120 seconds, allowed to recover for 10 minutes, then stimulated again at 10 Hz for 150 seconds to unload the FM dye.
(B) Representative trace from control experiment to verify that bafilomycin loaded into vesicles expressing VGLUT1-pHluorin increases the pH of these vesicles and the more neutral pH is stable for 10 minutes.
(C) Neurons from the NHE9 KO loaded simultaneously with bafilomycin as well as FM2-10 do not differ from WT neurons in the rate of FM dye destaining in response to 10 Hz stimulation.

(D) The time constant (tau) for destaining shows that bafilomycin rescues the exocytosis defect of NHE9 KO neurons but does not affect the destaining of WT cells. **, p<0.01; ****, p<0.0001 by one-way ANOVA with Bonferroni. Data represent the mean ± s.e.m. WT, n=19/15 coverslips/3 cultures; KO, n=20/15 coverslips/3 cultures

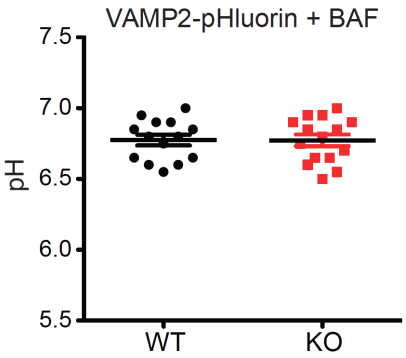

Supplemental Figure 2.S7. Bafilomycin Dissipates Synaptic Vesicle ΔpH
Calculation of synaptic vesicle pH in the presence of bafilomycin was performed as in Figure 4. Bafilomycin increases the pH of synaptic vesicles from both WT and NHE9 KO mice to ~6.8. WT, n=14 coverslips/3 cultures; KO, n=15 coverslips/3 cultures

Bafilomycin eliminates the difference between NHE9 KO and WT in the rate of FM dye destaining, but has no effect on the WT (Figure 2.7C,D), consistent with the previous report (Zhou et al., 2000). Excessive acidification due to the loss of NHE9 can thus impair synaptic vesicle exocytosis, and this does not reflect a problem with development or in response to network activity since it can be reversed acutely by simple dissipation of the H^+ electrochemical gradient.

2.5 Discussion

NHE9 Regulates the Endosome and Synaptic Vesicle H^+ Electrochemical Gradient

The results provide basic information about the biochemical function of NHE9 in the physiologically relevant setting of synaptic transmission. Although yeast *Nhx1* contributes to the regulation of cytosolic pH (Brett et al., 2005), loss of NHE9 has no effect on cytosolic pH in neurons. In contrast, loss of NHE9 lowers the pH of dendritic endosomes and synaptic vesicles. Despite a role for NHE7 in acidification (Milosavljevic et al., 2014), NHE9 catalyzes endosomal alkalinization. Since K^+ is the main cytosolic cation, the mechanism of H^+ exchange further predicts that NHE9 recognizes K^+.

NHE6 has a similar role in regulation of the endosome H^+ electrochemical gradient. Loss of NHE6 also results in the hyperacidification of endosomes (Ouyang et al., 2013), indicating an analogous role as H^+ leak and predicting the recognition of K^+. However, the two isoforms are not redundant since loss of either produces a phenotype. This may reflect differences in subcellular localization, as originally suggested (Nakamura et al., 2005). However, NHE6 localizes to endosomes (Brett et al., 2002; Deane et al., 2013; Ouyang et al., 2013) much like NHE9, although we find that the colocalization is not complete. Alternatively, normal function may depend on the total amount of NHE activity expressed. NHE6 and 9 presumably operate together with other mechanisms that set endosome pH, each contributing in a quantitative way to the outcome. The more severe phenotype of NHE6 inactivation may indeed simply reflect the greater abundance of this isoform. The difficulty detecting endogenous NHE9 with the available antibodies suggests that it is expressed at very low levels, perhaps accounting for the more subtle phenotype of the NHE9 cKO. Consistent with the importance of total endosome NHE activity, we also observed no up-regulation of brain NHE6 mRNA by qPCR or NHE6 protein by western blot in the NHE9 cKO (data not shown).

Recent work has also suggested that VGLUT1 itself confers cation/H^+ exchange activity independent of the known NHE isoforms (Preobraschenski et al., 2014). However, NHE9 colocalizes with synaptic vesicle components by immunofluorescence and previous proteomic analysis has demonstrated the localization of NHE6 to highly purified synaptic vesicles (Gronborg et al., 2010). In addition, the hyperacidification of synaptic vesicles in KO neurons indicates a role for NHE9 at this site. NHE9 and presumably NHE6 thus contribute to regulation of the synaptic vesicle H^+ electrochemical gradient, perhaps in combination with the VGLUTs.

Loss of NHE9 Reproduces Behavioral Features of ASD

In contrast to the severe phenotype produced by loss of NHE6 in humans and mice (Gilfillan et al., 2008; Ouyang et al., 2013), loss of NHE9 has more selective effects. The NHE9 cKO does not show any premature lethality, and has no apparent anxiety or defect in motor coordination by the standard assays. Although several of the individuals with mutations in NHE9 have epilepsy (Morrow et al., 2008), we detected only a single obvious seizure in cKO animals, so this does not appear to be a prominent feature of the mouse model.

The NHE9 cKO exhibits defects specifically related to social interactions. As juveniles, they solicit less play with other animals, and exhibit less affiliative and investigative behavior. As adults, they do not differ from WT in the three chamber test for sociability. However, they fail to habituate on repeat exposure to the same animal, indicating a defect in social recognition. Importantly, social recognition has recently been suggested to depend on the hippocampus (Hitti and Siegelbaum, 2014), which expresses particularly high levels of NHE9. The almost

invariable withdrawal of NHE9 cKO mice in the tube test further indicates social subordination. Thus, NHE9 cKO mice exhibit normal interest in social interactions, but do not interact normally.

In addition to the defects in social interaction, the NHE9 cKO show other behavioral features associated with ASD. They bury more marbles than WT mice, suggesting an element of repetitive behavior. They also climb more than WT. However, they manipulate pellets, rear and groom less than WT, and these behaviors can become stereotyped and repetitive in ASD. The NHE9 cKO also fail to distinguish socially relevant odors from those of food objects, even though they have no apparent defect in basic olfaction. Loss of NHE9 thus reproduces some of the repetitive behavior and problematic communication that may result from defective sensory processing and accompany social impairments in ASD.

Surprisingly, heterozygous NHE9 mice also exhibit multiple defects in juvenile play. The juvenile heterozygotes show less play soliciting and investigation but no difference in affiliative behavior from WT animals. In contrast, the adult heterozygotes show no defect in the tube test, marble burying or response to most olfactory cues, although they do have difficulty with social recognition. The quantitative role of NHEs in determination of endosome pH presumably accounts for the behavioral phenotype of heterozygotes, with the lower levels of NHE9 expressed early in life perhaps accounting for the relatively specific effect on juvenile behavior. Resolution of the behavioral phenotype in NHE9 heterozygotes with age may therefore reflect the developmental increase in NHE9 expression. Alternatively, neural systems may adapt to the disturbance produced by partial loss of NHE9, although this does not happen in the homozygote.

Loss of NHE9 Impairs Neurotransmitter Release

Considering the relatively subtle behavioral phenotype of NHE9 cKO mice, we were surprised to observe major effects on baseline synaptic transmission. First, we observed a reduction in the amount of transmitter released per vesicle. The low-affinity glutamate receptor antagonist γ-DGG inhibits the evoked response to a greater extent in the KO than in WT. Since the response in γ-DGG is normalized to the response in its absence, the assay provides a measure that is independent of receptor expression, release probability and synapse number, indicating a role for NHE9 in vesicle filling.

Second, loss of NHE9 impairs synaptic vesicle exocytosis. The paired-pulse ratio increases in both field and whole cell recordings, indicating reduced transmitter release in response to a single action potential (Zucker and Regehr, 2002). pHluorin-based and FM dye imaging confirm the defect in synaptic vesicle exocytosis inferred from postsynaptic recording.

Considering the defect in both synaptic vesicle exocytosis as well as filling, it is remarkable that NHE9 inactivation has a modest effect on baseline transmission assessed by field recordings. The discrepancy implies some form of compensation for the defect in release. One possibility is that glutamate receptors up-regulate, perhaps through synaptic scaling, a homeostatic mechanism that adjusts receptor expression to the level of activation (Turrigiano, 2008). Since quantal size reflects receptor sensitivity as well as the amount of transmitter released per vesicle, receptor up-regulation would affect mEPSC amplitude but not the inhibition by γ-DGG. Indeed, the mEPSCs of NHE9 cKO animals show no change in amplitude despite reduced vesicle filling demonstrated using γ-DGG. Alternatively, synapse number might increase to compensate for the reduced transmitter release. We do not observe a change in spine density, but mEPSC frequency increases in the NHE9 KO, and this might reflect an increase in the proportion of functional rather than morphologically identifiable synapses.

Dysregulation of the H^+ Electrochemical Gradient Underlies Synaptic Deficits in NHE9 KO Mice

Many genes implicated in ASD influence brain development. Mutations in the neuroligins (3 and 4) and neurexin 1 cause ASD, and these proteins interact to promote synapse formation (Scheiffele et al., 2000; Jamain et al., 2003; Sudhof, 2008). Mutations in another neurexin superfamily member contactin-associated protein 2 (CNTNAP2) can also produce ASD, and the mouse knockout shows defects in neuron migration as well as cell number (Strauss et al., 2006; Penagarikano et al., 2015). Mutations in the protocadherins that mediate selective cell adhesion and the semaphorins involved in axon guidance further implicate developmental processes in ASD (Morrow et al., 2008; Iossifov et al., 2014). The association of developmental genes with ASD suggests a disturbance in the formation of neural circuits. Indeed, ASD have been considered to reflect an alteration in excitation-inhibition balance (Rubenstein and Merzenich, 2003).

On the other hand, the role of NHE9 in the regulation of endosome pH and the synaptic impairment that results raise the possibility of a more direct effect on synapse function. The presynaptic reduction in vesicle filling revealed using γ-DGG presumably reflects an alteration in the driving force for vesicular glutamate transport. In previous work, we showed that synaptic vesicles express an NHE activity that promotes vesicle filling with glutamate by promoting the formation of $\Delta\psi$ at the expense of ΔpH (Goh et al., 2011). We cannot detect a change in NHE activity using purified synaptic vesicles from the NHE9 KO, but the contribution of other factors such as NHE6 and VGLUT1 presumably makes this difficult, and the reduced synaptic vesicle pH in KO neurons clearly indicates a role for NHE9 in this process.

Although previous work has suggested that the H^+ electrochemical gradient does not influence synaptic vesicle exocytosis, we now find that the dysregulation of ΔpH resulting from loss of NHE9 inhibits release. Using an FM dye due to its pH-independence, we show that acute dissipation of ΔpH by inhibiting the H^+ pump with bafilomycin rescues the defect in synaptic vesicle exocytosis produced by the loss of NHE9. The acute effect of bafilomycin shows that the defect in exocytosis results directly from excessive ΔpH, and the results agree with previous work since we find no effect of bafilomycin on the rate of exocytosis in WT neurons.

How does low lumenal pH influence synaptic vesicle exocytosis? Previous work has indicated a role for ΔpH in homotypic fusion of the yeast vacuole, but in that case it promotes the pairing of SNARE proteins from opposing membranes required for membrane fusion (Ungermann et al., 1999). A subunit of the vacuolar H^+-ATPase itself has also been implicated in membrane and even synaptic vesicle fusion, but this function appears independent of its role establishing the H^+ electrochemical gradient (Bayer et al., 2003; Hiesinger et al., 2005). We now find that the increase in ΔpH due to loss of NHE9 makes the evoked response of VGLUT1-pHluorin less steeply dependent on external Ca^{++}. This might reflect a change in the Ca^{++} sensitivity of response to a single action potential (i.e., in fusion) or specifically in the Ca^{++} sensitivity to high frequency stimulation (i.e., in vesicle mobilization). Since bafilomycin rescues the defect in regulated exocytosis, however, ΔpH is not required for either of these processes. With regard to regulated exocytosis, NHE9 thus serves primarily to dissipate excess ΔpH and enable a steeply cooperative response to Ca^{++}.

The acute rescue of synaptic vesicle exocytosis by inhibition of the H^+ pump raises the possibility that bafilomycin might also rescue other aspects of the NHE9-deficient phenotype.

However, inhibition of the H^+ pump is not a viable therapeutic strategy since this would collapse the entire H^+ electrochemical gradient, eliminating transmitter storage and release. Complete dissipation of even ΔpH alone would also affect filling and release. From these considerations, we infer that endogenous NHE9 must dissipate excess ΔpH without collapsing the gradient altogether, and this intermediate level of activity presumably requires appropriate regulation. Regulation might involve the precise tuning of catalytic activity, possibly in response to the magnitude of ΔpH. Alternatively, the regulation might involve sequential, NHE-mediated activation of first H^+ influx driven by the Na^+ gradient, then H^+ efflux driven by a K^+ gradient. Consistent with this, NHE9 appears to recognize Na^+ as well as K^+ (Kondapalli et al., 2013). Regardless of mechanism, the phenotype of NHE9 cKO mice demonstrates the potential for regulation of the H^+ electrochemical gradient to influence synaptic transmission and behavior.

2.6 Acknowledgements

This work was supported by a fellowship from NIMH F31 MH096447 and the Elizabeth Roboz Einstein Fellowship (to J.C,U.), grant MH50712 from NIMH (to R.H.E.) and a pilot award from the Simons Foundation (to R.H.E.).

Julie Ullman and Robert Edwards co-authored the manuscript. Jing Yang and Jon Levy performed and analyzed the acute slice recordings. Michael Sullivan and Ellen Pham assisted in all aspects of mouse husbandry, genotyping and behavioral assays. All other experiments designed, executed and analyzed by Julie Ullman.

We thank Roger Nicoll for thoughtful suggestions, Chantal Toupin for histological analysis, Jacob Bendor, Jacob Eriksen, James Maas and other members of the Edwards lab for helpful discussion.

2.7 References

Bayer, M.J., Reese, C., Buhler, S., Peters, C., and Mayer, A. (2003). Vacuole membrane fusion: V0 functions after trans-snare pairing and is coupled to the ca2+-releasing channel. J. Cell Biol. *162*, 211-222.

Bellocchio, E.E., Hu, H., Pohorille, A., Chan, J., Pickel, V.M., and Edwards, R.H. (1998). The localization of the brain-specific inorganic phosphate transporter suggests a specific presynaptic role in glutamatergic transmission. J. Neurosci. *18*, 8648-8659.

Bowers, K., Levi, B.P., Patel, F.I., and Stevens, T.H. (2000). The sodium/proton exchanger nhx1p is required for endosomal protein trafficking in the yeast saccharomyces cerevisiae. Mol. Biol. Cell *11*, 4277-4294.

Brett, C.L., Wei, Y., Donowitz, M., and Rao, R. (2002). Human na(+)/h(+) exchanger isoform 6 is found in recycling endosomes of cells, not in mitochondria. Am. J. Physiol. Cell Physiol. *282*, C1031-1041.

Brett, C.L., Tukaye, D.N., Mukherjee, S., and Rao, R. (2005). The yeast endosomal na+k+/h+ exchanger nhx1 regulates cellular ph to control vesicle trafficking. Mol. Biol. Cell *16*, 1396-1405.

Chaudhry, F.A., Reimer, R.J., Bellocchio, E.E., Danbolt, N.C., Osen, K.K., Edwards, R.H., and Storm-Mathisen, J. (1998). The vesicular gaba transporter vgat localizes to synaptic vesicles in sets of glycinergic as well as gabaergic neurons. J. Neurosci. *18*, 9733-9750.

Clift-O'Grady, L., Linstedt, A.D., Lowe, A.W., Grote, E., and Kelly, R.B. (1990). Biogenesis of synaptic vesicle-like structures in a pheochromocytoma cell line pc12. J. Cell Biol. *110*, 1693-1703.

de Silva, M.G., Elliott, K., Dahl, H.H., Fitzpatrick, E., Wilcox, S., Delatycki, M., Williamson, R., Efron, D., Lynch, M., and Forrest, S. (2003). Disruption of a novel member of a sodium/hydrogen exchanger family and dock3 is associated with an attention deficit hyperactivity disorder-like phenotype. J. Med. Gene. *40*, 733-740.

Deane, E.C., Ilie, A.E., Sizdahkhani, S., Das Gupta, M., Orlowski, J., and McKinney, R.A. (2013). Enhanced recruitment of endosomal na+/h+ exchanger nhe6 into dendritic spines of hippocampal pyramidal neurons during nmda receptor-dependent long-term potentiation. J. Neurosci. *33*, 595-610.

Del Campo, N., Chamberlain, S.R., Sahakian, B.J., and Robbins, T.W. (2011). The roles of dopamine and noradrenaline in the pathophysiology and treatment of attention-deficit/hyperactivity disorder. Biol. Psych. *69*, e145-157.

Edwards, R.H. (2007). The neurotransmitter cycle and quantal size. Neuron *55*, 835-858.

Ferguson, S.M., Brasnjo, G., Hayashi, M., Wolfel, M., Collesi, C., Giovedi, S., Raimondi, A., Gong, L.W., Ariel, P., Paradise, S., *et al*. (2007). A selective activity-dependent requirement for dynamin 1 in synaptic vesicle endocytosis. Science *316*, 570-574.

Fisher, S.E., Francks, C., McCracken, J.T., McGough, J.J., Marlow, A.J., MacPhie, I.L., Newbury, D.F., Crawford, L.R., Palmer, C.G., Woodward, J.A., *et al*. (2002). A genomewide scan for loci involved in attention-deficit/hyperactivity disorder. American journal of human genetics *70*, 1183-1196.

Fremeau, R.T., Jr., Kam, K., Qureshi, T., Johnson, J., Copenhagen, D.R., Storm-Mathisen, J., Chaudhry, F.A., Nicoll, R.A., and Edwards, R.H. (2004). Vesicular glutamate transporters 1 and 2 target to functionally distinct synaptic release sites. Science *304*, 1815-1819.

Gilfillan, G.D., Selmer, K.K., Roxrud, I., Smith, R., Kyllerman, M., Eiklid, K., Kroken, M., Mattingsdal, M., Egeland, T., Stenmark, H., *et al*. (2008). Slc9a6 mutations cause x-linked mental retardation, microcephaly, epilepsy, and ataxia, a phenotype mimicking angelman syndrome. Am. J. Hum. Genet. *82*, 1003-1010.

Goh, G.Y., Huang, H., Ullman, J., Borre, L., Hnasko, T.S., Trussell, L.O., and Edwards, R.H. (2011). Presynaptic regulation of quantal size: K(+)/h(+) exchange stimulates vesicular glutamate transport. Nat. Neurosci. *14*, 1285-1292.

Gras, C., Amilhon, B., Lepicard, E.M., Poirel, O., Vinatier, J., Herbin, M., Dumas, S., Tzavara, E.T., Wade, M.R., Nomikos, G.G., *et al*. (2008). The vesicular glutamate transporter vglut3 synergizes striatal acetylcholine tone. Nat. Neurosci. *11*, 292-300.

Gronborg, M., Pavlos, N.J., Brunk, I., Chua, J.J., Munster-Wandowski, A., Riedel, D., Ahnert-Hilger, G., Urlaub, H., and Jahn, R. (2010). Quantitative comparison of glutamatergic and gabaergic synaptic vesicles unveils selectivity for few proteins including mal2, a novel synaptic vesicle protein. J. Neurosci. *30*, 2-12.

Han, S., Tai, C., Westenbroek, R.E., Yu, F.H., Cheah, C.S., Potter, G.B., Rubenstein, J.L., Scheuer, T., de la Iglesia, H.O., and Catterall, W.A. (2012). Autistic-like behaviour in scn1a+/- mice and rescue by enhanced gaba-mediated neurotransmission. Nature *489*, 385-390.

Herman, M.A., Ackermann, F., Trimbuch, T., and Rosenmund, C. (2014). Vesicular glutamate transporter expression level affects synaptic vesicle release probability at hippocampal synapses in culture. The Journal of neuroscience : the official journal of the Society for Neuroscience *34*, 11781-11791.

Hiesinger, P.R., Fayyazuddin, A., Mehta, S.Q., Rosenmund, T., Schulze, K.L., Zhai, R.G., Verstreken, P., Cao, Y., Zhou, Y., Kunz, J., *et al*. (2005). The v-atpase v0 subunit a1 is required for a late step in synaptic vesicle exocytosis in drosophila. Cell *121*, 607-620.

Hill, J.K., Brett, C.L., Chyou, A., Kallay, L.M., Sakaguchi, M., Rao, R., and Gillespie, P.G. (2006). Vestibular hair bundles control ph with (na+, k+)/h+ exchangers nhe6 and nhe9. J. Neurosci. *26*, 9944-9955.

Hitti, F.L., and Siegelbaum, S.A. (2014). The hippocampal ca2 region is essential for social memory. Nature *508*, 88-92.

Hnasko, T.S., Chuhma, N., Zhang, H., Goh, G.Y., Sulzer, D., Palmiter, R.D., Rayport, S., and Edwards, R.H. (2010). Vesicular glutamate transport promotes dopamine storage and glutamate corelease in vivo. Neuron *65*, 643-656.

Hua, Z., Leal-Ortiz, S., Foss, S.M., Waites, C.L., Garner, C.C., Voglmaier, S.M., and Edwards, R.H. (2011). V-snare composition distinguishes synaptic vesicle pools. Neuron *71*, 474-487.

Iossifov, I., O'Roak, B.J., Sanders, S.J., Ronemus, M., Krumm, N., Levy, D., Stessman, H.A., Witherspoon, K.T., Vives, L., Patterson, K.E., *et al*. (2014). The contribution of de novo coding mutations to autism spectrum disorder. Nature *515*, 216-221.

Jamain, S., Quach, H., Betancur, C., Rastam, M., Colineaux, C., Gillberg, I.C., Soderstrom, H., Giros, B., Leboyer, M., Gillberg, C., *et al*. (2003). Mutations of the x-linked genes encoding neuroligins nlgn3 and nlgn4 are associated with autism. Nat. Gen. *34*, 27-29.

Kallay, L.M., Brett, C.L., Tukaye, D.N., Wemmer, M.A., Chyou, A., Odorizzi, G., and Rao, R. (2011). Endosomal na+ (k+)/h+ exchanger nhx1/vps44 functions independently and downstream of multivesicular body formation. J. Biol. Chem. *286*, 44067-44077.

Kelley, A.E. (2001). Measurement of rodent stereotyped behavior. Curr Protoc Neurosci *Chapter 8*, Unit 8 8.

Knoepfler, P.S., Cheng, P.F., and Eisenman, R.N. (2002). N-myc is essential during neurogenesis for the rapid expansion of progenitor cell populations and the inhibition of neuronal differentiation. Genes Dev *16*, 2699-2712.

Kojima, A., Toshima, J.Y., Kanno, C., Kawata, C., and Toshima, J. (2012). Localization and functional requirement of yeast na+/h+ exchanger, nhx1p, in the endocytic and protein recycling pathway. Biochimica et biophysica acta *1823*, 534-543.

Kondapalli, K.C., Hack, A., Schushan, M., Landau, M., Ben-Tal, N., and Rao, R. (2013). Functional evaluation of autism-associated mutations in nhe9. Nat. Comm. *4*, 2510.

Kondapalli, K.C., Llongueras, J.P., Capilla-Gonzalez, V., Prasad, H., Hack, A., Smith, C., Guerrero-Cazares, H., Quinones-Hinojosa, A., and Rao, R. (2015). A leak pathway for luminal protons in endosomes drives oncogenic signalling in glioblastoma. Nat. Comm. *6*, 6289.

Lasky-Su, J., Neale, B.M., Franke, B., Anney, R.J., Zhou, K., Maller, J.B., Vasquez, A.A., Chen, W., Asherson, P., Buitelaar, J., *et al*. (2008). Genome-wide association scan of quantitative traits for attention deficit hyperactivity disorder identifies novel associations and confirms candidate gene associations. Am. J. Med. Genet. B Neuropsychiatr. Genet. *147B*, 1345-1354.

Lein, E.S., Hawrylycz, M.J., Ao, N., Ayres, M., Bensinger, A., Bernard, A., Boe, A.F., Boguski, M.S., Brockway, K.S., Byrnes, E.J., *et al*. (2007). Genome-wide atlas of gene expression in the adult mouse brain. Nature *445*, 168-176.

Lord, C., and Bishop, S.L. (2015). Recent advances in autism research as reflected in dsm-5 criteria for autism spectrum disorder. Ann. Rev. Clin. Psychol. *11*, 53-70. Neuron *71*, 474-487.

Martin, L.A., Goldowitz, D., and Mittleman, G. (2010). Repetitive behavior and increased activity in mice with purkinje cell loss: A model for understanding the role of cerebellar pathology in autism. The European journal of neuroscience *31*, 544-555.

McFarlane, H.G., Kusek, G.K., Yang, M., Phoenix, J.L., Bolivar, V.J., and Crawley, J.N. (2008). Autism-like behavioral phenotypes in btbr t+tf/j mice. Genes, brain, and behavior *7*, 152-163.

Miesenböck, G., De Angelis, D.A., and Rothman, J.E. (1998). Visualizing secretion and synaptic transmission with ph-sensitive green fluorescent proteins. Nature *394*, 192-195.

Milosavljevic, N., Monet, M., Lena, I., Brau, F., Lacas-Gervais, S., Feliciangeli, S., Counillon, L., and Poet, M. (2014). The intracellular na(+)/h(+) exchanger nhe7 effects a na(+)-coupled, but not k(+)-coupled proton-loading mechanism in endocytosis. Cell Rep. *7*, 689-696.

Mitchell, S.J., and Ryan, T.A. (2004). Syntaxin-1a is excluded from recycling synaptic vesicles at nerve terminals. J. Neurosci. *24*, 4884-4888.

Moretti, P., Bouwknecht, J.A., Teague, R., Paylor, R., and Zoghbi, H.Y. (2005). Abnormalities of social interactions and home-cage behavior in a mouse model of rett syndrome. Hum. Mol. Gen. *14*, 205-220.

Morrow, E.M., Yoo, S.Y., Flavell, S.W., Kim, T.K., Lin, Y., Hill, R.S., Mukaddes, N.M., Balkhy, S., Gascon, G., Hashmi, A., *et al*. (2008). Identifying autism loci and genes by tracing recent shared ancestry. Science *321*, 218-223.

Nakamura, N., Tanaka, S., Teko, Y., Mitsui, K., and Kanazawa, H. (2005). Four na+/h+ exchanger isoforms are distributed to golgi and post-golgi compartments and are involved in organelle ph regulation. J. Biol. Chem. *280*, 1561-1572.

Nemani, V.M., Lu, W., Berge, V., Nakamura, K., Onoa, B., Lee, M.K., Chaudhry, F.A., Nicoll, R.A., and Edwards, R.H. (2010). Increased expression of alpha-synuclein reduces

neurotransmitter release by inhibiting synaptic vesicle reclustering after endocytosis. Neuron *65*, 66-79.

Ohgaki, R., van, I.S.C., Matsushita, M., Hoekstra, D., and Kanazawa, H. (2011). Organellar na+/h+ exchangers: Novel players in organelle ph regulation and their emerging functions. Biochemistry *50*, 443-450.

Orlowski, J., and Grinstein, S. (2004). Diversity of the mammalian sodium/proton exchanger slc9 gene family. Pflugers Arch. *447*, 549-565.

Ouyang, Q., Lizarraga, S.B., Schmidt, M., Yang, U., Gong, J., Ellisor, D., Kauer, J.A., and Morrow, E.M. (2013). Christianson syndrome protein nhe6 modulates trkb endosomal signaling required for neuronal circuit development. Neuron *80*, 97-112.

Penagarikano, O., Lazaro, M.T., Lu, X.H., Gordon, A., Dong, H., Lam, H.A., Peles, E., Maidment, N.T., Murphy, N.P., Yang, X.W., *et al*. (2015). Exogenous and evoked oxytocin restores social behavior in the cntnap2 mouse model of autism. Sci. Trans. Med. *7*, 271ra278.

Preobraschenski, J., Zander, J.F., Suzuki, T., Ahnert-Hilger, G., and Jahn, R. (2014). Vesicular glutamate transporters use flexible anion and cation binding sites for efficient accumulation of neurotransmitter. Neuron *84*, 1287-1301.

Rab, S.M. (1963). Two cases of chloroquine psychosis. Brit. Med. J. *1*, 1275.

Rizzoli, S.O., and Betz, W.J. (2005). Synaptic vesicle pools. Nat. Rev. Neurosci. *6*, 57-69.

Rodriguez, C.I., Buchholz, F., Galloway, J., Sequerra, R., Kasper, J., Ayala, R., Stewart, A.F., and Dymecki, S.M. (2000). High-efficiency deleter mice show that flpe is an alternative to cre-loxp. Nat. Gen. *25*, 139-140.

Rosenmund, C., and Stevens, C.F. (1996). Definition of the readily releasable pool of vesicles at hippocampal synapses. Neuron *16*, 1197-1207.

Rubenstein, J.L., and Merzenich, M.M. (2003). Model of autism: Increased ratio of excitation/inhibition in key neural systems. Genes, brain, and behavior *2*, 255-267.

Sadakata, T., Shinoda, Y., Oka, M., Sekine, Y., Sato, Y., Saruta, C., Miwa, H., Tanaka, M., Itohara, S., and Furuichi, T. (2012). Reduced axonal localization of a caps2 splice variant impairs axonal release of bdnf and causes autistic-like behavior in mice. Proceedings of the National Academy of Sciences of the United States of America *109*, 21104-21109.

Sankaranarayanan, S., De Angelis, D., Rothman, J.E., and Ryan, T.A. (2000). The use of phluorins for optical measurements of presynaptic activity. Biophys. J. *79*, 2199-2208.

Scheiffele, P., Fan, J., Choih, J., Fetter, R., and Serafini, T. (2000). Neuroligin expressed in nonneuronal cells triggers presynaptic development in contacting axons. Cell *101*, 657-669.

Schmittgen, T.D., and Livak, K.J. (2008). Analyzing real-time pcr data by the comparative c(t) method. Nat. Protocols *3*, 1101-1108.

Schwede, M., Garbett, K., Mirnics, K., Geschwind, D.H., and Morrow, E.M. (2013). Genes for endosomal nhe6 and nhe9 are misregulated in autism brains. Mol. Psych. *19*, 277-279.

Silverman, J.L., Yang, M., Lord, C., and Crawley, J.N. (2010). Behavioural phenotyping assays for mouse models of autism. Nat. Rev. Neurosci. *11*, 490-502.

Soden, M.E., and Chen, L. (2010). Fragile x protein fmrp is required for homeostatic plasticity and regulation of synaptic strength by retinoic acid. J. Neurosci. *30*, 16910-16921.

Spencer, C.M., Alekseyenko, O., Hamilton, S.M., Thomas, A.M., Serysheva, E., Yuva-Paylor, L.A., and Paylor, R. (2011). Modifying behavioral phenotypes in fmr1ko mice: Genetic background differences reveal autistic-like responses. Autism research : official journal of the International Society for Autism Research *4*, 40-56.

Stauber, T., and Jentsch, T.J. (2013). Chloride in vesicular trafficking and function. Ann. Rev. Physiol. *75*, 453-477.

Stevens, T.H., and Forgac, M. (1997). Structure, function and regulation of the vacuolar h+-atpase. Ann. Rev. Cell Dev. Biol. *13*, 779-808.

Strauss, K.A., Puffenberger, E.G., Huentelman, M.J., Gottlieb, S., Dobrin, S.E., Parod, J.M., Stephan, D.A., and Morton, D.H. (2006). Recessive symptomatic focal epilepsy and mutant contactin-associated protein-like 2. New Engl. J. Med. *354*, 1370-1377.

Stromme, P., Dobrenis, K., Sillitoe, R.V., Gulinello, M., Ali, N.F., Davidson, C., Micsenyi, M.C., Stephney, G., Ellevog, L., Klungland, A.*, et al*. (2011). X-linked angelman-like syndrome caused by slc9a6 knockout in mice exhibits evidence of endosomal-lysosomal dysfunction. Brain *134*, 3369-3383.

Sudhof, T.C. (2008). Neuroligins and neurexins link synaptic function to cognitive disease. Nature *455*, 903-911.

Sulzer, D., and Rayport, S. (1990). Amphetamine and other psychostimulants reduce ph gradients in midbrain dopaminergic neurons and chromaffin granules: A mechanism of action. Neuron *5*, 797-808.

Sulzer, D., Chen, T.-K., Lau, Y.Y., Kristensen, H., Rayport, S., and Ewing, A. (1995). Amphetamine redistributes dopamine from synaptic vesicles to the cytosol and promotes reverse transport. J. Neurosci. *15*, 4102-4108.

Thomas, A., Burant, A., Bui, N., Graham, D., Yuva-Paylor, L.A., and Paylor, R. (2009). Marble burying reflects a repetitive and perseverative behavior more than novelty-induced anxiety. Psychopharmacology *204*, 361-373.

Tischbirek, C.H., Wenzel, E.M., Zheng, F., Huth, T., Amato, D., Trapp, S., Denker, A., Welzel, O., Lueke, K., Svetlitchny, A.*, et al*. (2012). Use-dependent inhibition of synaptic transmission by the secretion of intravesicularly accumulated antipsychotic drugs. Neuron *74*, 830-844.

Tronche, F., Kellendonk, C., Kretz, O., Gass, P., Anlag, K., Orban, P.C., Bock, R., Klein, R., and Schutz, G. (1999). Disruption of the glucocorticoid receptor gene in the nervous system results in reduced anxiety. Nat. Gen. *23*, 99-103.

Turrigiano, G.G. (2008). The self-tuning neuron: Synaptic scaling of excitatory synapses. Cell *135*, 422-435.

Ungermann, C., Wickner, W., and Xu, Z. (1999). Vacuole acidification is required for trans-snare pairing, lma1 release, and homotypic fusion. Proc. Natl. Acad. Sci. USA *96*, 11194-11199.

Voglmaier, S.M., Kam, K., Yang, H., Fortin, D.L., Hua, Z., Nicoll, R.A., and Edwards, R.H. (2006). Distinct endocytic pathways control the rate and extent of synaptic vesicle protein recycling. Neuron *51*, 71-84.

Xinhan, L., Matsushita, M., Numaza, M., Taguchi, A., Mitsui, K., and Kanazawa, H. (2011). Na+/h+ exchanger isoform 6 (nhe6/slc9a6) is involved in clathrin-dependent endocytosis of transferrin. Am. J. Physiol. Cell Physiol. *301*, C1431-1444.

Yang, M., and Crawley, J.N. (2009). Simple behavioral assessment of mouse olfaction. Curr Protoc Neurosci *Chapter 8*, Unit 8 24.

Yang, M., Silverman, J.L., and Crawley, J.N. (2011). Automated three-chambered social approach task for mice. Curr Protoc Neurosci *Chapter 8*, Unit 8 26.

Zhou, Q., Petersen, C.C.H., and Nicoll, R.A. (2000). Effects of reduced vesicular filling on synaptic transmission in rat hippocampal neurones. J. Physiol. *525*, 195-206.

Zucker, R.S., and Regehr, W.G. (2002). Short-term synaptic plasticity. Ann. Rev. Physiol. *64*, 355-405.

Chapter 3: Physiological Role of NHE6 in neurons

3.1 Introduction

The organellar cation/hydrogen exchanger NHE6 is highly expression across in the central nervous system. NHE6 was the first organellar NHE isoform identified and it was originally thought to localize to mitochondria. However, subsequent studies demonstrated that it is not in mitochondrial membranes but rather resides on vesicles within the endosomal pathway. As discussed in Chapter 1, human loss of function mutations in NHE6 result in a syndromic autism spectrum disorder known as Christianson Syndrome. This is a severe ASD with intellectual disability, seizures, no verbal communication and other features. Mice that lack NHE6 are also severely impaired, only 60% of them survive the first three weeks of life and those that do survive past that exhibit motor coordination defects and neurodegeneration. While it is clear that NHE6 is important for normal human behavior we still know very little about its physiological role in neurons.

3.2 Experimental Procedures

Biochemistry

Whole Brain Protein Lysate. After euthanasia, brains were dissected rapidly in cold Hepes-buffered saline (HBS), flash frozen in liquid nitrogen and stored on dry ice until homogenization. Tissue was disrupted in buffer containing 150 mM NaCl, 50 mM Tris, pH 7.5, 1 mM EGTA, 1% Triton-X 100, 0.5 % Na-deoxycholate and 1x Roche protease inhibitor cocktail using a rotor stator homogenizer at 900rpm for 9 strokes, and then solubilized by rotation at 4° C for 30 minutes. The homogenate was then sedimented at 1000 *g* for 10 minutes at 4° C to sediment large debris. The supernatant was then transferred to a new tube, total protein concentration determined by BCA, equal amounts of protein added to SDS loading buffer with 100mM DTT and 5% BME. The samples were incubated at 27° C for 30 minutes before separation by electrophoresis through SDS-polyacrylamide (10-15%) and immunoblotting.

Antibodies. We used the following antibodies at the titer indicated: VGLUT1 (Bellocchio et al., 1998) at 1:2000, VGAT (Chaudhry et al., 1998) at 1:2000, VACHT (RHE 819) at 1:1000, P38 (Sigma) at 1:2000, Syntaxin 1 (Sigma) at 1:1000, TfR (Invitrogen) at 1:500, Actin (Millipore) at 1:1000, NHE6 (J. Orlowski adsorbed). HRP-conjugated secondary antibodies were used for western blotting at 1:1000.

Western Blot Quantification. Scanned images of western blot films were quantified using ImageJ. Briefly, tiff files of imaged gels including the proteins of interest and actin (loading control) were analyzed in ImageJ by subtracting the background for each channel, measuring average pixel intensity for each band (in a fixed area), and normalizing each sample to actin. Results are presented as mean ± s.e.m. for 4 animals/genotype.

Synaptic vesicle isolation & radiolabelled glutamate uptake. Synaptic vesicles were purified as described before (Clift-O'Grady et al., 1990; Goh et al., 2011). Briefly, the standard buffer for glutamate uptake contained 148 mM choline or potassium gluconate, 2 or 20 mM choline or KCl, 4 mM MgATP, 10 mM HEPES-Tris, pH 7.4, 1 mM choline glutamate, and 40 μCi ml^{-1} [^{3}H]L-glutamate (Perkin Elmer). Transport was initiated by adding 100 μg LP2 protein to 200 μl reaction buffer (pre-warmed to 30° C). The reaction was incubated at 30° C for 10 min and stopped by rapid filtration and washing four times with 2 ml cold reaction buffer with no

glutamate. Bound radioactivity was detected by liquid scintillation, and background transport measured in the presence of 100 μM Evans Blue subtracted. In every experiment, each condition was assayed in triplicate and at least three independent experiments were performed using at least three different synaptic vesicle preparations. Results are presented as mean ± s.e.m and the statistics analyzed by two-way ANOVA test with Bonferroni post-hoc comparison.

Velocity gradient fractionation of Synaptic Vesicles. A continuous glycerol gradient from 5-25% was layered on top of a 50% sucrose cushion through the use of an auto densi-flow. Synaptic vesicles were then added to the top of the gradient. Samples were then centrifuged in an SW41 rotor for 60 minutes at 270K G. The auto densi-flow was then used to collect fraction from the sedimented solution. Aliquots of fractions were then added to SDS-PAGE loading buffer with reducing agents and run on 10% SDS-PAGE gels.

Immunoisolation of Synaptic Vesicles. Protocol is adapted with minor modifications from Hnsako et al., 2010. Dynabeads Protein G (300ul, Invitrogen) were incubated with 1-2ug antibody in 1mL citrate-phosphate buffer pH 5.8 for 60 minutes at room temperature while rotating on a nutator. Beads were then placed in magnetic holder and washed with 0.2M triethanolamine (TEA) buffer pH 8.4 three times. Beads were then resuspended in 1 ml 20 mM dimethy pimelimidate (DMP) (5.4 mg/ml) in 0.2 M TEA and placed on a nutator for 30 minutes at room temperature to crosslink. Crosslinking solution was then removed and beads washed with 1 ml 50 mM Tris ph7.5 for 15 minutes and then washed again three times with PBS. Synaptic vesicles were then added to beads with 0.35% BSA + Protease Inhibitors, and incubated for 1 hour. Beads were then washed and unbound supernatants removed. Bound beads were incubated with SDS-PAGE loading buffer + DTT, and supernatant was run on 10% SDS-PAGE gel.

Neuronal culture

Hippocampal neurons were isolated from newborn mouse pups following guidelines approved by the UCSF IACUC. Hippocampi were digested for 20 minutes in Hanks buffered saline + 0.36% glucose (HBS+) containing 0.00025% trypsin, washed three times with HBS+ and triturated thirty times in 2.25 ml MEM containing 21 mM glucose, 5% FBS, 2% B27 and 1x Glutamax (Serum Neuronal Media, SNM). Coverslips pretreated with L-polylysine (PLL) were rinsed in water and dried before plating neurons. For live cell imaging experiments, neurons in SNM were plated into 10 mm cloning rings secured onto 25 mm coverslips at a density of 30-35,000/79mm^2. The next day, 50% of the SNM media was removed and 3 volumes Neurobasal Media (NBM) DIV1 (NBM with 2% B27, 1.3X Glutamax) was added. At 7 days *in vitro* (DIV7), 50% of the media was removed and one volume NBM DIV7 (1 part SNM: 3 part NBM DIV1, 4 μM AraC) added. Neurons were infected with lentivirus expressing VGLUT2-pHluorin at DIV6, resulting in transduction efficiencies ~100%.

Live Imaging

To image the cycling of synaptic vesicles, neurons were infected with VGLUT2-pHluorin expressing lentivirus at DIV6. Cultured neurons were imaged at DIV14–17 as previously described (Voglmaier et al., 2006; Nemani et al., 2010; Hua et al., 2011). VGLUT2-pHluorin was imaged with 470/40 nm excitation and 525/50 nm emission filters. pHluorin images were acquired at 0.2 Hz, and the fluorescence normalized to total intracellular fluorescence (in NH_4Cl) after subtracting the initial fluorescence, or $F_{NH4Cl} - F_{initial.}$. Background fluorescence was

determined by averaging 10 ROIs of 5 x 5 pixels over an area of non-transfected cell background, and subtracted from the fluorescence of each puncta in each frame.

3.3 Results & Discussion

In recent years, unpublished work from the Edwards lab and publications from three separate groups have explored the function of NHE6 in neurons; and the complex picture of its physiological role in neuron biology is slowly beginning to emerge. NHE6 is a highly abundant protein expressed in all regions of the brain (Allen Brain Atlas) and at high levels throughout development (Figure 3.1, J. Ullman unpublished data).

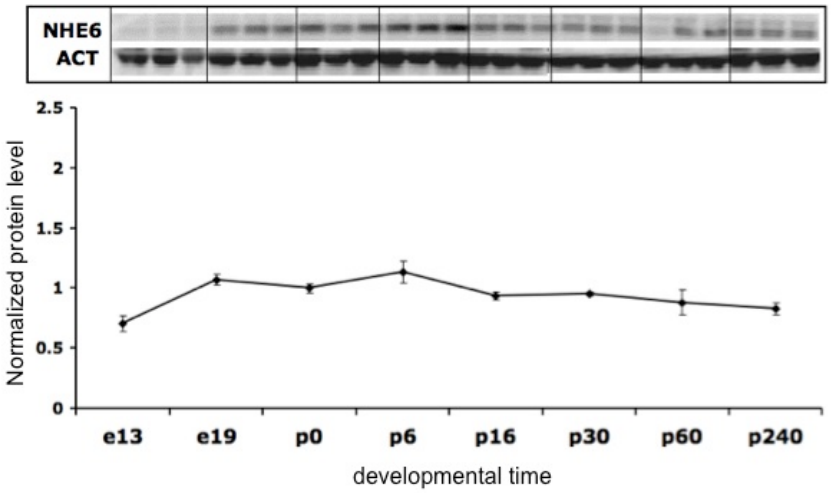

Figure 3.1 NHE6 protein levels over development
Brains of 3 C57Bl6 mice/timepoint were homogenized, protein lysates solubilized, denatured samples run on an SDS-PAGE gel, immunoblotted with rb anti-NHE6 (rb antibody generous gift of J. Orlowski) and HRP secondary visualized with ECL reagent. [mean, error bars s.e.m.]

The physiological importance of this protein is highlighted not only by humans with NHE6 mutations but also by the severity of phenotypes observed the NHE6 knock-out (KO) mouse. Only 60% of these mice survive to postnatal day 21 and those remaining suffer from seizures, are grossly under-weight and become severely ataxic with age (Stromme et al., 2011, J. Ullman unpublished data).

In cortical neurons NHE6 localizes exclusively to pre and post-synaptic endosomal vesicles. In dendrites at steady state, NHE6 has very high overlap with transferrin receptor in recycling endosomes and shows little to no enrichment in PSD95 positive spines (Ouyang et al., 2013, Deane et al., 2013, J. Ullman unpublished data). However, live-imaging of GFP-tagged NHE6 protein has revealed it to be highly mobile and actively recruited into spine heads during long-term potentiation; thus suggesting an unexplored role for NHE6 and cation/hydrogen exchange activity in synaptic plasticity (Deane et al., 2013). In developing neurons the cation/hydrogen exchange activity of NHE6 is important for proper circuit development. In cultures made from the NHE6 KO mouse neurons, dendritic endosomes are hyper-acidified (Ouyang et al., 2013). This results in attenuated TRKB signaling, and altered dendrite branching that can be rescued by exogenously applied BDNF (Ouyang et al., 2013). In brains from mature

NHE6 KO mice, loss of the protein results in cerebellar degeneration and accumulation of classic ganglioside markers for lysosomal storage dysfunction (Stromme et al., 2011).

Based on localization data NHE6 must have a role in axons, yet its function there remains unknown. By immunostaining of cultured neurons, it has been demonstrated by several groups that NHE6 colocalizes with markers for synaptic vesicles including VGLUT1, VGAT and P38, in some but not all presynaptic boutons (Deane et al., 2013, Ouyang et al., 2013, J. Ullman unpublished data). Furthermore, proteomic analysis of excitatory (VGLUT1 containing) and inhibitory (VGAT containing) synaptic vesicles identified NHE6 peptides in both populations (Gronborg et al., 2010). This work has been confirmed by velocity gradient sedimentation of purified synaptic vesicles, which shows that NHE6 migrates like a typical synaptic vesicle protein (Figure 3.2, J. Ullman unpublished data).

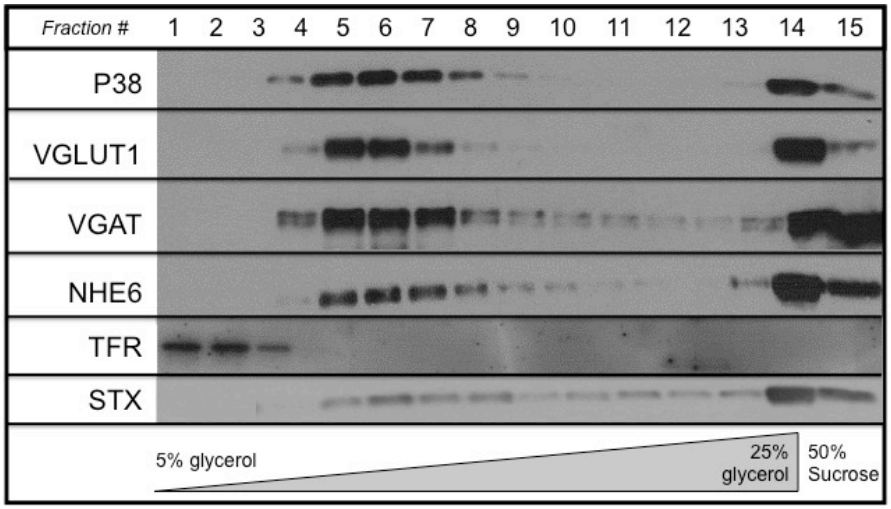

Figure 3.2: NHE6 sediments with synaptic vesicle proteins in velocity gradient fractionation
Purified synaptic vesicles (see Chapter 2, Experimental Methods for details) were further separated by size via glycerol gradient fractionation. Briefly, vesicles were loaded onto a continuous gradient of 5-25% glycerol and then centrifuged for one hour at 270K G. Fractions were collected and protein lysates analyzed by western blot.

The presence of NHE6 on different synaptic vesicles subtypes was further investigated by immunoisolation of NHE6 containing synaptic vesicles via NHE6 affinity purified antibody bound to magnetic beads. These experiments revealed NHE6 co-immunoisolation with vesicular neurotransmitter transporters for glutamate (VGLUT1), GABA (VGAT) and acetylcholine (VACHT) (Figure 3.3, J. Ullman unpublished data).

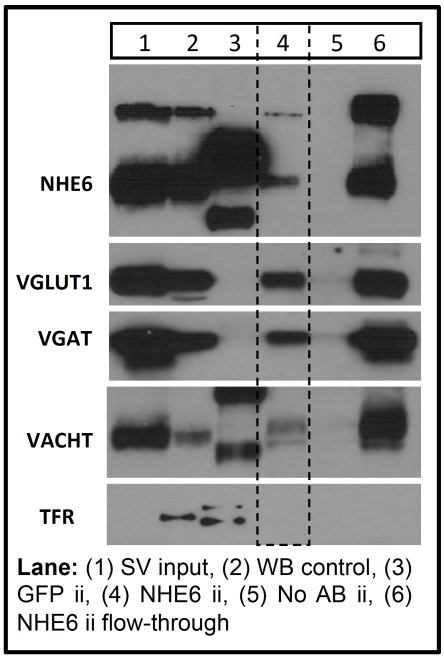

Figure 3.3: Co-Immunoisolation of NHE6 with neurotransmitter transporters

Rabbit anti-NHE6 (generous gift of J. Orlowski) was bound to dynabeads and used to immunoisolate synaptic vesicles containing NHE6. These samples were then subjected to western blot analysis by antibodies against NHE6 and other proteins. Abbreviations: (SV) synaptic vesicles, (WB) whole brain protein lysate, (GFP ii) negative control pull down of dynabeads bound with GFP antibody, (NHE6 ii) pull down of dynabeads bound with NHE6 antibody, (No AB ii) no antibody negative control, (NHE6 ii flow-through) unbound synaptic vesicles from the NHE6 ii incubation.

The enrichment of NHE6 on synaptic vesicles is intriguing in light of work from the Edwards' lab which discovered that NHE activity has a crucial role in generation of the proton electrochemical driving force that drives the uptake of the neurotransmitter glutamate into synaptic vesicles (Goh et al., 2011). Vesicular glutamate transporters (VGLUTs) rely specifically on the electrical component of the H+ electrochemical driving force (ΔμH+) across the vesicle membrane. ΔμH+ is comprised of the chemical component (ΔpH) and electrical component (Δψ), and although certain neurotransmitter transporters rely more on ΔpH, the VGLUTs rely primarily on Δψ (Maycox et al., 1988, Tabb et al., 1992). Goh et al. established that cation/H+ exchange (NHE) activity converts ΔpH into Δψ, and this conversion promotes glutamate transport into synaptic vesicles (2011). Given its enrichment on synaptic vesicles, the Edwards lab originally hypothesized that NHE6 was the isoform responsible for this activity. However, functional data supporting this hypothesis is lacking. In an assay of radiolabelled glutamate uptake into synaptic vesicles purified from either wild-type (WT) or NHE6 KO brains, there was no difference in potassium stimulation of glutamate transport (Figure 3.4, J. Ullman unpublished data).

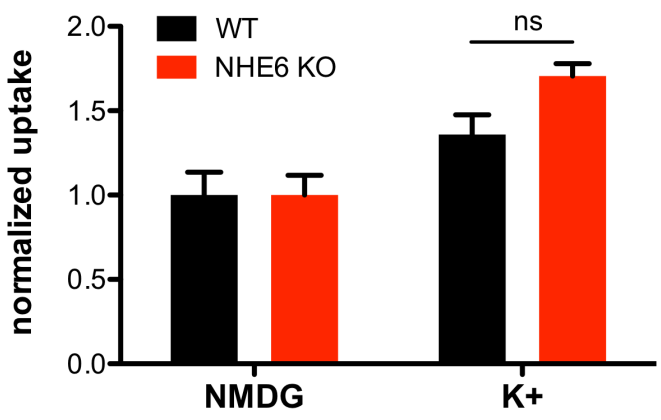

Figure 3.4: K+ stimulation of glutamate uptake is normal in NHE6 KO vesicles

Isolated synaptic vesicles were incubated with 3H-gluatmate and ATP in buffer contatining either NMDG-gluconate or K+-gluconate. There is no significant difference in K+ stimulation of glutamate uptake in the NHE6 KO vesicles. N=3, mean, s.e.m., 2-Way ANOVA with Bonferroni.

However, it is possible that the in vitro uptake experiments are not sensitive enough to capture a small difference and thus electrophysiological analysis of quantal size by gamma-DGG is suggested. Alternatively, the primary role of NHE6 on synaptic vesicles could be independent of its catalytic activity. Considerable work has established that for the plasma membrane isoforms, the c-terminal tail recruits a vast array of interacting partners with the interactions influencing protein trafficking, altering exchange activity and many other effects. Perhaps then the c-terminal tail of NHE6 is important for synaptic vesicle cycling? This possibility was investigated in neurons cultured from NHE6 KO hippocampi expressing VGLUT2-pHluorin. This pH sensitive genetic probe is expressed exclusively on synaptic vesicles and is normally quenched inside the acidic lumen of the vesicles. Upon electrical stimulation, vesicles are exocytosed whereby the pHluorin fluorescence increases upon exposure to the imaging solution neutral pH before it is rapidly endocytosed and quenched again. Live imaging of VGLUT2-pHluorin fluorescence in response to stimulation thus provides a direct measurement of the synaptic vesicle cycle. However, there was no difference in synaptic vesicle cycling between the NHE6 KO and WT neurons suggesting that NHE6 does not have a role in this pathway (Figure 3.5, J. Ullman unpublished data).

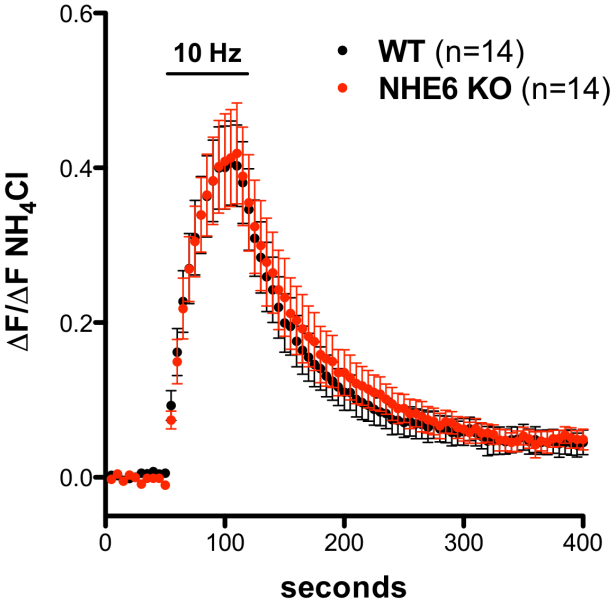

Figure 3.5: Loss of NHE6 KO does not alter synaptic vesicle cycling

Cultured hippocampal neurons div14 from NHE6 KO mice show a similar VGLUT2-pHluorin fluorescence response to 10 Hz stimulation for 60 seconds relative to WT cells. N=14 coverslips from 4 cultures, mean, s.e.m.

Furthermore, electrophysiological analysis of field response in acute hippocampal slice recordings from NHE6 KO mice show no disturbance in presynaptic release of neurotransmitter (Ouyang et al., 2013). The role of NHE6 in axons and synaptic vesicles thus remains an open and intriguing question.

3.4 Chapter 3 References

Bellocchio, E.E., Hu, H., Pohorille, A., Chan, J., Pickel, V.M., and Edwards, R.H. (1998). The localization of the brain-specific inorganic phosphate transporter suggests a specific presynaptic role in glutamatergic transmission. J. Neurosci. *18*, 8648-8659.

Chaudhry, F.A., Reimer, R.J., Bellocchio, E.E., Danbolt, N.C., Osen, K.K., Edwards, R.H., and Storm-Mathisen, J. (1998). The vesicular gaba transporter vgat localizes to synaptic \ vesicles in sets of glycinergic as well as gabaergic neurons. J. Neurosci. *18*, 9733-9750.

Clift-O'Grady, L., Linstedt, A.D., Lowe, A.W., Grote, E., and Kelly, R.B. (1990). Biogenesis of synaptic vesicle-like structures in a pheochromocytoma cell line pc12. J. Cell Biol. *110*, 1693-1703.

Deane, E.C., Ilie, A.E., Sizdahkhani, S., Das Gupta, M., Orlowski, J., and McKinney, R.A. (2013). Enhanced recruitment of endosomal na+/h+ exchanger nhe6 into dendritic spines of hippocampal pyramidal neurons during nmda receptor-dependent long-term potentiation. J. Neurosci. *33*, 595-610.

Goh GY, Huang H, Ullman J, Borre L, Hnasko TS, Trussell LO, Edwards RH. (2011) Presynaptic regulation of quantal size: K+/H+ exchange stimulates vesicular glutamate transport. Nature Neuroscience, 14: 1285-1292.

Gronborg M, Pavlos NJ, Brunk I, Chua JJ, Munster-Wandowskit A, Reidel D, Ahnert HIlger G, Urlaub H, Jahn R. (2010) Quantitative comparison of glutamatergic and GABAergic synaptic vesicles unveils selectivity for few proteins including MAL2, a novel synaptic vesicle protein. Journal of Neuroscience, 30: 2-12.

Hnasko, T.S., Chuhma, N., Zhang, H., Goh, G.Y., Sulzer, D., Palmiter, R.D., Rayport, S., and Edwards, R.H. (2010). Vesicular glutamate transport promotes dopamine storage and glutamate corelease in vivo. Neuron *65*, 643-656.

Maycox PR, Deckerwerth T, Hell JW, Jahn R. (1988) Glutamate uptake by brain synaptic vesicles. Energy dependence of transport and functional reconstitution in proteoliposomes. Journal of Biological Chemistry, 263: 15423-28.

Ouyang, Q., Lizarraga, S.B., Schmidt, M., Yang, U., Gong, J., Ellisor, D., Kauer, J.A., and Morrow, E.M. (2013). Christianson syndrome protein nhe6 modulates trkb endosomal signaling required for neuronal circuit development. Neuron *80*, 97-112.

Strømme P, Dobrenis K, Sillitoe RV, Gulinello M, Ali NF, Davidson C, Micsenyi MC, Stephney G, Ellevog L, Klungland A, Walkley SU. (2011) X-linked Angelman like syndrome caused by Slc9a6 knockout in mice exhibits evidence of endosomal-lysosomal dysfunction. Brain, 134: 3369-3383.

Tabb JS, Kish PE, Van Dyke R, Ueda T. (1992) Glutamate transport into synaptic vesicles. Roles of membrane potential, pH gradient, and intravesicular pH. Journal of Biological Chemistry, 267: 15412-18.

Chapter 4: Future Directions & Closing Remarks

4.1 Future Directions

The studies presented in this dissertation highlight the importance of the proton electrochemical gradient (ΔμH+) in synaptic transmission and autism. While these findings mark a significant advancement in our understanding of the specific role for NHE9 in neuronal biology there is still much to be learned about the broader role of the ΔμH+ in vesicular biology and synaptic transmission. The diverse physiological functions that rely on ΔμH+ require precise balance between the chemical component (ΔpH) and electrical component (Δψ). While much is known about their respective roles in neurotransmitter loading, understanding the unique contributions of each gradient to other aspects of neuronal biology is of great importance. Towards this end, there are both general questions relating to ΔpH & Δψ, as well as specific questions relating to the endosomal NHE proteins that require further investigation. A discussion of general questions relating to ΔμH+ will first be addressed, followed by more specific consideration of the roles of NHE6 and NHE9 in vesicular and neuronal biology.

The membrane transporter proteins within the endo-lysosomal pathway have biochemical functions that co-evolved based on dynamic pH and cation regulation along the pathway. Lysosomal proteases remain inactive until they reach a steady state pH lower than ~5.0. Upon endocytosis, ligands stay bound to their respective GPCR prolonging signaling until the vesicle acidifies which then dissociates the ligand from its receptor, and finally terminates the signal. The unique neurotransmitter transporters are the Goldilocks proteins in the pathway- each require a specific balance between ΔpH and Δψ to maximally load transmitter; not too much nor too little, but just right. Yet, this requirement is probably true for all the biochemically active membrane proteins on endo-lysosomal vesicles. However, we are limited in our ability to interpret these requirements for specific proteins due to a lack of direct measurements for neuron endosomal ΔpH, Δψ as well as absolute [H+] and [ion] in response to various biological challenges. There are excellent pH sensitive fluorescent probes to monitor vesicular pH in live neurons and every year new probes are being developed that allow greater and more targeted precision. The fluorescent probes used to monitor live fluxes of K+ and Na+ are rapidly evolving; and electrophysiological recordings from endosomes is now a tractable technique. With these methods, quantification of endosomal alkali cation concentration and analysis of their driving forces is possible. What is the precise concentration of K+ or Na+ in various vesicle subtypes? Does neuronal activity acutely change these concentrations? In vesicles undergoing endocytosis, how are these gradients dynamically altered? How do the changes in cation concentrations correlate to changes in pH? What is the role of vesicle osmolarity in exo and endocytosis; and does absolute osmolarity vary dramatically along different parts of the pathway? Characterization of these fundamental properties will allow us to more precisely formulate hypothesis about the potential role of specific proteins in various neuronal physiological responses.

The same techniques can also be used to further our understanding of the function of NHE6 in synaptic transmission and neuronal physiology. The cation/hydrogen exchange activity of NHE6 clearly has an important role in BDNF signaling during development. Yet, this alone cannot explain the multitude and magnitude of pathologies observed in both humans and mice, lacking NHE6, over the course of their lifetime. Given the observation that NHE6 containing vesicles are recruited to spines during LTP, the obvious question remains- how does $[pH]_i$ and

$[K+]_i$ influence this process? and is LTP impaired in NHE6 KO neurons? Given the role of NHE6 in BDNF signaling, are there other neurotrophic factors whose signaling is altered by loss of NHE6? Does NHE6 directly influence dense-core vesicle pH or osmolarity, and does this influence cargo processing? NHE6 immunostaining localizes the protein to only a subset of synaptic vesicles, why? The imaging thus far performed, only resolves NHE6 localization to the level of boutons- employing electron micrograph imaging, with immunostaining, to visualize NHE6 on individual vesicles within a bouton could be incredibly helpful. However, immuno-EM labeling is always sparse and localization to specific vesicle sub-types is limited by the availability of high affinity antibodies to specific proteins. The Edwards lab has an excellent collection of antibodies against synaptic vesicles markers and to date we have yet to find one whose immunofluorescence localization matches NHE6 perfectly. This argues that an EM approach could be very difficult. It has been speculated that perhaps the role of NHE6 is on axonal endosomes and not actively recycling synaptic vesicles. This population of vesicles is extremely difficult to study as there are no proteins that have been exclusively localized to this population. The biochemical isolation of purified synaptic vesicles surely includes these vesicles; and indeed these vesicles might make up what is commonly referred to as the resting pool of synaptic vesicles. Functional assays do exist to measure the relative size of the resting pool and analysis of this property in the NHE6 KO neurons could be very informative. Alternatively, NHE6 might be important for axonal transport vesicles and live imaging of fluorescently tagged NHE6 in axons would be an excellent experiment to begin this line of inquiry. There are still many questions unanswered in the study of NHE6, and all of them have the potential of yielding great insight not only to our understanding of endosomal biology but also for ASDs.

While our study marks significant advancement in our understanding of the precise role of NHE9 in neuron endosomal biology and synaptic transmission there are still many questions that require further study. Indeed, the conclusions from our study directly highlight specific questions that need to be resolved. First, how is calcium cooperativity influenced by vesicle pH? This could be through direct interaction of one protein with protons, or there could be a cascading effect of pH on calcium buffering or transients within the terminal. Live imaging of calcium in boutons, in response to different types of activity, can tell us how much calcium is entering presynaptic boutons and whether the kinetics of calcium buffering are altered in the NHE9 KO neurons. If no change in calcium is observed, then analysis of the SNARES required for vesicle fusion could yield important insights into the nature of the NHE9 KO exocytosis dysfunction. The second set of questions for NHE9 are totally unexplored in our study- what is NHE9 doing post-synaptically? and how does loss of the protein affect synaptic transmission? Dendritic recycling endosomes are acidified in the absence of NHE9, and surely there are consequences to this change. For the purpose of clarity in our study, we chose to focus on understanding the presynaptic role of NHE9. However, we do have evidence to suggest that there might be altered post-synaptic receptor trafficking given that we see changes in amplitude of miniature inhibitory post synaptic currents this could directly reflect a decrease in receptors on the surface. Additionally, the increased frequency and normal amplitude of miniature excitatory post synaptic currents cannot be resolved with our other physiology data unless some idea of homeostatic scaling is evoked. We are currently testing this idea first by looking at AMPA/NMDA ratios to see if the proportion of active synapses is higher in he NHE9 KO neurons, but it is possible that the situation is more complex than that. Regardless, more work is needed to clarify the nature of the synaptic transmission defect in these neurons and then to link these defects to either altered endosomal pH or loss of interaction with NHE9. The third area of

inquiry for NHE9 is understanding its role in the olfactory bulb. NHE9 expression is highest in this area of the brain and the animals display a prominent defect in odorant processing. Understanding how loss of NHE9 affects this circuit could be tremendously interesting. The fourth area of study, that is speculated on in Chapter 2, is whether the behavioral phenotypes of the NHE9 cKO mice can be reversed by weak base treatment. We have already begun to explore this possibility by treating mice with chloroquine for 2-4 weeks. This treatment does affect aspects of their behavior that may suggest an improvement in social recognition. However, WT and KO animals alike become extremely hyperactive due to the treatment which makes it very difficult to interpret the results of our experiments. Thus, we are considering alternative drugs or more acute treatments as possible avenues to explore this question. The fifth and final line of questions, that will be very interesting, aims to understand the biochemical consequences of the human and mouse mutations on the function of NHE9. We performed two behavioral experiments that address different aspects ADHD behavior in mice: hyperactivity and impulsivity. Both were normal in the cKO mouse. Perhaps this suggests that the ADHD mutations are gain of function mutations. By expressing these mutant cDNAs in NHE9 KO neurons we can determine if they alter endosomal pH, trafficking or synaptic vesicle filling. Understanding the nature of this defect could yield important insights into the cellular pathology of ADHD.

These questions are offered to evoke investigation of the proton electrochemical gradient ($\Delta\mu H+$) in synaptic transmission and autism. $\Delta\mu H+$ is a fascinating and complex biophysical force. While it is clearly important for normal cognition we know so little about its specific role in synaptic physiology. The endosomal NHE proteins, NHE6 & 9, offer an exciting and rewarding entryway into the study of this biophysical property and the consequences of its dysregulation.

4.2 Closing Remarks

This dissertation work has evolved in many ways over many years, yet it ultimately ended where it began: with the desire to offer a new insight into the molecular biology of autism spectrum disorders. This work would not have been possible without the unwavering support, mentorship and enthusiasm of Robert Edwards. He is an amazing scientist and a terrific PhD advisor. The analysis of the behavioral phenotype of the NHE9 cKO mice would have been next to impossible without the commitment and ingenuity of Michael Sullivan and Ellen Pham. They both volunteered hundreds of hours for this project while enrolled fulltime as UC Berkeley undergraduates. The collaboration with Jing Yang for the electrophysiological analysis of the NHE9 KO slices marked a wonderful turning point in the investigations, and it was her findings that put into context the meaning of the cellular defects we were observing. She demonstrated the very best of what a collaborator should be- intelligent, curious and devoted to the success of the project. It cannot go without saying, that all the members of the Edwards Lab had a tremendous role in shaping this work- their inquisitiveness and technical expertise were invaluable assets throughout these investigations. Finally, this dissertation would not have been possible without David Whitfield. He is amazing.